



Growth yields and light-capture in PhycoCyanin and PhycoErythrin-rich picocyanobacteria, across photic regimes and growth phases

Journal:	<i>Limnology and Oceanography</i>
Manuscript ID:	Draft
Wiley - Manuscript type:	Original Article
Date Submitted by the Author:	n/a
Complete List of Authors:	Śliwińska-Wilczewska, Sylwia; Mount Allison University Department of Biology; University of Gdańsk, Department of Marine Ecosystems Functioning, Faculty of Oceanography and Geography Konik, Marta; University of Victoria, Department of Geography; Polish Academy of Sciences, Institute of Oceanology Savoie, Mireille; Mount Allison University Department of Biology Aguilera, Anabella; Linnaeus University, Department of Biology and Environmental Science, Centre for Ecology and Evolution in Microbial Model Systems (EEMiS); Swedish University of Agricultural Sciences, Department of Aquatic Sciences and Assessment Omar, Naaman; Mount Allison University Department of Biology Campbell, Douglas; Mount Allison University Department of Biology
Keywords:	Cumulative diel photon dose, Light-capture, PAR, Photic regime, Phase of growth, Photoperiod, Picocyanobacteria, PUR
Abstract:	The genus <i>Synechococcus</i> occurs from tropical to arctic zones, with climate scenarios forecasting range expansions of this picocyanobacteria into new photic regimes. We found that coastal PhycoCyanin(PC)-rich and PhycoErythrin(PE)-rich <i>Synechococcus</i> strains grew fastest under moderate photosynthetically active radiation, and a 24-hour photoperiod, despite a cumulative diel photon dose equivalent to conditions where growth was slower, under higher light and shorter photoperiods. Under optimal conditions, a PE-rich <i>Synechococcus</i> sp. achieved a highest recorded cyanobacterial chlorophyll-specific exponential growth rate of 4.5 d ⁻¹ . PE-rich strains demonstrated wider ability to modulate light capture capacity, whereas PC-rich strains showed less change in light capture across increasing cumulative diel photon dose. We found the coastal picocyanobacteria show consistent patterns of an exponential decay of effective absorption cross section for PSII photochemistry, versus increasing cumulative diel PAR doses. Effective absorption cross section for PSII excited through phycobilisome absorbance at 590 nm was positively correlated with phycobiliprotein:Chl a, particularly during pre-stationary growth phase. Within each strain, μ showed consistent saturating responses to increasing cumulative diel PSII electron flux. As photoperiod opportunists coastal picocyanobacteria show potential to expand into longer photic regimes at warming higher latitudes.



SCHOLARONE™
Manuscripts

Scientific Significance Statement Topic

In PhycoCyanin(PC)-rich, and particularly in PhycoErythrin(PE)-rich phenotypes of *Synechococcus*, photoperiod alters the responses of growth rates to cumulative diel photons, with both 8 and 24 h photoperiods provoking increased photoinhibition of growth. In contrast, growth rates show simpler saturating responses to cumulative diel reductant generation, accessed through a chlorophyll fluorescence measure of electron flux, across a matrix of photoperiods and photosynthetically active radiation levels.

Under optimal conditions of 24 h photoperiod and moderate photosynthetically active radiation, a PE-rich *Synechococcus* sp. reached a chlorophyll-specific exponential growth rate of 4.5 d^{-1} , a record for cyanobacteria, comparable with genetically-modified industrial strains.

As photoperiod opportunitists, with capacity to grow rapidly under 24 h photoperiod, coastal *Synechococcus* sp. show potential to emerge as phytoplankton components during summer in future, warmed, polar regions.

Scientific Significance Statement Outlet

Dear Editor-in-Chief

K. David Hambright,

Our work indicating that picocyanobacteria have the potential to expand into new photic regimes while PE-rich picocyanobacteria may emerge as the dominant phytoplankton.

The findings of this study are helpful for further research on picocyanobacteria ecophysiology, and should be of interest to readers of Limnology and Oceanography, which has previously published articles on similar topics.

1 **Growth yields and light-capture in PhycoCyanin and**
2 **PhycoErythrin-rich picocyanobacteria, across photic**
3 **regimes and growth phases**

4

5 **Sylwia Śliwińska-Wilczewska^{1,2}, Marta Konik^{3,4}, Mireille Savoie¹, Anabella**
6 **Aguilera^{5,6§}, Naaman M. Omar¹, and Douglas A. Campbell^{1,*}**

7

8 ¹ Department of Biology, Mount Allison University, 53 York St., Sackville, NB, E4L 1C9,
9 Canada

10 ² Institute of Oceanography, University of Gdańsk, 46 Piłsudskiego St, 81-378, Gdynia, Poland

11 ³ Department of Geography, University of Victoria, Victoria, BC, V8P 5C2, Canada

12 ⁴ Institute of Oceanology, Polish Academy of Sciences, 81-712 Sopot, Poland

13 ⁵ Department of Biology and Environmental Science, Centre for Ecology and Evolution in
14 Microbial Model Systems (EEMiS), Linnaeus University, Kalmar, Sweden

15 ^{6§} Department of Aquatic Sciences and Assessment, Swedish University of Agricultural
16 Sciences, Uppsala, Sweden

17 * Correspondence: Douglas A. Campbell: dubhglascambeuil@gmail.com

18

19 **Running head:** *Picocyanobacteria across photic regimes*

20 **Keywords:** Cumulative diel photon dose; Light-capture, PAR; Photic regime; Phase of growth;
21 Photoperiod; Picocyanobacteria; PUR

22

23 **Abstract**

24 The genus *Synechococcus* occurs from tropical to arctic zones, with climate scenarios
25 forecasting range expansions of this picocyanobacteria into new photic regimes. We found that
26 coastal PhycoCyanin(PC)-rich and PhycoErythrin(PE)-rich *Synechococcus* strains grew fastest
27 under moderate photosynthetically active radiation, and a 24-hour photoperiod, despite a
28 cumulative diel photon dose equivalent to conditions where growth was slower, under higher
29 light and shorter photoperiods. Under optimal conditions, a PE-rich *Synechococcus* sp. achieved
30 a highest recorded cyanobacterial chlorophyll-specific exponential growth rate of 4.5 d^{-1} . PE-
31 rich strains demonstrated wider ability to modulate light capture capacity, whereas PC-rich
32 strains showed less change in light capture across increasing cumulative diel photon dose. We
33 found the coastal picocyanobacteria show consistent patterns of an exponential decay of effective
34 absorption cross section for PSII photochemistry, versus increasing cumulative diel PAR doses.
35 Effective absorption cross section for PSII excited through phycobilisome absorbance at 590 nm
36 was positively correlated with phycobiliprotein:Chl *a*, particularly during pre-stationary growth
37 phase. Within each strain, μ showed consistent saturating responses to increasing cumulative diel
38 PSII electron flux. As photoperiod opportunists, coastal picocyanobacteria show potential to
39 expand into longer photic regimes at warming higher latitudes.

40

41 **Introduction**

42 The photic regime, comprised of Photosynthetically Active Radiation (PAR), spectral
43 quality, and photoperiod, is a pivotal influence on the growth and productivity of phytoplankton
44 within aquatic ecosystems. PAR refers to the spectral range of solar radiation, approximately

45 400-700 nm, that is capable of driving photosynthesis. The availability and distribution of PAR
46 in aquatic ecosystems is influenced by cloud cover, water depth, and light attenuation due to
47 water turbidity and suspended particles, including phytoplankton cells (Field et al. 1998;
48 Torremorell et al. 2009). Photosynthetically Usable Radiation (PUR), in turn is the fraction of
49 PAR that can be absorbed for photosynthesis by pigments of a given cyanobacteria or algae
50 (Morel 1978). PUR thus depends upon the interaction of PAR, and the phytoplankter expression
51 of genomic capacities for light capture (Moejes et al. 2017). Cyanobacteria also respond to
52 changes in photoperiod, which serves as a key environmental cue for photosynthesis, growth,
53 reproduction, and nutrient assimilation (LaRoche and Robicheau 2022). Thus, in polar regions,
54 characterized by prolonged periods of wintertime darkness and continuous daylight during
55 summer, cyanobacteria encounter unique challenges. Light is the primary limitation on biomass
56 production in winter, suppressing cyanobacteria growth and metabolic activity, whereas
57 extended daylight in summer boosts photosynthetic activity (Arrigo 2014). In temperate regions,
58 seasonal variation in light-limitation is less pronounced, but cyanobacteria are still influenced by
59 daily and seasonal fluctuations, with a contrast between more favorable conditions for
60 cyanobacteria growth in spring and summer, compared to fall and winter (Huisman et al. 2002;
61 Holtrop et al. 2021). In the tropics, daylight hours remain nearly constant throughout the year
62 (Behrenfeld et al. 2006), and cyanobacteria productivity is rather controlled by nutrients
63 resupplied into the euphotic zone (Li et al. 2015), and mortality through viral lysis (Ortmann et
64 al. 2002) and zooplankton grazing (Christaki et al. 1999).

65 *Synechococcus*, a diverse genus of picocyanobacteria, exhibits a distribution spanning
66 diverse geographical regions (Flombaum et al. 2013), with strains demonstrating a remarkable
67 range of adaptations to environmental conditions (Śliwińska-Wilczewska et al. 2018a; Aguilera

et al. 2023). *Synechococcus* capacities to thrive across diverse marine and freshwater habitats positions it as a pivotal agent in energy and nutrient transfer within food webs, connecting the microbial loop with higher trophic levels, offering direct sustenance to grazers, including zooplankton and small fish (Li 1995). As one of the two dominant picocyanobacterial genera in oceanic waters, *Synechococcus* contribute significantly to light attenuation and light availability for other photosynthetic marine organisms, thereby influencing ocean colour and allowing satellite detection of *Synechococcus*-rich communities (Xi et al. 2020). General relations among optical absorption spectra and pigment compositions have been used to determine diagnostic pigment indices of major phytoplankton functional types (Hirata et al. 2011). Modeling suggests that *Synechococcus* abundance and ranges will increase due to climate warming (Flombaum et al. 2013). The projected changes may vary geographically and may include shifts in the spatial distribution of the main picocyanobacteria, as well as changes in the proportions among *Synechococcus* sp. lineages (Six et al. 2021), potentially pushing lineages into new photic regimes. *Synechococcus* exhibits significant phenotypic diversity across lineages, encompassing strains rich in phycobiliprotein pigments, phycoerythrin (PE-rich) or phycocyanin (PC-rich) (Haverkamp et al. 2009; Aguilera et al. 2023). Phycobiliprotein pigments are pivotal for light absorption during photosynthesis and confer distinctive colours to the picocyanobacteria (Stomp et al. 2007). The disparate light preferences between PC-rich and PE-rich *Synechococcus* sp. strains influence their ecological niches. PC-rich strains thrive in environments with elevated light levels, such as surface waters and coastal regions. PE-rich strains exhibit adaptation to lower-light conditions, primarily inhabiting the deeper layers of the water column. PC-rich and PE-rich *Synechococcus* sp. strains thus predominantly occupy complementary habitats (Six et al. 2007; Haverkamp et al. 2009; Six et al. 2021), although differential responses of *Synechococcus*

91 lineages to photoperiod, have not been studied in detail, except for thermophilic PC-rich
92 *Synechococcus* PCC 6715 (Klepacz-Smółka et al. 2020).

93 Cyanobacteria growth includes lag, exponential growth, stationary, and death phases
94 (Reynolds 2006). During the lag phase, cyanobacteria acclimate to the environment and prepare
95 for active growth by synthesizing essential cellular components. Exponential growth phase is
96 marked by cell division and biomass accumulation, fueled by nutrient and light availability. If
97 growth is limited by declining nutrients, by light, or by accumulation of inhibitory factors, algae
98 enter stationary phase, characterized by a balance between cell division and death, leading to a
99 plateau in population. The death phase occurs when cyanobacteria cell death outruns division,
100 leading to net decomposition, contributing to nutrient recycling in aquatic ecosystems (Reynolds
101 2006). Moreover, Schuurmans et al. (2017) proposed an additional phase between the
102 exponential and stationary phases of picocyanobacteria growth, which is often neglected in
103 physiological studies. Herein, we examined the physiological responses of PC-rich and PE-rich
104 *Synechococcus* sp. in this phase, which we termed the pre-stationary phase of growth.

105 Picocyanobacteria are the most abundant phytoplankters in aquatic ecosystems and are
106 crucial to the optical properties of ocean water, by influencing its colour and transparency. PC-
107 rich and PE-rich *Synechococcus* sp. may have different costs and physiological strategies for
108 growth under different photic regimes, which could drive spatial and temporal variability of
109 picocyanobacteria biomass and community composition, in current and potential future aquatic
110 habitats. Therefore, our aim was to determine whether photic regimes and growth phases
111 differentially affect growth and light-capture, between representative PC-rich and PE-rich
112 *Synechococcus* sp.

113

114 **Materials and Methods**

115 **Experimental setup**

116 Two xenic PhycoCyanin(PC)-rich (CCBA_056 or CCBA_077) strains and two
117 PhycoErythrin(PE)-rich (CCBA_048 or CCBA_127) strains of *Synechococcus* were obtained
118 from the Culture Collection of Baltic Algae (CCBA; <https://ccba.ug.edu.pl/pages/en/home.php>).
119 Pre-cultures of picocyanobacteria strains were maintained in Tissue Culture Flasks (VWR
120 International, Cat. No. 10062-872, PA, USA) and were transferred to fresh f/2 media (Guillard
121 1975) at salinity of 8 PSU (which corresponds to their natural habitat) every two weeks, under a
122 photoperiod of 12 h and Photosynthetically Active Radiation (PAR) of 10 $\mu\text{mol photons m}^{-2}\text{s}^{-1}$
123 supplied from cool white fluorescent tubes, at 22°C.

124 Experimental cultures of each strain were grown in 8 x 80 mL round bottom cylindrical
125 glass tubes in a Multi-Cultivator MC 1000-OD (Photon Systems Instruments, Drásov, Czech
126 Republic). Each culture tube contained 75 mL of f/2 medium inoculated with 5 mL of growing
127 pre-culture, to achieve exponential growth from the beginning of the experiment, with little to no
128 lag phase upon inoculation. Culture tubes were inoculated in the afternoon while the
129 photoregime of a sinusoidal photoperiod commenced the following morning such that peak PAR
130 occurred at noon each day.

131 Cultures grew at 22°C, with photoperiods of 8, 12, 16, or 24 h, with peak PAR of 30, 90,
132 180, 300, 600, or 900 $\mu\text{mol photons m}^{-2}\text{s}^{-1}$ independently supplied to each culture tube from
133 white LED lamps. To approximate diel cycles, the photoperiods of 8 – 16 h were applied in a
134 sinusoidal shape, while the 24-hour photoperiod was applied continuously in a square shape.
135 The area under the sinusoidal curve is 1/2 the area under a square of equal width, therefore at

136 equivalent peak PAR the 24 h square photoperiod cultures received 4 times the diel photon doses
137 of the 12 h sinusoidal photoperiod cultures.

138 Culture tubes were closed with a silicone inert silicone stopper perforated by an aeration
139 input tube extending to the bottom of the culture tube, and a pressure outlet tube. Aeration with a
140 total air flow rate of around $\sim 140 \text{ mL min}^{-1} \text{ tube}^{-1}$ through a $0.2\mu\text{m}$ filter ensured mixing and
141 provided sufficient air/ CO_2 supply to cultures through the entire culture volume. The pH of
142 tested cultures did not fluctuate fiercely during the experiment and remained at approximately 8
143 – 9. Light, temperature, optical density, and aeration gas of the Multi-Cultivator system were
144 monitored and controlled via the Photobioreactor Control Software (Photon Systems
145 Instruments, Drásov, Czech Republic).

146

147 **DNA extractions**

148 Samples for total genomic DNA were collected by harvesting 10 mL of each culture and
149 centrifuging for 8 minutes at 8,000 x. DNA was extracted using the FastDNATM SPIN Kit for
150 Soil (MP Biomedicals) with Matrix E columns following manufacturer instructions with the
151 addition of an incubation with proteinase-K (1% final concentration) at 55°C for one hour. DNA
152 concentration was measured using an Invitrogen Qubit 2.0 fluorometer (Thermo Fisher Scientific
153 Inc.) and purity was assessed using a Thermo ScientificTM NanoDrop 2000 spectrophotometer
154 (Thermo Fisher Scientific Inc.).

155 The phylogenetic placement of CCBA strains (Fig. S1 in Supporting Information) within
156 cluster 5 picocyanobacteria was explored by amplifying and sequencing a fragment of the 16S
157 rRNA gene using universal primers 27F and 1492R (Lane 1991). 16S rRNA gene sequences
158 were aligned with MAFFT v. 7.5 using the G-INS-I algorithm (Katoh et al. 2019). Phylogenetic

159 trees were created using IQ-TREE v. 1.6.12 (Hoang et al. 2018), using GTR+F+I+R3 model
160 determined by ModelFinder (Kalyaanamoorthy et al. 2017). Bootstrap values were calculated
161 with 1000 replicates (Hoang et al. 2018).

162

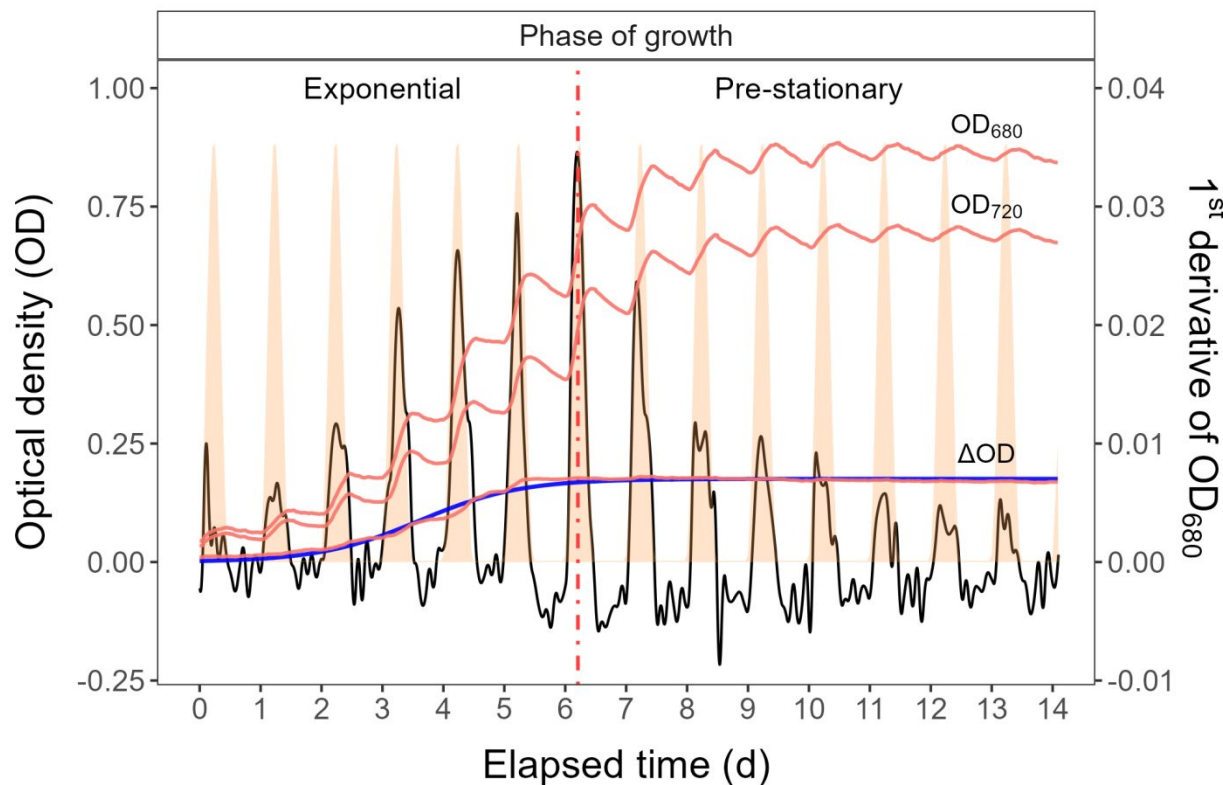
163 **Growth curves and chlorophyll-specific exponential growth rates**

164 Picocyanobacterial growth was monitored every 5 minutes by automatically recording
165 OD₆₈₀, OD₇₂₀, and ΔOD ($\Delta\text{OD} = \text{OD}_{680} - \text{OD}_{720}$) for 14 days, independently for each culture
166 tube. The exceptions were experiments conducted with a photoperiod of 24 h and light of 600 or
167 900 $\mu\text{mol photons m}^{-2}\text{s}^{-1}$, which lasted 7 days (Fig. S2). The chlorophyll-specific exponential
168 growth rates (μ) were determined by fitting logistic growth curves using a modified Levenberg-
169 Marquardt fitting algorithm (Elzhov et al. 2023) to plots of the chlorophyll *a* proxy of ΔOD
170 vs. elapsed time for each combination of strain, photoperiod, and peak PAR (Fig. S3).

171 To summarize the growth responses of the four picocyanobacterial strains we used a
172 Generalized Additive Model (GAM) (Wood 2017) was applied to the relation of chlorophyll-
173 specific μ , d^{-1} to photoperiod and PAR level. The R package *mgcv* (Wood 2017) was used to
174 model the growth rate with smoothing terms and indicate the 90, 50 and 10% quantiles for
175 growth rate across the levels of factors. Only growth rate estimates for which the amplitude of
176 standard error was smaller than 50% of the fitted growth rate were included in the GAM. We
177 visually compared the GAM contours to isolines of equal cumulative diel PAR ($\mu\text{mol photons}$
178 $\text{m}^{-2}\text{d}^{-1}$).

179 The 1st derivative of OD₆₈₀ taken over 1 h increments was computed using *xts*: eXtensible
180 Time Series (Ryan et al. 2024) and *signal*: Signal Processing (Ligges et al. 2024) R packages.
181 The time when the cultures reached their maximum absolute hourly growth (tMaxAHG) of the

182 1st derivative of OD₆₈₀ was taken as the time of transition from exponential to pre-stationary
 183 growth phases (Fig. 1).



184

185 **Fig. 1.** Example of a growth curve (tracked as OD₇₂₀, OD₆₈₀, or ΔOD; red solid lines, left y-axis) of PE-rich culture
 186 of *Synechococcus* sp. (048) vs. elapsed time (d, x-axis). 1st derivative of OD₆₈₀ taken over 1 h increments (black
 187 solid line, right y-axis); solid blue line shows logistic fits of chlorophyll proxy OD₆₈₀ – OD₇₂₀ (ΔOD) vs. elapsed
 188 time. The vertical red dot dash line represents the time when the culture reached the maximum of the 1st derivative
 189 of OD₆₈₀, or maximum absolute hourly growth (tMaxAHG), taken as the time of transition from exponential to pre-
 190 stationary growth phases.

191

192 Whole-cell absorbance spectra

193 Absorbance measurements on intact cells in suspension were conducted in an integrating
 194 cavity upgrade spectrophotometer (CLARiT^Y 17 UV/Vis/NIR, On-Line Instrument Systems,
 195 Inc., Bogart, GA, USA). 8 mL of f/2 medium were added to both the sample and reference

196 observation cavities of the spectrophotometer. After recording a baseline from 375 to 710 nm, 1
197 mL was withdrawn from the sample cavity and replaced with 1 mL of picocyanobacteria cell
198 suspension. The pathlength corrected absorbance per cm was performed by determining the
199 Javorfi coefficients (Javorfi et al. 2006) as described in the equipment manual.

200

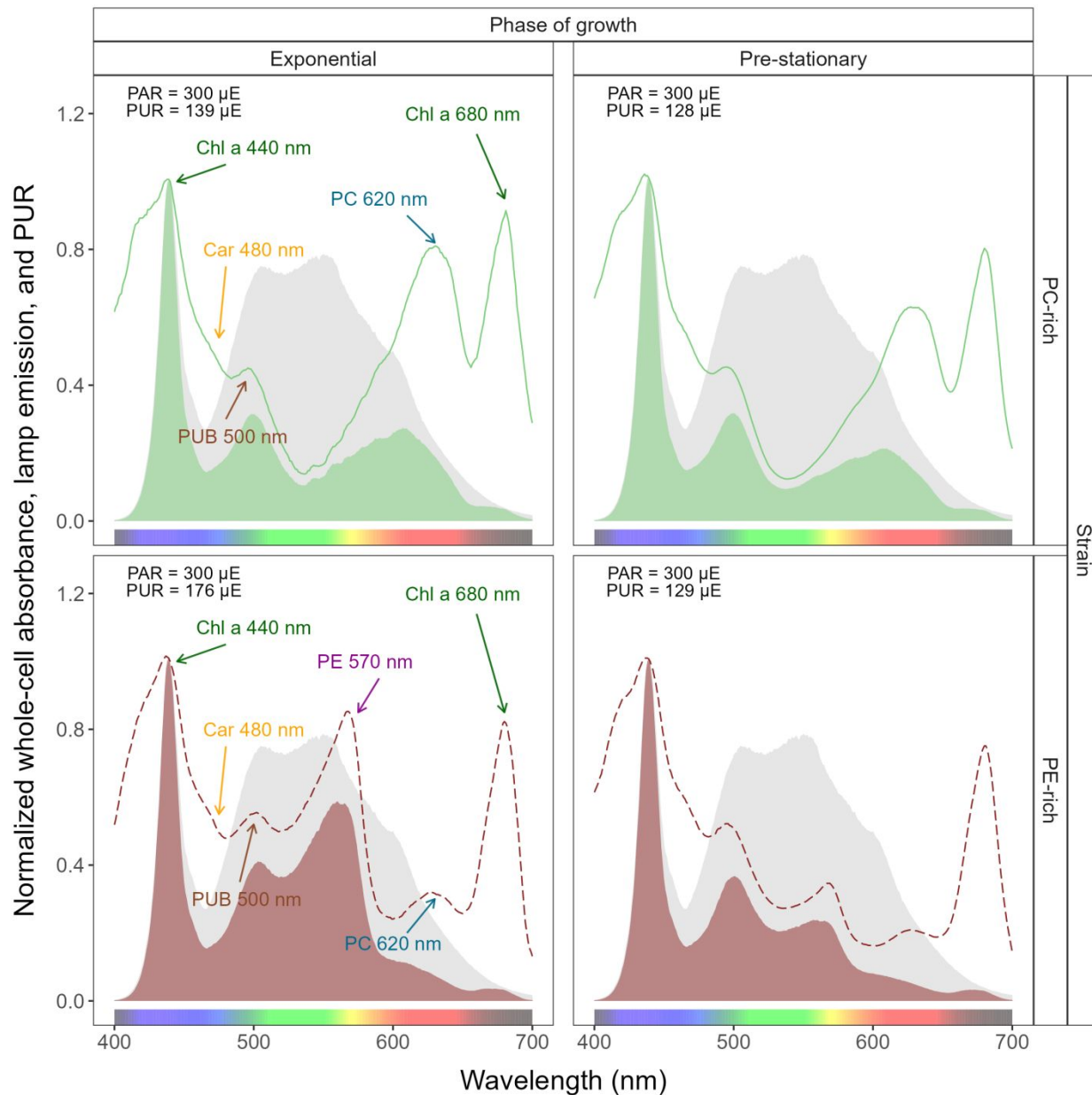
201 Photosynthetically Usable Radiation (PUR)

202 Using whole-cell absorbance spectra of *Synechococcus* sp. cultures (Fig. 2, we estimated
203 Photosynthetically Usable Radiation (PUR; $\mu E = \mu\text{mol photons m}^{-2}\text{s}^{-1}$) according to (Morel
204 1978). We normalized the obtained whole-cell Absorbances (A) and the Emission spectra of the
205 white LED lamps (Em) from 400 nm to 700 nm to a reference wavelength of 440 nm. PUR is
206 then the ratio of the sum of Absorbance Normalized to 440 nm (NormA₄₄₀) multiplied by the
207 sum of Emission spectra Normalized to 440 nm (NormEm₄₄₀) to the sum of the Emission spectra
208 Normalized to 440 nm (NormEm₄₄₀), multiplied by the PAR (Eq. (1)).

209

$$PUR (\mu E) = \frac{\sum(NormA_{440} \times NormEm_{440})}{\sum(NormEm_{440})} \times PAR (\mu E) \quad (1)$$

210



211

212 **Fig. 2.** Whole-cell absorbance spectra of PC-rich (solid green lines) or PE-rich (dashed red lines) cultures of
 213 *Synechococcus* sp. Representative absorbance spectra, normalized to 440 nm (NormA_{440}), were measured from the
 214 exponential or pre-stationary phases of growth, together with emission spectra of the white LED lamp used for PAR,
 215 normalized to emission at 440 nm (NormEm_{440} , light gray area), in this example PAR was $300 \mu\text{mol photons m}^{-2}\text{s}^{-1}$.
 216 Estimated Photosynthetically Usable Radiation (PUR) is shown as a darker green area for the PC-rich strain and a
 217 darker red area for the PE-rich strain, with PUR given for each culture ($\mu\text{E} = \mu\text{mol photons m}^{-2}\text{s}^{-1}$). Peaks

218 characteristic of known pigments are labeled; Chl *a*, chlorophyll *a*; PC, phycocyanin; PE, phycoerythrin; PUB,
219 phycobilin; Car, carotenoids.

220

221 Cumulative diel PAR and PUR

222 Based on the length and shape of the photoperiod (sinusoidal wave for photoperiods of 8,
223 12, 16 h; square for photoperiod of 24 h) and the peak PAR ($\mu\text{E} = \mu\text{mol photons m}^{-2}\text{s}^{-1}$), we
224 estimated the value of the cumulative diel PAR ($\mu\text{mol photons m}^{-2}\text{d}^{-1}$). For sinusoidal
225 photoperiods we used Eq. (2); for the continuous 24 h photoperiod we used Eq. (3). Cumulative
226 diel PUR was estimated similarly after estimation of peak PUR from peak PAR.

$$227 \frac{\text{Cumulative diel PAR } (\mu\text{mol photons m}^{-2} \text{ d}^{-1})}{\text{PAR } (\mu\text{E}) \times 60 \text{ (s min}^{-1}\text{)} \times 60 \text{ (min h}^{-1}\text{)} \times \text{photoperiod (h d}^{-1}\text{)}}{2} \quad (2)$$

$$228 \frac{\text{Cumulative diel PAR } (\mu\text{mol photons m}^{-2} \text{ d}^{-1})}{\text{PAR } (\mu\text{E}) \times 60 \text{ (s min}^{-1}\text{)} \times 60 \text{ (min h}^{-1}\text{)} \times \text{photoperiod (h d}^{-1}\text{)}} \quad (3)$$

229

230 Pigment content

231 Chlorophyll *a* (Chl *a*) ($\mu\text{g mL}^{-1}$) was measured using Trilogy Laboratory Fluorometer
232 (Turner Designs, Inc., CA, USA) equipped with Chlorophyll In-Vivo Module, previously
233 calibrated using 20 mL ampoules with known Chl *a* concentrations in 3:2 90% acetone:DMSO
234 solution. Quantitative analysis of Chl *a* was obtained after adding 50 μL of culture and 2 mL of a
235 90% acetone:DMSO solution in a 3:2 ratio.

236 We also estimated the pigment content ($\mu\text{g mL}^{-1}$): chlorophyll *a* (Chl *a*), carotenoids (Car),
237 phycoerythrin (PE), phycocyanin (PC), and allophycocyanin (APC) in *Synechococcus* sp.
238 cultures over time using previously determined linear correlations between pigment content
239 obtained by extraction (Strickland and Parsons 1972; Bennett and Bogorad 1973) and absorbance

240 values of individual pigment peaks (Car; 480, PE; 565, PC; 620, APC; 650, and Chl *a*; 665 nm)
241 obtained from the whole-cell absorbance spectra using integrating cavity upgrade
242 spectrophotometer (CLARiT^Y 17 UV/Vis/NIR, On-Line Instrument Systems, Inc., Bogart, GA,
243 USA) (Tab. S1 in Supporting Information). The sum of phycobiliproteins (PE, PC, APC protein)
244 to Chl *a* ratio ($\mu\text{g}:\mu\text{g}$) for individual strains was also calculated.

245

246 **PSII effective absorption cross section of PSII and electron flux**

247 We harvested 2 mL of cultures for photophysiological characterizations repeatedly across
248 the growth trajectories. We used Fast Repetition Rate fluorometry (Kolber et al. 1998) (FRRf,
249 Solisense, USA), with a lab built temperature control jacket (22°C), to apply series of flashlets to
250 drive saturation induction/relaxation trajectories, fit using the onboard Solisense LIFT software
251 (Falkowski and Kolber 1993; Kolber et al. 1998). From the model fits we took the initial
252 fluorescence before induction (F_0 , F_0' , or F_S , depending upon the level of actinic light and step
253 in the light response curve); the maximum fluorescence (F_M or F_M') once Photosystem II (PSII)
254 was driven to closure; and the effective absorption cross section for PSII photochemistry (σ_{PSII} or
255 σ_{PSII}' ; $\text{nm}^2 \text{ quanta}^{-1}$) (Tortell and Suggett 2021). We used a double tap protocol (Xu et al. 2017),
256 where FRRf induction/relaxation trajectories were collected during a rapid light curve sequence
257 increasing in steps of 10 s at 0, 20, 40, 80, 160, and 320 $\mu\text{mol photons m}^{-2}\text{s}^{-1}$ PAR, delivered
258 from LED emitters centred at 445, preferentially exciting chlorophyll, or 590 nm, preferentially
259 exciting phycobiliproteins. Flash Power for 445 nm excitation was 60000 $\mu\text{mol photons m}^{-2}\text{s}^{-1}$
260 PAR, while for 590 nm excitation power was 14000 $\mu\text{mol photons m}^{-2}\text{s}^{-1}$, calibrated using a
261 quantum sensor (LI-250, LI-COR, Inc.). We applied 1 s darkness between sequential light steps,

262 to allow re-opening of PSII. FRRf excitation flashlets were applied at the same wavebands, 445
263 or 590 nm, as the actinic light steps.

264 We calculated (Eq. (4)) an uncalibrated fluorescence based estimator for volumetric
265 electron transport, JV_{PSII} , ($\text{km} \times \text{e}^- \text{ L}^{-1} \text{ s}^{-1}$) under both 445 and 590 nm excitation bands
266 (Oxborough et al. 2012; Boatman et al. 2019; Tortell and Suggett 2021).

267

$$JV_{PSII} = \frac{\sigma_{PSII}' \times qP \times I \times F_O}{\sigma_{PSII}} \quad (4)$$

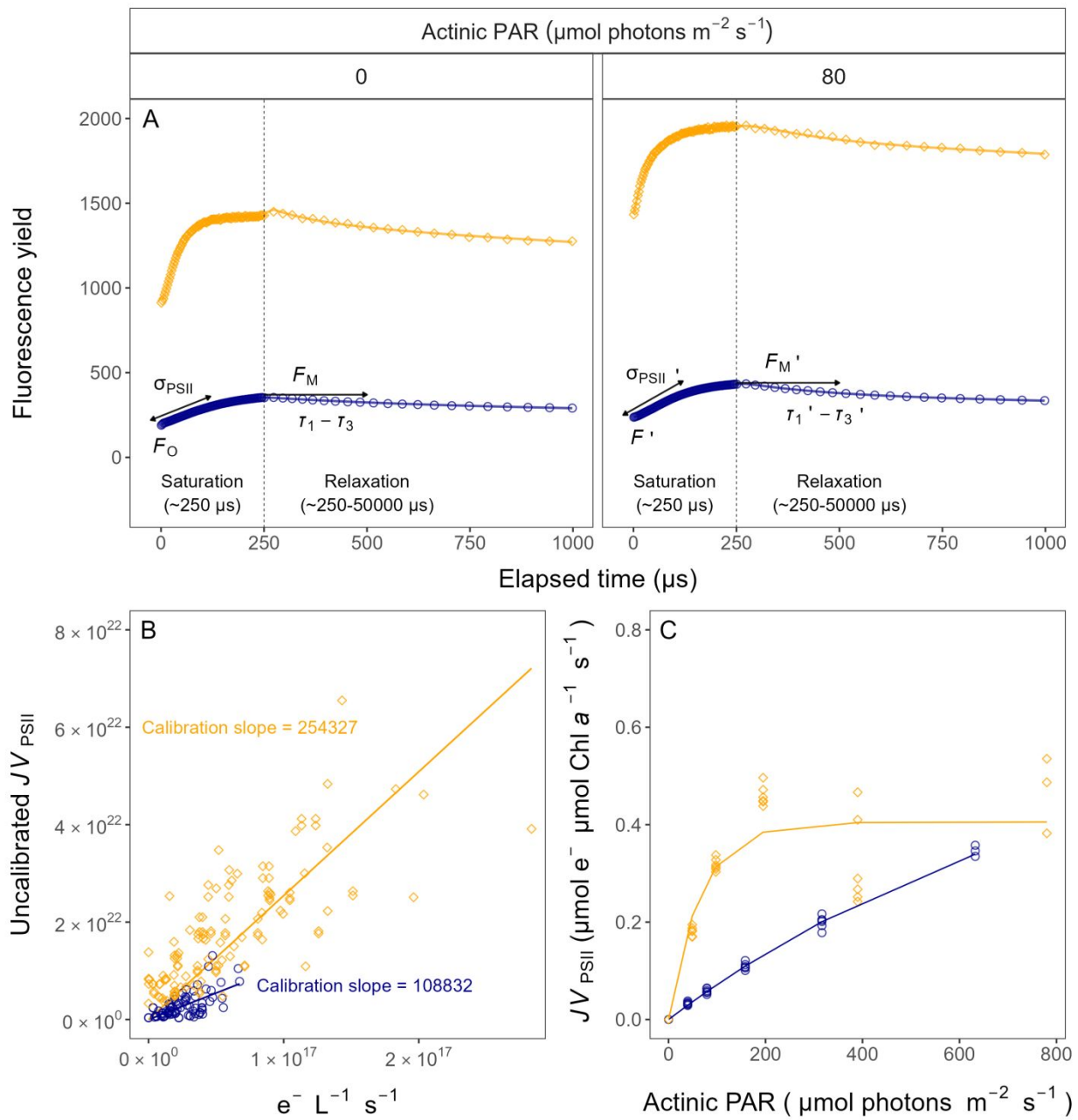
268 where σ_{PSII}' is effective absorption cross section for PSII photochemistry under the relevant
269 actinic PAR step ($\text{nm}^2 \text{ quanta}^{-1}$); qP is an estimate of the fraction of PSII open for
270 photochemistry estimated according to Oxborough and Baker (1997); I is the applied PAR (μmol
271 photons $\text{m}^{-2}\text{s}^{-1}$); F_O is the minimum fluorescence from a given sample and excitation bandwidth
272 (relative fluorescence) and σ_{PSII} is the maximum effective absorption cross section for PSII
273 photochemistry from a given sample and excitation bandwidth ($\text{nm}^2 \text{ quanta}^{-1}$). We compared
274 several other algorithms for JV_{PSII} (Tortell and Suggett 2021) and found similar results.

275 We calibrated the JV_{PSII} estimator to absolute rates of electron transport (Eq. (5)) using
276 parallel measures of oxygen evolution ($\mu\text{mol O}_2 \text{ L}^{-1} \text{ s}^{-1}$), captured simultaneously with the FRRf
277 measures, below light saturation of electron transport, using a FireSting robust oxygen probe
278 (PyroScience, Germany) inserted in the cuvette for select Rapid Light Curve (RLC) runs (Fig. 3).
279 For the blue LED ($\text{Ex}_{445\text{nm}}$) excitation we used a calibration slope of 108832, while for orange
280 LED ($\text{Ex}_{590\text{nm}}$) excitation we used a calibration slope of 254327

281

$$JV_{PSII}(\text{e}^- \text{ L}^{-1} \text{ s}^{-1}) = \frac{\text{Uncalibrated } JV_{PSII}(\text{e}^- \text{ L}^{-1} \text{ s}^{-1})}{\text{Calibration slope}} \quad (5)$$

282



283

284 **Fig. 3.** Single turnover (ST) fluorescence induction by Fast Repetition Rate fluorometry (FRRf). (A) Examples of
 285 fluorescence yield vs. elapsed time (μs) for PE-rich culture of *Synechococcus* sp. (048) in the dark (dark-relaxed; 0
 286 $\mu\text{mol photons m}^{-2}\text{s}^{-1}$) and under actinic PAR (in this example $80 \mu\text{mol photons m}^{-2}\text{s}^{-1}$) using blue LED (Ex_{445nm};
 287 open blue circles) or orange (Ex_{590nm}; open orange diamonds) excitation. The ST technique delivers a series of
 288 flashlets for non-intrusive, repeated monitoring of chlorophyll fluorescence parameters (including F_O , F' , F_M , F'_M ,
 289 $\tau_1 - \tau_3$, $\tau'_1 - \tau'_3$, σ_{PSII} , and σ_{PSII}'). (B) Linear regressions of uncalibrated PSII electron flux (JV_{PSII}) vs. $e^- L^{-1} s^{-1}$ derived

290 from simultaneously measured oxygen evolution Light Response Curves (LRC) under blue LED ($\text{Ex}_{445\text{nm}}$; open blue
291 circles) or orange ($\text{Ex}_{590\text{nm}}$; open orange diamonds) excitation. (C) Rapid Light Curve (RLC), fit with a three
292 parameter model (Harrison and Platt 1986), for PSII electron flux (JV_{PSII} ; $\mu\text{mol e}^{-} \mu\text{mol Chl } a^{-1} s^{-1}$) vs. actinic PAR
293 measured under blue LED ($\text{Ex}_{445\text{nm}}$; open blue circles) or orange ($\text{Ex}_{590\text{nm}}$; open orange diamonds) excitation.
294

295 Statistical analysis

296 We used R version 4.3.0 (R Core Team 2023) running under RStudio (Posit team 2022).
297 We performed three-way factorial ANOVA (*aov()* function; R Base package) to determine
298 whether peak PAR, photoperiod, strain, and their interactions, significantly influence the
299 chlorophyll-specific exponential growth rate (μ ; d^{-1}), estimated from logistic fits (*nlsLM()*
300 function; Elzhov et al. (2023)) of chlorophyll proxy $OD_{680} - OD_{720}$ vs. cumulative diel PUR
301 (Table S2). We also used the *nlsLM()* function to fit a three parameter light response model
302 (Harrison and Platt 1986) of growth rates (α , initial slope of curve; β , reflecting the
303 photoinhibition process; P_{max} , the maximum rate of growth curve).

304 To examine statistical differences between fits of light responses, we performed one-way
305 ANOVA (*aov()* function) of the three parameter model (Harrison and Platt 1986) fit to pooled
306 data for each taxa, compared to separate fits for each different photoperiod (8, 12, 16, or 24); or
307 to separate fits for each different peak PAR (30, 90, 180, 300, 600 together with 900). These
308 comparisons were run for chlorophyll-specific exponential growth rate vs. cumulative diel PUR
309 (Table S3, S4); vs. cumulative diel PAR (Table S5, S6) or vs. PSII electron flux (JV_{PSII} ; $\mu\text{mol e}^{-}$
310 $\mu\text{mol Chl } a^{-1} d^{-1}$; Table S7, S8). One-way ANOVA was also used to examine statistical
311 differences between single phase exponential decay fits (*SSasymp()* function; Serway et al.
312 (2004)) of pooled data across different strains for a given phase of growth and across different
313 phase of growth for a given strain for PUR/PAR ratio (Table S9); Phycobiliprotein to Chl a ratio

314 (Table S10); or effective absorption cross section of PSII (σ_{PSII}' ; nm² quanta⁻¹) measured under
315 diel peak PAR growth light under Ex_{590nm} (orange) excitation in relation to the cumulative diel
316 PAR ($\mu\text{mol photons m}^{-2}\text{d}^{-1}$) (Table S11).

317 We used *t*-tests (*t.test()* function; R Base package) of linear fits (*lm()* function) to compare
318 pooled data across different strains for a given phase of growth, and across different phases of
319 growth, for a given strain, for effective absorption cross section of PSII (σ_{PSII}' ; nm² quanta⁻¹)
320 measured under diel peak PAR growth light under Ex_{445nm} (blue) excitation vs. the cumulative
321 diel PAR ($\mu\text{mol photons m}^{-2}\text{d}^{-1}$; Table S12); or vs. the Phycobiliprotein to Chl *a* ratio (Table
322 S13). The same *t*-test analyses were performed for effective absorption cross section of PSII
323 (σ_{PSII}' or σ_{PSII} ; nm² quanta⁻¹) measured under Ex_{590nm} (orange) excitation vs. the Phycobiliprotein
324 to Chl *a* ratio (Table S14, S15).

325 Statistical differences for all analyses were determined at significance level $\alpha = 0.05$. The
326 manuscript was prepared as a Rmarkdown document (Handel 2020) with figures plotted using
327 ggplot2 (Wickham 2016) and patchwork (Pedersen 2024) packages. All metadata, data and code
328 is available on GitHub (<https://github.com/FundyPhytoPhys/BalticPhotoperiod>).

329

330 **Results**

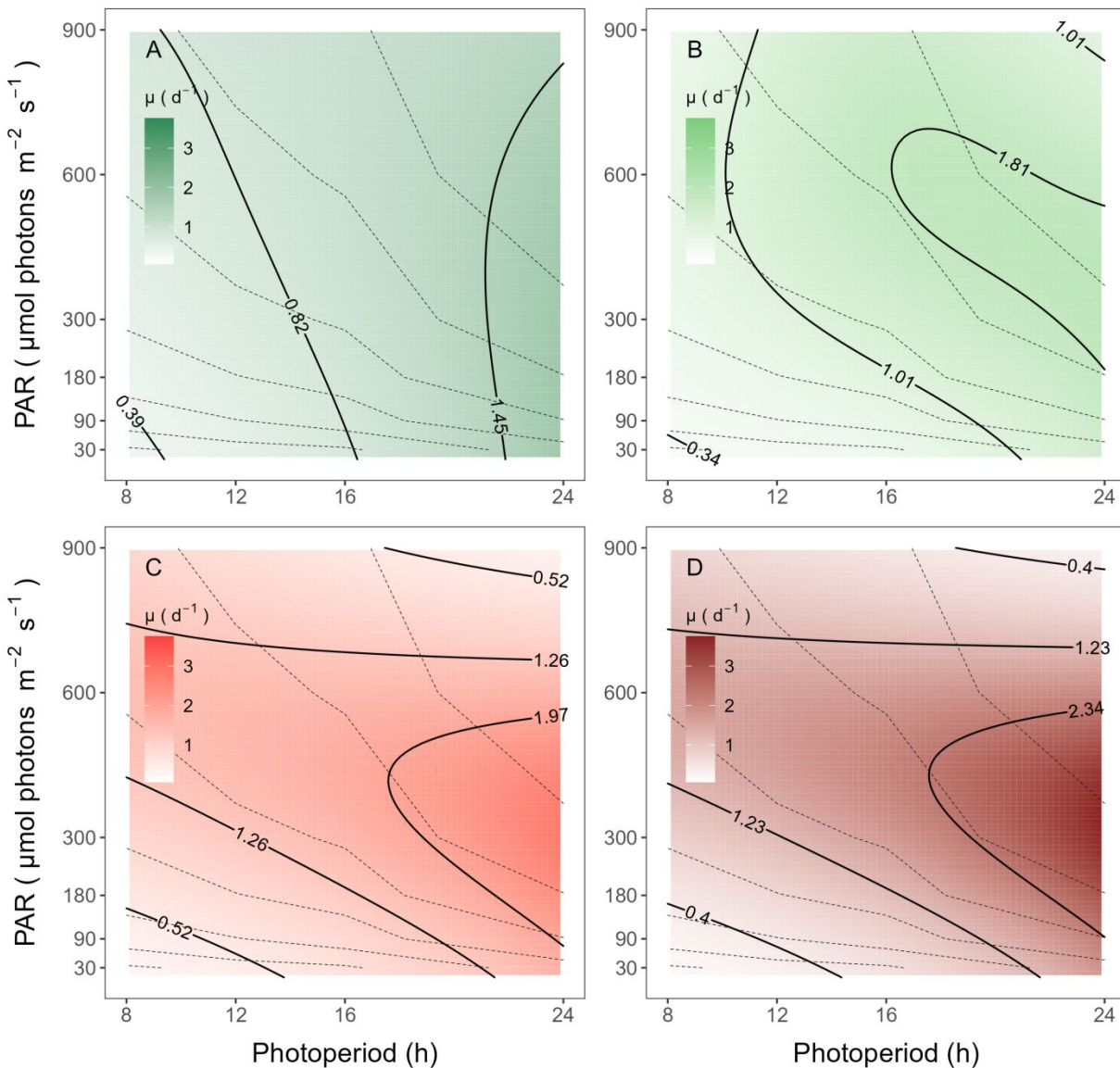
331 **Chlorophyll-specific exponential growth rate**

332 We used logistic curve fits (Fig. S3B) to determine chlorophyll-specific exponential
333 growth rates (μ ; d⁻¹), for two PhycoCyanin(PC)-rich cultures (056, 077) and two
334 PhycoErythrin(PE)-rich cultures (048, 127) of *Synechococcus* sp. grown at 30, 90, 180, 300, 600,
335 or 900 peak PAR $\mu\text{mol photons m}^{-2}\text{s}^{-1}$ (μE); and photoperiods of 8, 12, 16, or 24 h. Three-way
336 factorial ANOVA showed that peak PAR, photoperiod, strain, and their interactions,

337 significantly affected μ (ANOVA, $p < 0.05$ for all; Table S2). All tested strains, except PE-
338 rich_048, grew even under peak PAR 900 $\mu\text{mol photons m}^{-2}\text{s}^{-1}$ and 24 h photoperiod. The
339 highest growth rate was recorded for *Synechococcus* sp. PE-rich_127 ($\mu = 4.5 \text{ d}^{-1}$; 3.7 h doubling
340 time) and PC-rich_056 ($\mu = 3.4 \text{ d}^{-1}$; 4.9 h doubling time) at 180 $\mu\text{mol photons m}^{-2}\text{s}^{-1}$ peak PAR
341 and photoperiod of 24 h.

342 The GAM model in Fig. 4 summarizes the growth responses of the PC-rich and PE-rich
343 picocyanobacteria to peak PAR and photoperiod. PC-rich_056 *Synechococcus* sp. showed
344 highest growth rates under a photoperiod of 24 h, across a wide range of peak PAR indicated by
345 the contour line labeled 1.45 d^{-1} , representing the 90th percentile of achieved growth rates for the
346 strain. On the other hand, the other tested PC-rich strain (077) showed highest growth rates in the
347 range of photoperiod 16-24 h and peak PAR between 300 – 700 $\mu\text{mol photons m}^{-2}\text{s}^{-1}$, indicated
348 by the 1.81 d^{-1} contour line again representing the 90th percentile of maximum achieved growth
349 rates for the strain. For both PC-rich strains, growth was slowest under 30 $\mu\text{mol photons m}^{-2}\text{s}^{-1}$
350 and a photoperiod of 8 h.

351 Both PE-rich strains achieved fastest growth rates above peak PAR of ~300 $\mu\text{mol photons}$
352 $\text{m}^{-2}\text{s}^{-1}$, under the longest photoperiod of 24 h, indicated by the 1.97 d^{-1} for PE-rich_048, and
353 2.34 d^{-1} for PE-rich_127, contour lines. For the PE-rich strains growth decreased with decreasing
354 photoperiod and decreasing peak PAR. Moreover, PE-rich strains showed photoinhibition of
355 growth at peak PAR of 900 $\mu\text{mol photons m}^{-2}\text{s}^{-1}$ and photoperiods of 16- 24 h. The growth rate
356 contours for PC-rich and PE-rich *Synechococcus* sp. did not generally follow isoclines of
357 cumulative diel photon dose ($\mu\text{mol photons m}^{-2}\text{d}^{-1}$, dashed lines), showing that photoperiod, and
358 peak PAR influenced growth rates beyond cumulative diel photon dose.



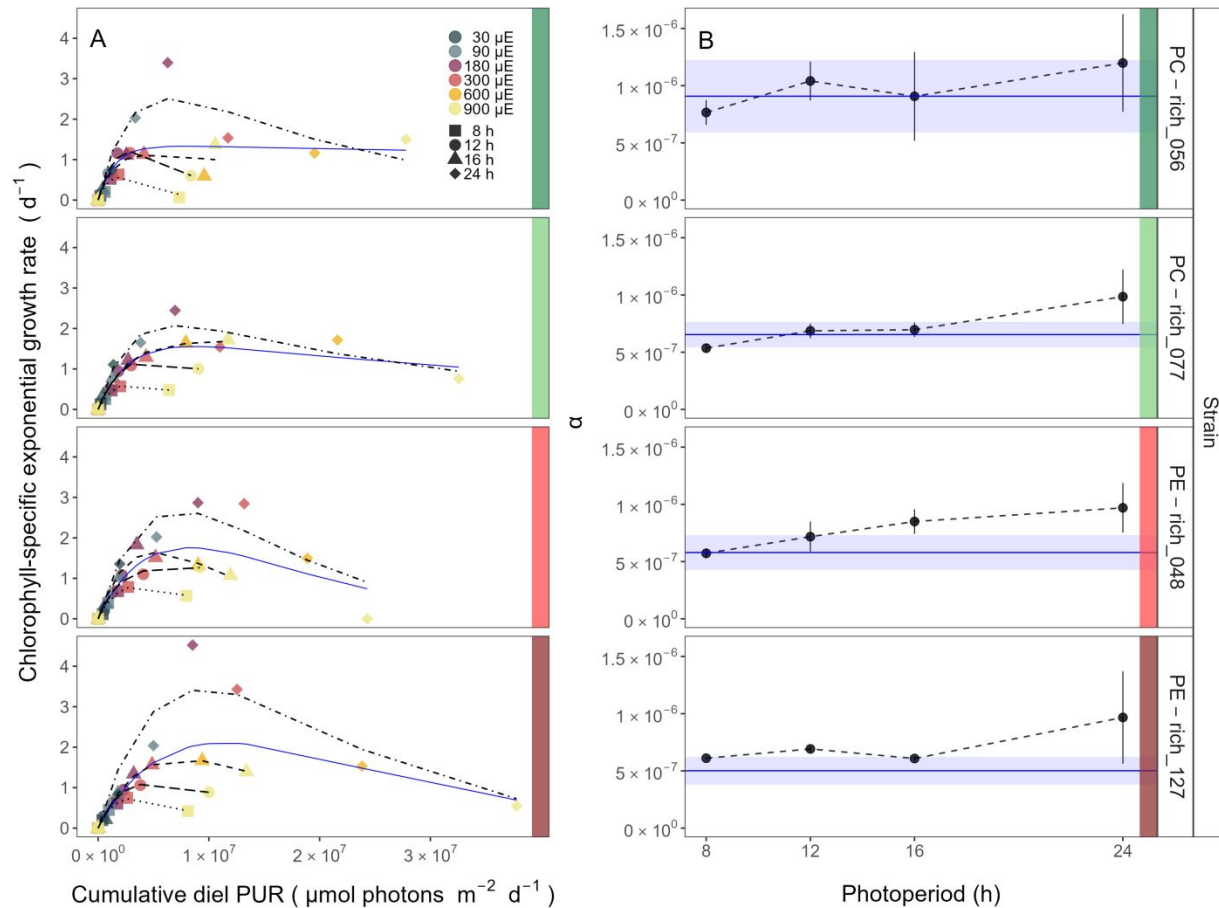
359

360 **Fig. 4.** A contour plot of a Generalized Additive Model (GAM) of chlorophyll-specific growth rates (d^{-1}) for two
 361 PC-rich cultures: **(A)** 056, **(B)** 077 and two PE-rich cultures: **(C)** 048, **(D)** 127 of *Synechococcus* sp. grown at 30, 90,
 362 180, 300, 600, or 900 peak PAR $\mu\text{mol photons m}^{-2}\text{s}^{-1}$; and photoperiods of 8, 12, 16, or 24 h. Legends show colour
 363 gradients of growth rate (μ ; d^{-1}) from no growth (white) to 3.0 d^{-1} (dark green for PC-rich_056, light green for PC-
 364 rich_077, light red for PE-rich_048 or dark red for PE-rich_127 strains). Labeled contour lines indicate the 90%,
 365 50%, and 10% quantiles for achieved growth rate. Dotted lines show isoclines of cumulative diel photon dose (μmol
 366 $\text{photons m}^{-2} d^{-1}$).

367

368 A three parameter light response model fit (Harrison and Platt 1986) of chlorophyll-
369 specific exponential growth rates vs. cumulative diel PUR dose for two PC-rich and two PE-rich
370 cultures of *Synechococcus* sp. showed significant differences between model fits of the pooled
371 data vs. fits for all tested photoperiods (8, 12, 16, or 24 h; ANOVA, $p < 0.05$; Fig. 5A, Table S3).
372 The alpha parameters of the initial rise of growth rate (α) vs. cumulative diel PUR, estimated
373 from data pooled for each photoperiod increased with increasing photoperiod for all strains. The
374 highest increase (>2-fold) of α with increasing photoperiod was recorded for PC-rich_056 (Fig.
375 5B). Strains also showed distinct growth rate responses to cumulative diel PUR, depending upon
376 peak PAR (Fig. S4A, Table S4), that differ from a single light response model fit to the pooled
377 data across all peak PAR from a strain. Exceptions were observed in the strains PC-rich_077 and
378 PE-rich_048 with the peak PAR of 600 or 900 $\mu\text{mol photons m}^{-2}\text{s}^{-1}$, which were not
379 significantly different from the pooled data model. A caveat to these findings is that cumulative
380 diel photon dose is a product of photoperiod and PAR, so the highest levels of cumulative PUR
381 dose are only achieved under the 600 or 900 $\mu\text{mol photons m}^{-2}\text{s}^{-1}$. The alpha parameters of the
382 initial rise of growth rate (α) vs. cumulative diel PUR, estimated from data pooled for each peak
383 PAR decreased across peak PAR for all tested strains (Fig. S4B).

384 Growth rate saturated under increasing cumulative diel PUR for all strains, however, the
385 achieved estimates of μ_{\max} varied depending upon photoperiod and peak diel PAR. Growth rates
386 vs. cumulative diel PAR relationships, estimated for exponential phase cultures, followed similar
387 patterns (Fig. S5, Fig. S6 and Table S5, S6 in Supporting Information).



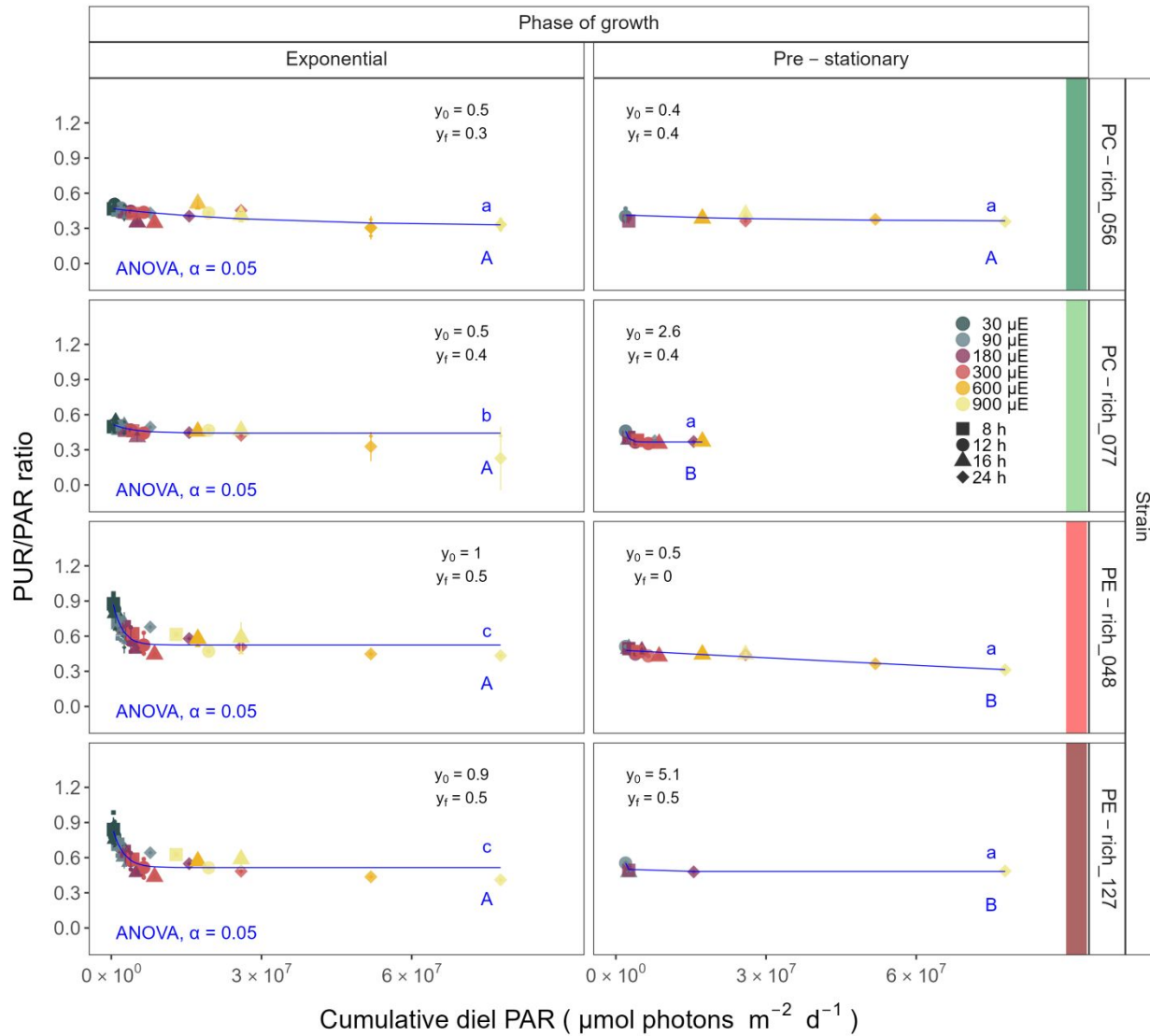
388

389 **Fig. 5.** (A) Chlorophyll-specific exponential growth rates (d^{-1}) vs. cumulative diel Photosynthetically Usable
 390 Radiation (PUR, $\mu\text{mol photons m}^{-2}\text{d}^{-1}$). Growth rates (\pm SE falling within symbols) were estimated from logistic fits
 391 of chlorophyll proxy $\text{OD}_{680} - \text{OD}_{720}$ (ΔOD) vs. elapsed time (Fig. 1, Fig. S3B), for two PC-rich cultures (056; dark
 392 green, 077; light green) and two PE-rich cultures (048; light red, 127; dark red) of *Synechococcus* sp. grown at 30
 393 (μE), 90 (light gray), 180 (purple), 300 (red), 600 (orange), or 900 (yellow) peak PAR $\mu\text{mol photons m}^{-2}\text{s}^{-1}$
 394 (μE); and photoperiods of 8 (square), 12 (circle), 16 (triangle), or 24 (diamond) h. Solid blue line shows a fit of the
 395 pooled growth rates through photoperiods for each strain, with a three parameter model (Harrison and Platt 1986).
 396 We also fit the same model separately for 8 (dotted line), 12 (long dash line), 16 (dashed line), or 24 (two dash line)
 397 h photoperiods, since for all strains they were each significantly different (ANOVA, $p < 0.05$) from the fit of pooled
 398 data. (B) Alpha parameters of the initial rise of growth rate (α) vs. cumulative diel Photosynthetically Usable
 399 Radiation (PUR), estimated from data pooled for each photoperiod (points (\pm SE) connected by dashed lines), and
 400 estimated for all data across photoperiods (solid blue horizontal line \pm SE), for each strain.

401

402 **PUR/PAR ratio vs. cumulative diel PAR**

403 The PUR/PAR ratio is an index of the efficacy of light capture for a culture under a given
404 growth condition; showing the fraction of PAR that can be captured by the absorbance of the
405 cells (Fig. 6). For the two PC-rich and, particularly, for the two PE-rich cultures of
406 *Synechococcus* sp. PUR/PAR decayed exponentially to a plateau, with increasing cumulative
407 diel PAR, when pooling PUR/PAR data across different combinations of photoperiod and peak
408 PAR. Although all strains followed a similar trend, the single phase exponential decay model fit
409 parameters varied significantly among strains, during their exponential phase of growth
410 (ANOVA, $p < 0.05$), except the model fits from PE-rich_048 and PE-rich_127 (ANOVA, $p >$
411 0.05; Table S9). Moreover, the PUR/PAR ratio was higher in the PE-rich strains under low
412 cumulative diel photon dose during their exponential phase of growth (y_0 greater or equal to 0.9),
413 but decayed towards a plateau close to the PC-rich strains as cumulative diel photon dose
414 increases ($y_f = 0.5$). On the other hand, the single phase exponential decay model fits did not
415 differ significantly among strains, during their pre-stationary phase of growth (ANOVA, $p >$
416 0.05; Table S9). During this phase, response of PUR/PAR ratio to increasing cumulative diel
417 PAR exhibits damping, maintaining a consistent trend across all strains within the y_f range of 0.4
418 to 0.5, with the exception of the PE-rich_048 strain. We also find that model fits from different
419 phases of growth differed within a given strain, with the exception of PC-rich_056 (ANOVA; p
420 < 0.05 , Table S9). A similar decay trend was observed for Phycobiliprotein to Chl *a* ratio
421 ($\mu\text{g}:\mu\text{g}$) across cumulative diel PAR (Fig. S7).



422

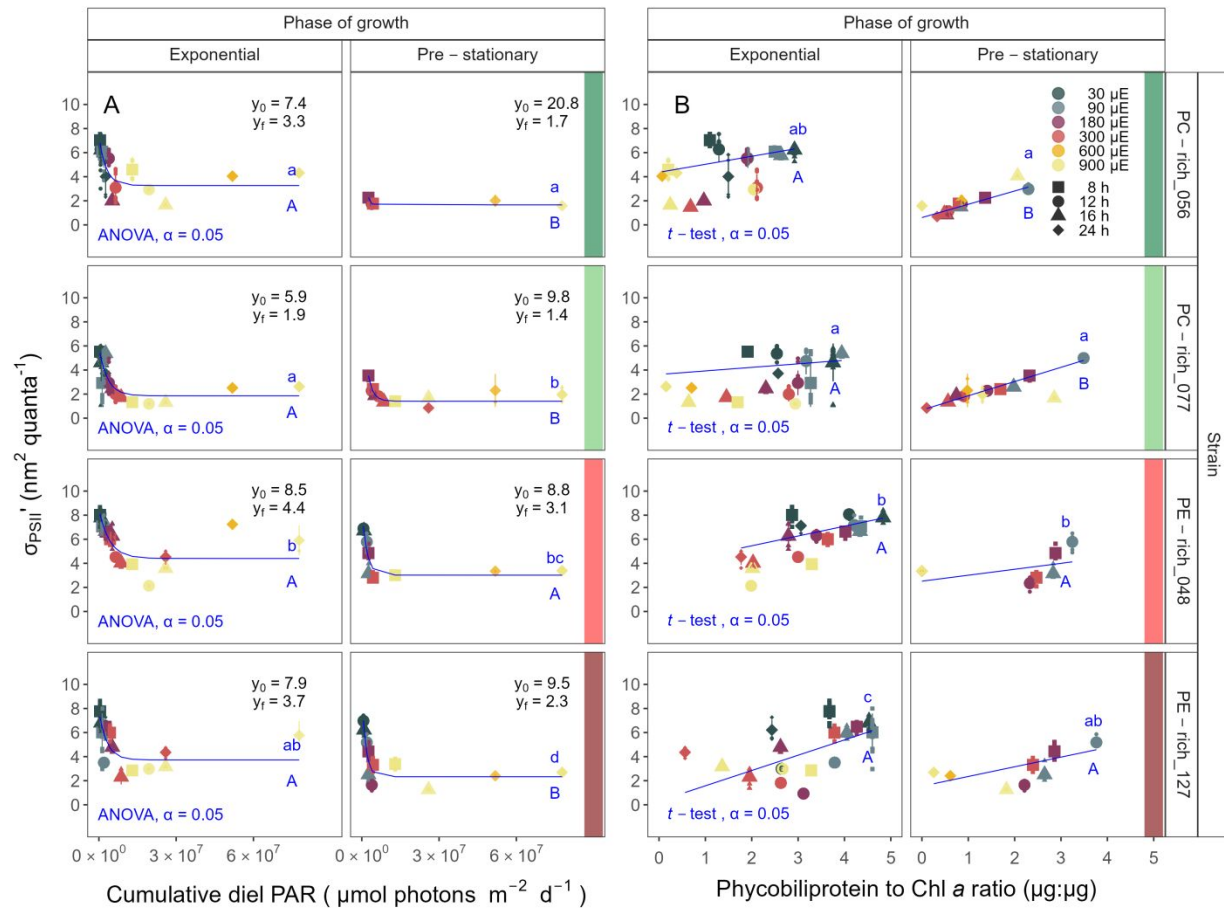
423 **Fig. 6.** Changes in PUR/PAR ratio vs. cumulative diel PAR ($\mu\text{mol photons m}^{-2} \text{d}^{-1}$). PUR/PAR ratio was estimated
 424 for two PC-rich cultures (056; dark green, 077; light green) and two PE-rich cultures (048; light red, 127; dark red)
 425 of *Synechococcus* sp. grown at 30 (dark gray), 90 (light gray), 180 (purple), 300 (red), 600 (orange), or 900 (yellow)
 426 peak PAR $\mu\text{mol photons m}^{-2} \text{s}^{-1}$ (μE); and photoperiods of 8 (square), 12 (circle), 16 (triangle), or 24 (diamond) h.
 427 Figure presents data (smaller symbols) and means (bigger symbols) from exponential or pre-stationary phase of
 428 growth. Blue solid line shows single phase exponential decay fit for data from each strain and growth phase, with fit
 429 parameters presented. Different lowercase letters indicate statistically significant differences between the fit models
 430 for different strains within a given phase of growth. Different uppercase letters indicate statistically significant
 431 differences between the fit models for different phases of growth within a given strain (ANOVA; $p < 0.05$).

432

433 **Effective absorption cross section of PSII of picocyanobacteria**

434 The effective absorption cross section of PSII (σ_{PSII}' , $\text{nm}^2 \text{ quanta}^{-1}$), was estimated using
435 FRRf induction curves using $\text{Ex}_{590\text{nm}}$ (orange) excitation, for two PC-rich (056, 077) and two PE-
436 rich (048, 127) cultures of *Synechococcus* sp. grown at 30, 90, 180, 300, 600, or 900 peak PAR
437 $\mu\text{mol photons m}^{-2}\text{s}^{-1}$ (μE); and photoperiods of 8, 12, 16, or 24 h (Fig. 7). The σ_{PSII}' measured
438 under diel peak PAR growth light under $\text{Ex}_{445\text{nm}}$ (blue) excitation vs. cumulative diel photon
439 dose is shown in Supporting Information (Fig. S8, Table S12).

440 All strains showed consistent patterns of sharp, exponential decay of effective absorption
441 cross section for PSII photochemistry vs. cumulative diel photon doses, across different
442 combinations of photoperiod and peak PAR (Fig. 7A). Although all strains showed this response
443 pattern, the exponential decay fits differed significantly among two PC-rich strains and PE-
444 rich_048 strains during their exponential phase of growth (ANOVA, $p < 0.05$; Table S11). PE-
445 rich strains showed higher σ_{PSII}' under low cumulative diel photon dose (y_0 about 0.8 and y_f
446 about 4) than did PC-rich strains. During pre-stationary phase this response dampens in the PC-
447 rich strains but persists in the PE-rich strains (Table S11). σ_{PSII}' for the PE-rich strains during
448 pre-stationary phase of growth still remain higher (y_f between 2.3 – 3.0) than in the PC-rich
449 strains (y_f between 1.4 – 1.7) even as cumulative diel photon dose increases. Model fits from
450 different phases of growth differed within a given strain, with the exception of PE-rich_048
451 (ANOVA; $p < 0.05$, Table S11).



452

453 **Fig. 7. (A)** Effective absorption cross section of PSII (σ_{PSII}' ; $\text{nm}^2 \text{ quanta}^{-1}$) measured under diel peak PAR growth
 454 light vs. cumulative diel PAR ($\mu\text{mol photons m}^{-2} \text{ d}^{-1}$); blue solid line shows single phase exponential decay fit for
 455 data from each strain and growth phase. **(B)** Changes of σ_{PSII}' measured under diel peak PAR growth light vs. the
 456 ratio of sum of μg phycobilins (PE, PC, APC protein, Phycobiliprotein) to $\mu\text{g Chl a}$; blue solid line shows linear
 457 model fit for data from each strain and growth phase. σ_{PSII}' was estimated using FRRf induction curves with
 458 excitation of phycobilisomes (Ex_{590nm}, orange), for two PC-rich cultures (056; dark green, 077; light green) and two
 459 PE-rich cultures (048; light red, 127; dark red) of *Synechococcus* sp. grown at 30 (dark gray), 90 (light gray), 180
 460 (purple), 300 (red), 600 (orange), or 900 (yellow) peak PAR $\mu\text{mol photons m}^{-2} \text{ s}^{-1}$ (μE); and photoperiods of 8
 461 (square), 12 (circle), 16 (triangle), or 24 (diamond) h. Figure presents data (smaller symbols) and means (bigger
 462 symbols) from exponential or pre-stationary phase of growth. Different lowercase letters indicate statistically
 463 significant differences between the fit models for different strains within a given phase of growth. Different

464 uppercase letters indicate statistically significant differences between the fit models for different phases of growth
465 within a given strain ($p < 0.05$).

466

467 Effective absorption cross section of PSII (σ_{PSII}' ; $\text{nm}^2 \text{ quanta}^{-1}$), measured under diel peak
468 PAR growth light with $\text{Ex}_{590\text{nm}}$ (orange) excitation, varies with Phycobiliprotein to Chl *a* ratio
469 (Fig. 7B). σ_{PSII}' excited through phycobilisome absorbance at $\text{Ex}_{590\text{nm}}$ shows positive linear
470 correlations with the Phycobiliprotein to Chl *a* ratio, although strains in exponential growth show
471 significant scatter around this positive relation, likely related to regulatory control of σ_{PSII}' under
472 different measurement PAR, beyond pigment composition. Under pre-stationary phase the
473 relationship between σ_{PSII}' and Phycobiliprotein to Chl *a* ratio was more consistent, suggesting
474 increased reliance upon compositional regulation to control light delivery to PSII, as opposed to
475 shorter-term physiological regulation under changing light. The linear fits of σ_{PSII}'
476 vs. Phycobiliprotein to Chl *a* ratio also vary significantly between PC-rich_077 and two PE-rich
477 strains during their exponential phase of growth. During pre-stationary phase we noted
478 significant differences between two PC-rich strains and PE-rich_048. Moreover, significant
479 differences between the fit models for varying phases of growth were noted for PC-rich strains
480 056 and 077 (*t*-test; $p < 0.05$, Table S14).

481 Changes in effective absorption cross section of PSII (σ_{PSII} ; $\text{nm}^2 \text{ quanta}^{-1}$) measured in the
482 dark with $\text{Ex}_{590\text{nm}}$ (orange) excitation vs. Phycobiliprotein to Chl *a* ratio (Fig. S9A, Table S15)
483 and σ_{PSII}' measured under diel peak PAR growth light under $\text{Ex}_{445\text{nm}}$ (blue) excitation
484 vs. Phycobiliprotein to Chl *a* ratio (Fig. S9B and Table S13) are shown in Supporting
485 Information.

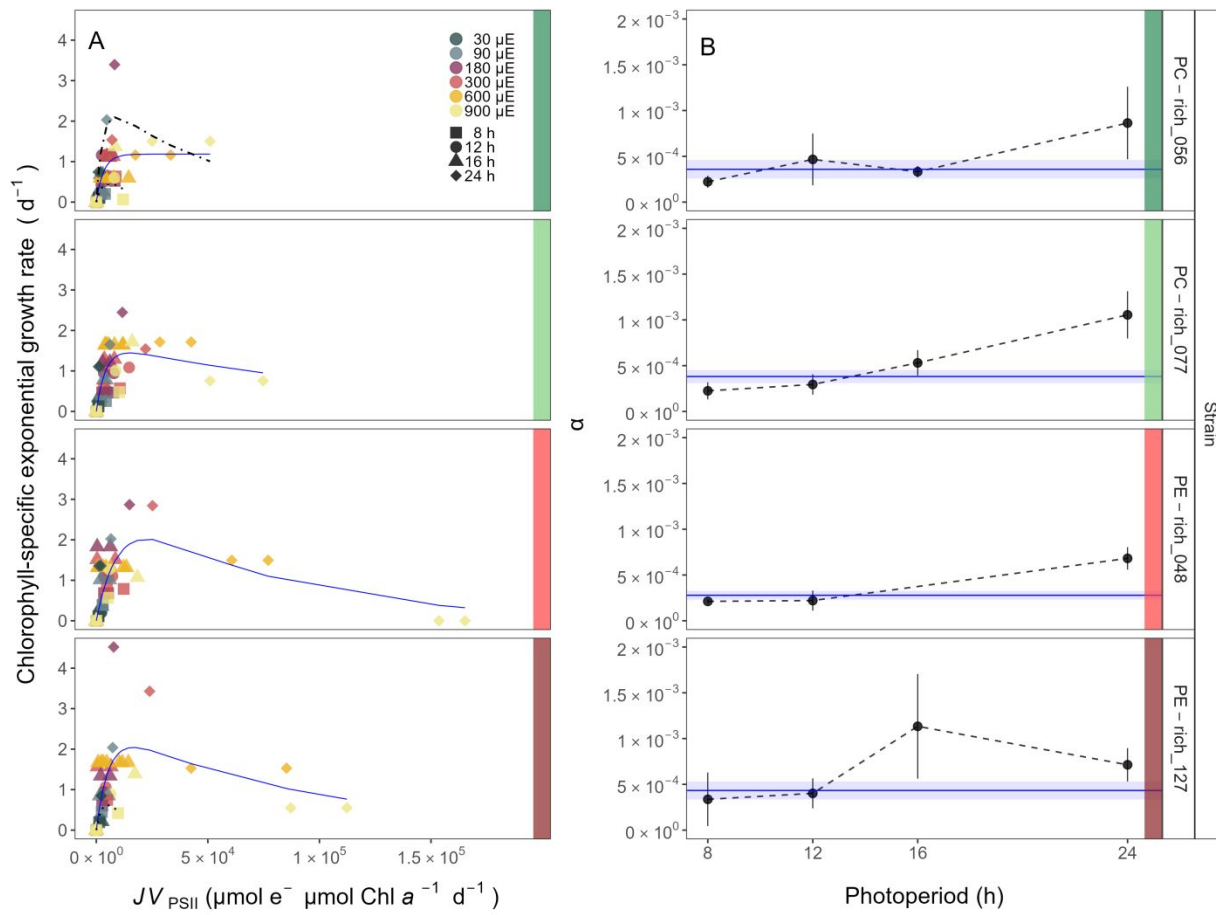
486

487 **Growth rates vs. cumulative diel PSII electron flux**

488 Chlorophyll-specific exponential growth rates (d^{-1}), within each strain, show fairly
489 consistent saturating responses to increasing cumulative diel PSII electron flux (JV_{PSII} ; $\mu\text{mol e}^-$
490 $\mu\text{mol Chl } a^{-1} d^{-1}$) estimated under diel peak PAR growth light, and estimated using FRRf
491 induction curves with excitation of chlorophyll (Ex_{445nm}, blue), although photoperiod (Fig. 8A,
492 Table S7) and peak PAR (Fig. S10, Table S8) retained a secondary influence on achieved growth
493 responses for some growth conditions.

494 A three parameter model fit of (Harrison and Platt 1986) vs. cumulative diel PSII electron
495 flux (JV_{PSII} ; $\mu\text{mol e}^- \mu\text{mol Chl } a^{-1} d^{-1}$) for two PC-rich and two PE-rich cultures of
496 *Synechococcus* sp. showed no significant differences between fits of the pooled data vs. fits for
497 different photoperiods (8, 12, 16, or 24 h; ANOVA, $p < 0.05$), with exception of 8 and 24 h
498 photoperiod for PC-rich_056 and 8 h photoperiod for PE-rich_127 strains (ANOVA, $p > 0.05$;
499 Table S7).

500 Alpha parameters of the initial rise of growth rate (α) vs. cumulative diel JV_{PSII} , estimated
501 from data pooled for each photoperiod showed an increase across increasing photoperiods for
502 each strain except for PE-rich_0127. The highest increase (>2-fold) of α from the lowest to the
503 highest photoperiod was recorded for PC-rich_077 (Fig. 8B).



504

505 **Fig. 8.** (A) Chlorophyll-specific exponential growth rates (d^{-1}) vs. cumulative diel PSII electron flux (JV_{PSII} ; $\mu\text{mol e}^-$
 506 $\mu\text{mol Chl } a^{-1} d^{-1}$) measured under diel peak PAR growth light. Growth rates (\pm SE falling within symbols) were
 507 estimated from logistic fits of chlorophyll proxy $OD_{680} - OD_{720}$ (ΔOD) vs. elapsed time (Fig. S3B). JV_{PSII} was
 508 estimated using FRRf induction curves with excitation of chlorophyll ($Ex_{445\text{nm}}$, blue), for two PC-rich cultures (056;
 509 dark green, 077; light green) and two PE-rich cultures (048; light red, 127; dark red) of *Synechococcus* sp. grown at
 510 30 (dark gray), 90 (light gray), 180 (purple), 300 (red), 600 (orange), or 900 (yellow) peak PAR $\mu\text{mol photons}$
 511 $\text{m}^{-2}\text{s}^{-1}$ (μE); and photoperiods of 8 (square), 12 (circle), 16 (triangle), or 24 (diamond) h. Solid blue line shows a fit
 512 of the pooled growth rates for each strain, with a three parameter model (Harrison and Platt 1986). We also fit the
 513 same model separately for 8 (dotted line) and 24 (two dash line) h photoperiods, when they were significantly
 514 different (ANOVA, $p < 0.05$) from the fit of pooled data. (B) Alpha parameters of the initial rise of growth rate (α)
 515 vs. cumulative diel JV_{PSII} , estimated from data pooled for each photoperiod (points (\pm SE) connected by dashed
 516 lines), and estimated for all data across photoperiods (horizontal line \pm SE), for each strain.

517

518 **Discussion**519 **Photic regimes - implications for picocyanobacteria growth and distribution**

520 Light regimes, including photoperiod, and peak PAR, are major factors affecting the
521 distribution and seasonality of phytoplankters (Erga and Heimdal 1984). Changes in photoperiod
522 trigger acclimation responses, shaping the temporal dynamics and community structure of
523 phytoplankton (Theus et al. 2022; Longobardi et al. 2022). Each tested picocyanobacterial strain
524 showed influences of photoperiod upon the responses of growth rate to cumulative diel PUR
525 (Fig. 5) and PAR (Fig. S5). To our surprise, increasing photoperiod increased the ranges of
526 response to PAR and PUR. Both the PC-rich and the PE-rich strains of *Synechococcus* sp.
527 exhibited their highest initial responses of growth to increasing PUR and PAR (alpha, (Fig. 5B),
528 Fig. S5B), and their fastest growth rates under continuous light (24 h photoperiod), consistent
529 with some other strains (Jacob-Lopes et al. 2009; Klepacz-Smólka et al. 2020). Yet, 24 h
530 photoperiod also exacerbated eventual photoinhibition under excess cumulative diel PUR and
531 PAR. Our temperate strains do not experience direct selective pressures to exploit a continuous
532 24 photoperiod (Brand and Guillard 1981), so achieving maximum growth under a 24 h
533 photoperiod rather suggests lack of a requirement for a dark period, and lack of requirement for a
534 regular photoperiod. Coastal phytoplankton strains are selected to exploit instantaneous light
535 (Brand and Guillard 1981), of whatever duration, to cope with fluctuating light and nutrients in
536 coastal environments (MacIntyre et al. 2000; Litchman et al. 2009), leading to a pleiotropic
537 capacity for exploiting continuous light. The ability of both PC-rich and PE-rich coastal
538 picocyanobacteria to exploit continuous light means they could, potentially, grow rapidly at
539 higher latitudes, in a future warmer polar summer water.

540 Light level is another key driver of picocyanobacteria productivity (Pick 1991; Six et al.
541 2007; Aguilera et al. 2023). The spatial and temporal distribution of PAR within aquatic
542 ecosystems is influenced by solar angle, water depth, water clarity, and the presence of light-
543 absorbing substances such as dissolved organic matter (Morel 1978, 1988) and phytoplankton
544 cells. PUR then represents the light potentially available for phytoplankton to photosynthesize.
545 PUR is always smaller than PAR ($\text{PUR} < \text{PAR}$), and depends on the spectral composition of the
546 PAR, versus the phytoplankton pigment composition, determining cellular spectral absorption
547 (Morel 1978), which changes depending upon growth conditions and the phase of growth.

548 PE-rich and PC-rich *Synechococcus* sp. strains show distinct growth responses to
549 cumulative diel photon dose, depending upon the peak PAR of the applied photoregime (Fig. S4,
550 Fig. S6). Chlorophyll-specific exponential growth rates of the PE-rich and PC-rich
551 *Synechococcus* sp. strains increased with increasing light levels, to a plateau in the range of 180
552 – 300 $\mu\text{mol photons m}^{-2}\text{s}^{-1}$. Growth above 600 $\mu\text{mol photons m}^{-2}\text{s}^{-1}$ occurred with a growth
553 yield per cumulative diel photon lower than under moderate light, particularly when combined
554 with short 8 h or long 24 h photoperiods. Even though PE-rich *Synechococcus* sp. are more
555 adapted to lower-light conditions deeper in the water column (Stomp et al. 2007), our findings
556 show that PE-rich strains will grow under higher irradiance.

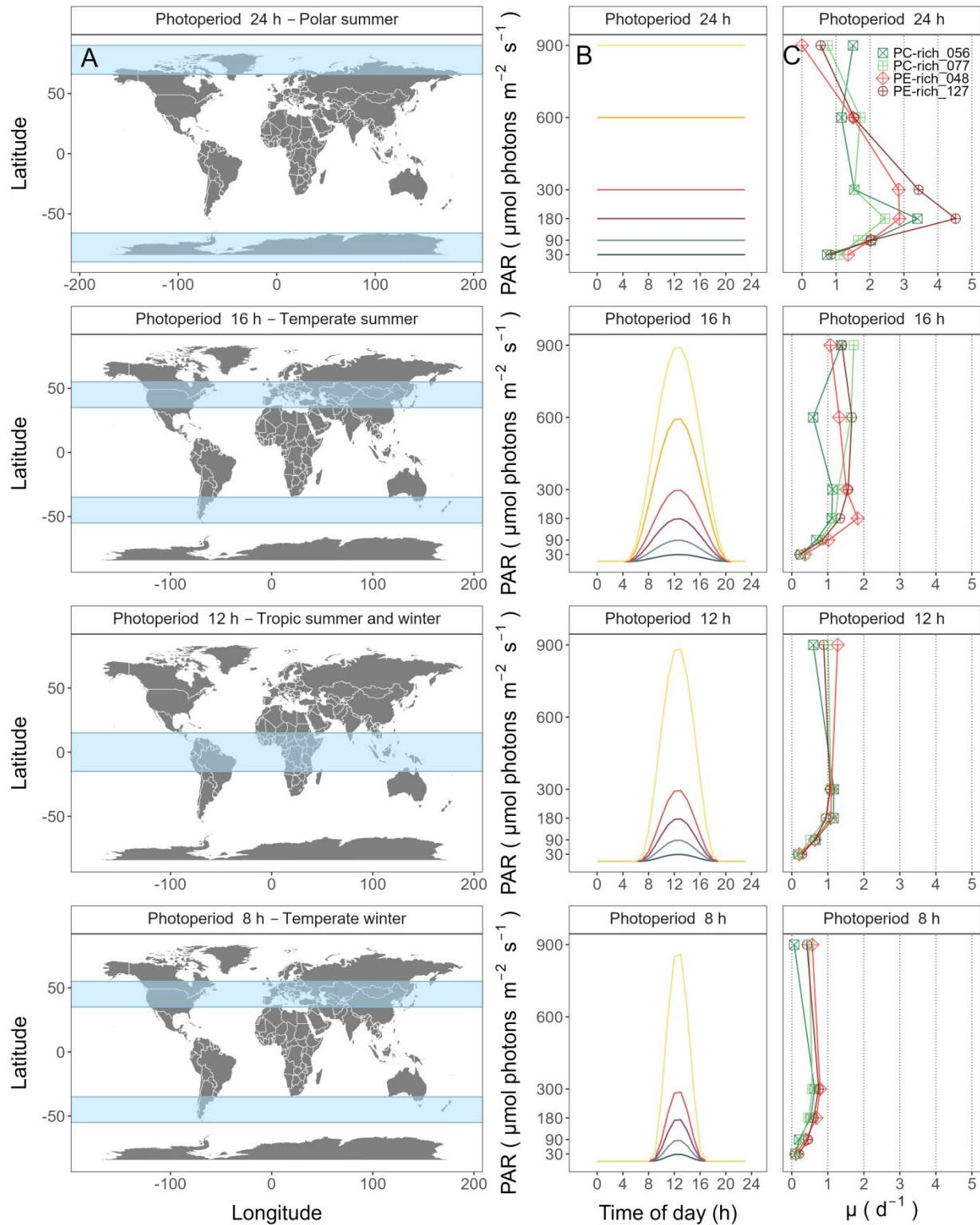
557 The maximum growth rate of *Synechococcus* sp. PE-rich_127 strain under 24 h
558 photoperiod and peak PAR of 180 $\mu\text{mol photons m}^{-2}\text{s}^{-1}$ was 4.5 d^{-1} ($\mu = 0.187 \text{ h}^{-1}$),
559 corresponding to a doubling time of 3.7 h (Fig. 5, Fig. S4); faster than previously reported for
560 marine picocyanobacteria, and indeed faster than for the model freshwater cyanobacteria
561 *Synechococcus* sp. PCC6301 (doubling time of 4.5–5 h under constant illumination and 250 μmol
562 $\text{photons m}^{-2}\text{s}^{-1}$) (Sakamoto and Bryant 1999), or *Synechocystis* sp. PCC 6803 (doubling time of

563 4.3 h) (van Alphen et al. 2018). The fastest growth rate as yet achieved for any phytoplankton
564 occurs in a genetically modified green algae *Picochlorum celeri*, with a maximum of about 6.8
565 d⁻¹ and ~2.5 h doubling time, in bioreactors (Krishnan et al. 2021). The Baltic *Synechococcus* sp.
566 strains, not genetically modified, preferred 24 h photoperiod and moderate peak PAR of 180
567 μmol photons m⁻²s⁻¹, suggesting they could, potentially, thrive in warming polar latitude waters.
568 *Synechococcus* sp. strains indeed already occur across geographical regions (Śliwińska-
569 Wilczewska et al. 2018b) with different photic regimes, including polar regions (reviewed by
570 Velichko et al. (2021)), exceeding latitude 80°S and 80°N. The prolonged daylight hours of polar
571 summers, coupled with nutrient-rich waters, promote growth of genetically diverse
572 *Synechococcus* populations (Vincent et al. 2000), contributing significantly to primary
573 productivity. Gradinger and Lenz (1989) suggested that *Synechococcus*-type picocyanobacteria
574 may serve as indicator organisms for the advection of warm water masses into polar regions,
575 important in the context of monitoring upcoming climate changes.

576 The coastal PC-rich and PE-rich strains of *Synechococcus* showed saturation, and then
577 photoinhibition of growth rates under increasing cumulative diel PUR, although the achieved
578 estimates of μ_{\max} , and the onset of photoinhibition of growth, varied depending upon strain,
579 photoperiod and peak PAR (Fig. 4). The tested strains were generally opportunistic in exploiting
580 longer photoperiods to achieve faster μ , although PE-rich strains suffered strong photoinhibition
581 of growth under peak PAR above 600 μmol photons m⁻²s⁻¹ and 24 h photoperiod (Fig. 5, Fig.
582 S4), suggesting the PE-rich strains are better adapted to lower light and deeper parts of the water
583 column. The least favorable growth conditions for both PE-rich and PC-rich strains of
584 *Synechococcus* sp. were under high light (> 600 μmol photons m⁻²s⁻¹) and the shortest
585 photoperiod (8 h), even though the cumulative diel PUR dose was equivalent to conditions where

586 the light intensity was lower and the photoperiod was longer. Thus these Baltic
587 picocyanobacteria are prone to photoinhibition under both the longest, and the shortest,
588 photoperiod regimes, with flatter light responses of growth under intermediate photoperiods.
589 Thus, in regions and periods with a longer photoperiod, both PC-rich and PE-rich *Synechococcus*
590 sp. could become dominant species in surface waters, but could suffer under shorter
591 photoperiods (Fig. 9).

For Review Only



592

593 **Fig. 9.** Latitudinal bands, equivalent summer or winter photoperiods, and picocyanobacterial growth responses. **(A)**
 594 Latitudinal bands corresponding to tested growth photoperiods. **(B)** Tested photoperiod and peak PAR regimes used

595 for growth experiments. (C) Chlorophyll specific exponential growth rates (\pm SE falling within symbols) for two
596 PhycoCyanin(PC)-rich cultures (056; dark green, 077; light green) and two PhycoErythrin(PE)-rich cultures (048;
597 light red, 127; dark red) of *Synechococcus* sp. under tested photoperiod and peak PAR regimes.

598

599 **Photic regimes and growth phase both influence cellular absorbance and light
600 use**

601 Under nutrient replete exponential growth the picocyanobacterial strains show consistent
602 patterns of an exponential decline in PUR/PAR ratio versus cumulative diel photon doses, across
603 different combinations of photoperiod and peak PAR. Thus, under nutrient repletion the
604 picocyanobacteria balance pigment composition to match light conditions (Fig. 6). In addition to
605 chlorophyll *a*, picocyanobacteria use phycobilins, including phycocyanin (harvesting red light at
606 620 nm) and phycoerythrin (harvesting yellow light at 570 nm), as accessory pigments to
607 enhance light harvesting efficiency. Picocyanobacteria enhance phycobilin production to
608 compensate for limited irradiance, thereby optimizing their photosynthetic capabilities
609 (Śliwińska-Wilczewska et al. 2018a) and increasing their PUR/PAR.

610 The effective absorption cross section for photochemistry of PSII in the light (σ_{PSII}')
611 comprises the probability of light capture by PSII and the quantum yield for subsequent
612 photochemistry. PC-rich and PE-rich strains of *Synechococcus* again show consistent patterns of
613 an exponential decay to a plateau with increasing cumulative diel PAR doses, for σ_{PSII}' (nm^2
614 quanta $^{-1}$, measured under diel peak PAR growth light under Ex_{590nm} (orange) excitation), without
615 detectable influences of photoperiod, nor of peak PAR (Fig. 7A). σ_{PSII}' excited through
616 chlorophyll absorbance at 445 nm was, in contrast, consistently small across strains and growth
617 conditions (Fig. S8, Fig. S9), since in cyanobacteria the number of chlorophyll serving each PSII
618 is nearly fixed (Xu et al. 2018). σ_{PSII}' excited through phycobilisome absorbance at 590 nm

619 shows, as expected, a positive correlation with Phycobiliprotein:Chl *a*. Growth under low
620 cumulative diel PAR results in an increased Phycobiliprotein:Chl *a*, as the picocyanobacteria
621 allocate protein resources towards phycobiliprotein-mediated light capture (Beale 1994;
622 Stadnichuk et al. 2015; Chakdar and Pabbi 2016). PC-rich and PE-rich strains of *Synechococcus*
623 sp. in exponential growth nonetheless show significant scatter around this pattern, likely related
624 to regulatory control of σ_{PSII}' , beyond pigment composition. In pre-stationary phase σ_{PSII}'
625 vs. Phycobiliprotein:Chl *a* was better aligned, suggesting reliance upon fixed compositional
626 regulation of phycobiliprotein content to control light delivery to PSII, as opposed to shorter-
627 term regulation.

628 A phylogeny 16S rRNA gene phylogeny (amplicon average 1385 bp) placed the tested
629 strains in order Synechoccales and family Synechoccaceae, within the cluster 5
630 picocyanobacterial lineage, in sub-cluster 5.2 together with freshwater, brackish and halotolerant
631 strains, separated from marine sub-clusters 5.1 and 5.3 (Fig. 1S). The 16S rRNA of the strains
632 showed ~100% identity with strains assigned to *Synechococcus* spp. or to *Cyanobium* spp. It is
633 worth emphasizing that light capture and light absorption abilities differed significantly among
634 tested strains (Six et al. 2021). The PE-rich strains show a much higher PUR/PAR ratio under
635 low cumulative diel photon doses during exponential phase, but decay towards a plateau and
636 reach a similar value to the PC-rich strains as cumulative diel photon dose increases. Thus the
637 PE-rich strains in exponential phase demonstrated higher ability to modulate light absorbance
638 capacity, whereas PC-rich strains retained a more stable PUR/PAR across cumulative diel
639 photon doses. What is more, during exponential phase, the PE-rich strains show a much higher
640 σ_{PSII}' under low cumulative diel photon dose, and their σ_{PSII}' remains higher than the PC-rich
641 strains, even as cumulative diel photon dose increases. Hence, PE-rich strains exhibit higher light

642 harvesting efficiency, at the expense of susceptibility to higher light levels, particularly under the
643 shortest (8h) and longest (24h) photoperiods.

644 *Synechococcus* exhibits remarkable acclimation within a strain to different environmental
645 conditions (Śliwińska-Wilczewska et al. 2018a, 2020; Aguilera et al. 2023). Under high
646 cumulative diel photon dose, *Synechococcus* employs photoprotective mechanisms to prevent the
647 harmful effects of excess light energy. These include the dissipation of excess energy as heat via
648 non-photochemical quenching (NPQ) and the regulation of phycobilisome antenna pigments, to
649 balance light absorption and energy transfer. In contrast, under conditions of low cumulative diel
650 PAR dose, *Synechococcus* sp. increases the expression of light-harvesting complexes to enhance
651 light absorption (Fig. 6) and capture (Fig. 7).

652 Available photic regimes, combining photoperiod and peak PAR, may determine the
653 occurrences of PC-rich and PE-rich picocyanobacterial phenotypes. Nitrogen (N) is an essential
654 element for cyanobacteria, while the N costs to produce photosynthetic pigments varies. The
655 molecular weight of the two phycoerythrin (PE; phycoerythrobilin) subunits is about 20,000 and
656 18,300 g mol⁻¹, while the two phycocyanin (PC; phycocyanobilin) subunits are about 17,600 and
657 16,300 g mol⁻¹, and allophycocyanin (APC) is lower still, about 16,000 g mol⁻¹ (Bennett and
658 Bogorad 1971) and cell-specific content of this pigment is usually low in both phenotypes
659 (Śliwińska-Wilczewska et al. 2020). It follows that N-cost of producing PE is higher than that of
660 PC, even though PE-rich picocyanobacteria capture light better than PC-rich phenotypes (Fig. 6;
661 Fig. 7. Our results confirm that PE-rich strains are stronger light-harvesting competitors, while
662 the PC-rich strains have lower N-quotients for their phycobilin light capture system.

663

664 **Photic regimes - implications for cumulative diel PSII electron flux**

665 Algal dynamics respond rapidly to changes in environmental conditions (Connor 2018).
666 We used Fast Repetition Rate fluorometry (FRRf; Fig. 3) (Kolber et al. 1998) to generate an
667 index of PSII electron transport rate per unit volume (JV_{PSII}) (Oxborough et al. 2012; Tortell and
668 Suggett 2021; Berman-Frank et al. 2023), calibrated to absolute rates of electron transport
669 measured through oxygen evolution. Across different photic regimes the growth rates, μ , of PC-
670 rich and PE-rich picocyanobacteria show fairly consistent saturating responses to increasing
671 cumulative diel PSII electron flux (JV_{PSII} ; $\mu\text{mol e}^- \mu\text{mol Chl } \alpha^{-1} \text{ d}^{-1}$; Fig. 8). As previously found
672 for diatoms (Li et al. 2017) cumulative diel reductant generation was indeed a better predictor of
673 μ than was cumulative diel PUR, although photoperiod and peak PAR retain secondary
674 influences on achieved growth responses of the picocyanobacteria under some conditions.

675

676 **Conclusions**

677 Coastal picocyanobacteria show different growth responses to photoperiod and light level,
678 even under combinations giving equivalent cumulative diel PUR. Both PE-rich and PC-rich
679 strains of *Synechococcus* sp., grew fastest under moderate light and a 24 h photoperiod.
680 Consequently, *Synechococcus* sp. has the potential to emerge as components of the
681 phytoplankton during the Arctic or Antarctic summer under future, warmed, polar regions. In
682 optimal conditions (24 h of photoperiod and a peak PAR of 180 $\mu\text{mol photons m}^{-2}\text{s}^{-1}$), one of the
683 PE-rich *Synechococcus* sp., reached a chlorophyll-specific exponential growth rate of 4.5 d^{-1} (3.7
684 h doubling time), a record for a cyanobacteria. PE-rich strains in the exponential phase of growth
685 also demonstrated high ability to modulate their PUR/PAR ratio by adjusting pigment
686 composition, giving an advantage in the competition for light. We determined that growth yields

687 of PC-rich and PE-rich picocyanobacteria are well predicted by cumulative diel PSII electron
688 fluxes, across different photic regimes. PE-rich phenotypes of picocyanobacteria currently
689 predominate in abundance and genetic diversity in the Baltic Sea (Aguilera et al. 2023). This
690 dominance may be the result of eutrophication in the Baltic Sea, providing higher nitrogen for
691 phycobiliprotein synthesis, and leading to lower light even in near-surface waters. Our results
692 suggest possible expansion of the range of picocyanobacteria to new photic regimes in a warmed
693 future and indicate that PE-rich *Synechococcus* sp. may be a dominant component of
694 picophytoplankton in nutrient-rich environments.

695

696 **Additional Supporting Information may be found in the online version of this article.**

697

698 **Authors Contribution Statement:** S.S-W. designed the study with input from D.A.C. M.K.
699 estimated the transition point between exponential and pre-stationary phase of growth. M.S.
700 ensured the proper operation of the photobioreactors. A.A. conducted genetic analysis. N.M.O.
701 solved technical problems related to computer operation and software. S.S-W., M.S., N.M.O.,
702 D.A.C. contributed to R coding and data analysis. S.S-W. conducted the experiments, created
703 plots and wrote the manuscript, with support from D.A.C. All authors contributed to the
704 discussion of the results, supported manuscript preparation, and approved the final submitted
705 manuscript.

706

707 **Data availability statement**

708 Data supporting this study is available on:

709 <https://github.com/FundyPhytoPhys/BalticPhotoperiod> (public GitHub Repository) and

710 https://docs.google.com/spreadsheets/d/1ZXpwR7Gfto-
711 uRzVdXzMpQF4frbrvMLH_IyLqonFZRSw/edit#gid=0 (URL for MetaDataCatalog).
712 Code to perform data processing and analyses is available at
713 https://github.com/FundyPhytoPhys/BalticPhotoperiod.
714 16S rRNA sequences used in this study are available in GenBank under the accession
715 numbers PP034393, PP034394, PP034396 and PP034403.

716

717 Acknowledgements

718 We thank Maximilian Berthold for the code for the GAM model; Miranda Corkum who
719 maintained cultures and trained personnel in culture handling; Laurel Genge, and Carlie Barnhill
720 (Mount Allison students) who assisted with R code. This work was supported by Canada
721 Research Chair in Phytoplankton Ecophysiology (D.A.C) and Latitude & Light; NSERC of
722 Canada Discovery Grant (D.A.C).

723

724 Conflict of Interest

725 None declared.

726

727 References

728 Aguilera, A., J. Alegria Zufia, L. Bas Conn, and others. 2023. Ecophysiological analysis reveals
729 distinct environmental preferences in closely related Baltic Sea picocyanobacteria.
730 Environmental Microbiology **25**: 1674–1695. doi:10.1111/1462-2920.16384

- 731 Arrigo, K. R. 2014. Sea ice ecosystems. *Annual Review of Marine Science* **6**: 439–467.
- 732 doi:10.1146/annurev-marine-010213-135103
- 733 Beale, S. I. 1994. Biosynthesis of cyanobacterial tetrapyrrole pigments: Hemes, chlorophylls,
734 and phycobilins, p. 519–558. In D.A. Bryant [ed.], *The Molecular Biology of Cyanobacteria*.
735 Springer Netherlands.
- 736 Behrenfeld, M. J., R. T. O'Malley, D. A. Siegel, and others. 2006. Climate-driven trends in
737 contemporary ocean productivity. *Nature* **444**: 752–755. doi:10.1038/nature05317
- 738 Bennett, A., and L. Bogorad. 1971. Properties of subunits and aggregates of blue-green algal
739 biliproteins. *Biochemistry* **10**: 3625–3634. doi:10.1021/bi00795a022
- 740 Bennett, A., and L. Bogorad. 1973. Complementary Chromatic Adaptation in a filamentous blue-
741 green alga. *Journal of Cell Biology* **58**: 419–435. doi:10.1083/jcb.58.2.419
- 742 Berman-Frank, I., D. Campbell, A. Ciotti, and others. 2023. Application of Single Turnover
743 Active Chlorophyll Fluorescence for Phytoplankton Productivity Measurements. Version 2.0,
744 June, 26, 2023. Report Scientific Committee on Oceanic Research (SCOR) Working Group 156.
- 745 Boatman, T. G., R. J. Geider, and K. Oxborough. 2019. Improving the accuracy of Single
746 Turnover Active Fluorometry (STAF) for the estimation of Phytoplankton Primary Productivity
747 (PhytoPP). *Frontiers in Marine Science* **6**. doi:10.3389/fmars.2019.00319
- 748 Brand, L. E., and R. R. L. Guillard. 1981. The effects of continuous light and light intensity on
749 the reproduction rates of twenty-two species of marine phytoplankton. *Journal of Experimental
750 Marine Biology and Ecology* **50**: 119–132. doi:10.1016/0022-0981(81)90045-9

- 751 Chakdar, H., and S. Pabbi. 2016. Cyanobacterial phycobilins: Production, purification, and
752 regulation, p. 45–69. In P. Shukla [ed.], *Frontier Discoveries and Innovations in Interdisciplinary*
753 *Microbiology*. Springer India.
- 754 Christaki, U., S. Jacquet, J. R. Dolan, D. Vaultot, and F. Rassoulzadegan. 1999. Growth and
755 grazing on *Prochlorococcus* and *Synechococcus* by two marine ciliates. *Limnology and*
756 *Oceanography* **44**: 52–61. doi:10.4319/lo.1999.44.1.0052
- 757 Connor, D. 2018. Investigating the use of fast repetition rate fluorometry in understanding algal
758 physiology in optically complex oceans.
- 759 Elzhov, T. V., K. M. Mullen, A.-N. Spiess, and B. Bolker. 2023. Minpack.lm: R Interface to the
760 Levenberg-Marquardt Nonlinear Least-Squares Algorithm Found in MINPACK, Plus Support
761 for Bounds.
- 762 Erga, S. R., and B. R. Heimdal. 1984. Ecological studies on the phytoplankton of Korsfjorden,
763 western Norway. The dynamics of a spring bloom seen in relation to hydrographical conditions
764 and light regime. *Journal of Plankton Research* **6**: 67–90. doi:10.1093/plankt/6.1.67
- 765 Falkowski, P., and Z. Kolber. 1993. Estimation of phytoplankton photosynthesis by active
766 fluorescence. *ICES Marine Science Symposium* **197**: 92–103.
- 767 Field, C. B., M. J. Behrenfeld, J. T. Randerson, and P. Falkowski. 1998. Primary production of
768 the biosphere: Integrating terrestrial and oceanic components. *Science* **281**: 237–240.
769 doi:10.1126/science.281.5374.237

- 770 Flombaum, P., J. L. Gallegos, R. A. Gordillo, and others. 2013. Present and future global
771 distributions of the marine Cyanobacteria *Prochlorococcus* and *Synechococcus*. Proceedings of
772 the National Academy of Sciences **110**: 9824–9829. doi:10.1073/pnas.1307701110
- 773 Gradinger, R., and J. Lenz. 1989. Picocyanobacteria in the high Arctic. Marine Ecology Progress
774 Series **52**: 99–101. doi:10.3354/meps052099
- 775 Guillard, R. R. L. 1975. Culture of phytoplankton for feeding marine invertebrates, p. 29–60. In
776 W.L. Smith and M.H. Chanley [eds.], Culture of Marine Invertebrate Animals: Proceedings —
777 1st Conference on Culture of Marine Invertebrate Animals Greenport. Springer US.
- 778 Handel, A. 2020. Andreas Handel - Custom Word formatting using R Markdown.
- 779 Harrison, W. G., and T. Platt. 1986. Photosynthesis-irradiance relationships in polar and
780 temperate phytoplankton populations. Polar biology **5**: 153–164.
- 781 Haverkamp, T. H. A., D. Schouten, M. Doeleman, U. Wollenzien, J. Huisman, and L. J. Stal.
782 2009. Colorful microdiversity of *Synechococcus* strains (picocyanobacteria) isolated from the
783 Baltic Sea. The ISME Journal **3**: 397–408. doi:10.1038/ismej.2008.118
- 784 Hirata, T., N. J. Hardman-Mountford, R. J. W. Brewin, and others. 2011. Synoptic relationships
785 between surface Chlorophyll-*a* and diagnostic pigments specific to phytoplankton functional
786 types. Biogeosciences **8**: 311–327. doi:10.5194/bg-8-311-2011
- 787 Hoang, D. T., O. Chernomor, A. von Haeseler, B. Q. Minh, and L. S. Vinh. 2018. UFBoot2:
788 Improving the Ultrafast Bootstrap Approximation. Molecular Biology and Evolution **35**: 518–
789 522. doi:10.1093/molbev/msx281

- 790 Holtrop, T., J. Huisman, M. Stomp, and others. 2021. Vibrational modes of water predict spectral
791 niches for photosynthesis in lakes and oceans. *Nature Ecology & Evolution* **5**: 55–66.
792 doi:10.1038/s41559-020-01330-x
- 793 Huisman, J., M. Arrayás, U. Ebert, and B. Sommeijer. 2002. How do sinking phytoplankton
794 species manage to persist? *The American Naturalist* **159**: 245–254. doi:10.1086/338511
- 795 Jacob-Lopes, E., C. H. G. Scoparo, L. M. C. F. Lacerda, and T. T. Franco. 2009. Effect of light
796 cycles (night/day) on CO₂ fixation and biomass production by microalgae in photobioreactors.
797 *Chemical Engineering and Processing: Process Intensification* **48**: 306–310.
798 doi:10.1016/j.cep.2008.04.007
- 799 Jávorfi, T., J. Erostyák, J. Gál, A. Buzády, L. Menczel, G. Garab, and K. Razi Naqvi. 2006.
800 Quantitative spectrophotometry using integrating cavities. *Journal of Photochemistry and
801 Photobiology B: Biology* **82**: 127–131. doi:10.1016/j.jphotobiol.2005.10.002
- 802 Kalyaanamoorthy, S., B. Q. Minh, T. K. F. Wong, A. von Haeseler, and L. S. Jermiin. 2017.
803 ModelFinder: Fast model selection for accurate phylogenetic estimates. *Nature Methods* **14**:
804 587–589. doi:10.1038/nmeth.4285
- 805 Katoh, K., J. Rozewicki, and K. D. Yamada. 2019. MAFFT online service: Multiple sequence
806 alignment, interactive sequence choice and visualization. *Briefings in Bioinformatics* **20**: 1160–
807 1166. doi:10.1093/bib/bbx108
- 808 Klepacz-Smólka, A., D. Pietrzyk, R. Szeląg, P. Głuscz, M. Daroch, J. Tang, and S. Ledakowicz.
809 2020. Effect of light colour and photoperiod on biomass growth and phycocyanin production by

- 810 *Synechococcus* PCC 6715. Bioresource Technology **313**: 123700.
811 doi:10.1016/j.biortech.2020.123700
- 812 Kolber, Z. S., O. Prášil, and P. G. Falkowski. 1998. Measurements of variable chlorophyll
813 fluorescence using fast repetition rate techniques: Defining methodology and experimental
814 protocols. Biochimica et Biophysica Acta (BBA) - Bioenergetics **1367**: 88–106.
815 doi:10.1016/S0005-2728(98)00135-2
- 816 Krishnan, A., M. Likhogrud, M. Cano, and others. 2021. *Picochlorum Celere* as a model system
817 for robust outdoor algal growth in seawater. Scientific Reports **11**: 11649. doi:10.1038/s41598-
818 021-91106-5
- 819 Lane, D. J. 1991. 16S/23S rRNA sequencing. Nucleic acid techniques in bacterial systematics
820 115–175.
- 821 LaRoche, J., and B. M. Robicheau. 2022. The Pelagic Light-Dependent Microbiome, p. 395–
822 423. In L.J. Stal and M.S. Cretoiu [eds.], The Marine Microbiome. Springer International
823 Publishing.
- 824 Li, G., D. Talmy, and D. A. Campbell. 2017. Diatom growth responses to photoperiod and light
825 are predictable from diel reductant generation. Journal of Phycology **53**: 95–107.
826 doi:10.1111/jpy.12483
- 827 Li, Q., L. Legendre, and N. Jiao. 2015. Phytoplankton responses to nitrogen and iron limitation
828 in the tropical and subtropical Pacific Ocean. Journal of Plankton Research **37**: 306–319.
829 doi:10.1093/plankt/fbv008

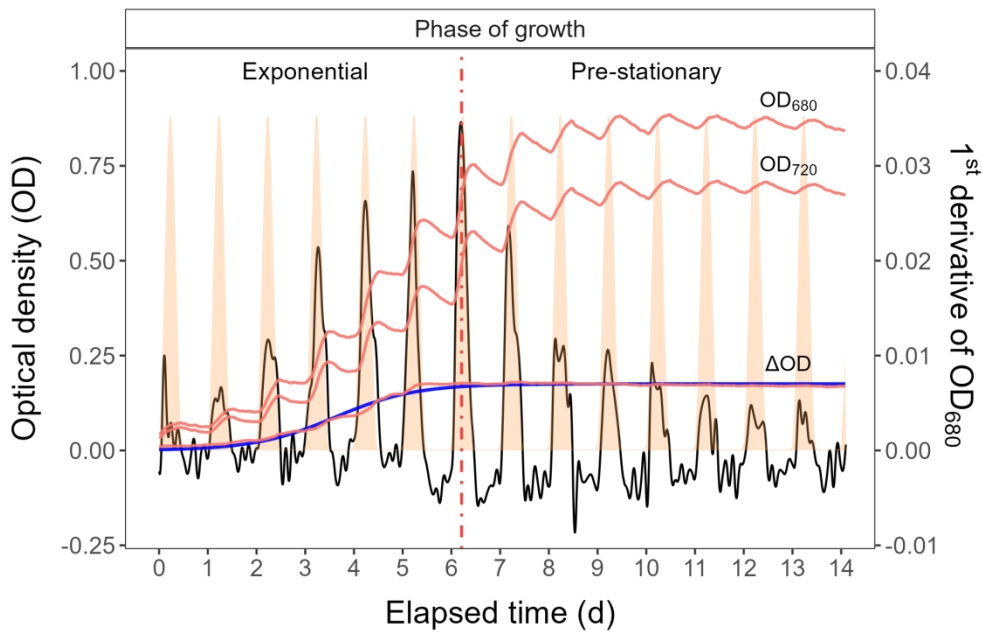
- 830 Li, W. K. W. 1995. Composition of ultraphytoplankton in the central North Atlantic. *Marine
831 Ecology Progress Series* **122**: 1–8.
- 832 Ligges, U., T. Short, P. Kienzle, and others. 2024. Signal: Signal Processing.
- 833 Litchman, E., C. A. Klausmeier, and K. Yoshiyama. 2009. Contrasting size evolution in marine
834 and freshwater diatoms. *Proceedings of the National Academy of Sciences* **106**: 2665–2670.
835 doi:10.1073/pnas.0810891106
- 836 Longobardi, L., L. Dubroca, F. Margiotta, D. Sarno, and A. Zingone. 2022. Photoperiod-driven
837 rhythms reveal multi-decadal stability of phytoplankton communities in a highly fluctuating
838 coastal environment. *Scientific Reports* **12**: 3908. doi:10.1038/s41598-022-07009-6
- 839 MacIntyre, H. L., T. M. Kana, R. J. Geider, H. L. MacIntyre, T. M. Kana, and R. J. Geider. 2000.
840 The effect of water motion on short-term rates of photosynthesis by marine phytoplankton.
841 *Trends in Plant Science* **5**: 12–17. doi:10.1016/S1360-1385(99)01504-6
- 842 Moejes, F. W., A. Matuszyńska, K. Adhikari, and others. 2017. A systems-wide understanding
843 of photosynthetic acclimation in algae and higher plants. *Journal of Experimental Botany* **68**:
844 2667–2681. doi:10.1093/jxb/erx137
- 845 Morel, A. 1978. Available, usable, and stored radiant energy in relation to marine
846 photosynthesis. *Deep Sea Research* **25**: 673–688. doi:10.1016/0146-6291(78)90623-9
- 847 Morel, A. 1988. Optical modeling of the upper ocean in relation to its biogenous matter content
848 (case I waters). *Journal of Geophysical Research: Oceans* **93**: 10749–10768.
849 doi:10.1029/JC093iC09p10749

- 850 Oxborough, K., and N. R. Baker. 1997. Resolving chlorophyll *a* fluorescence images of
851 photosynthetic efficiency into photochemical and non-photochemical components – calculation
852 of qP and Fv-/Fm-; without measuring Fo-; *Photosynthesis Research* **54**: 135–142.
853 doi:10.1023/A:1005936823310
- 854 Oxborough, K., C. M. Moore, D. J. Suggett, T. Lawson, H. G. Chan, and R. J. Geider. 2012.
855 Direct estimation of functional PSII reaction center concentration and PSII electron flux on a
856 volume basis: A new approach to the analysis of Fast Repetition Rate fluorometry (FRRf) data.
857 *Limnology and Oceanography: Methods* **10**: 142–154. doi:10.4319/lom.2012.10.142
- 858 Pedersen, T. L. 2024. Patchwork: The Composer of Plots.
- 859 Pick, F. R. 1991. The abundance and composition of freshwater picocyanobacteria in relation to
860 light penetration. *Limnology and Oceanography* **36**: 1457–1462. doi:10.4319/lo.1991.36.7.1457
- 861 Posit team. 2022. RStudio: Integrated development environment for r, Posit Software, PBC.
- 862 R Core Team. 2023. R: A language and environment for statistical computing, R Foundation for
863 Statistical Computing.
- 864 Reynolds, C. S. 2006. *The Ecology of Phytoplankton*, Cambridge University Press.
- 865 Ryan, J. A., J. M. Ulrich, R. Bennett, and C. Joy. 2024. Xts: eXtensible Time Series.
- 866 Sakamoto, T., and D. A. Bryant. 1999. Nitrate transport and not photoinhibition limits growth of
867 the freshwater cyanobacterium *Synechococcus* species PCC 6301 at low temperature. *Plant
868 Physiology* **119**: 785–794. doi:10.1104/pp.119.2.785

- 869 Schuurmans, R. M., J. C. P. Matthijs, and K. J. Hellingwerf. 2017. Transition from exponential
870 to linear photoautotrophic growth changes the physiology of *Synechocystis* sp. PCC 6803.
871 Photosynthesis Research **132**: 69–82. doi:10.1007/s11120-016-0329-8
- 872 Serway, R. A., C. J. Moses, and C. A. Moyer. 2004. Modern Physics, Cengage Learning.
- 873 Six, C., Z. V. Finkel, A. J. Irwin, and D. A. Campbell. 2007. Light variability illuminates niche-
874 partitioning among marine picocyanobacteria. PLOS ONE **2**: e1341.
875 doi:10.1371/journal.pone.0001341
- 876 Six, C., M. Ratin, D. Marie, and E. Corre. 2021. Marine *Synechococcus* picocyanobacteria: Light
877 utilization across latitudes. Proceedings of the National Academy of Sciences **118**: e2111300118.
878 doi:10.1073/pnas.2111300118
- 879 Śliwińska-Wilczewska, S., A. Cieszyńska, J. Maculewicz, and A. Latała. 2018a.
880 Ecophysiological characteristics of red, green, and brown strains of the Baltic
881 picocyanobacterium *Synechococcus* sp. – a laboratory study. Biogeosciences **15**: 6257–6276.
882 doi:10.5194/bg-15-6257-2018
- 883 Śliwińska-Wilczewska, S., Z. Konarzewska, K. Wiśniewska, and M. Konik. 2020.
884 Photosynthetic pigments changes of three phenotypes of picocyanobacteria *Synechococcus* sp.
885 Under different light and temperature conditions. Cells **9**: 2030. doi:10.3390/cells9092030
- 886 Śliwińska-Wilczewska, S., J. Maculewicz, A. Barreiro Felpeto, and A. Latała. 2018b.
887 Allelopathic and bloom-forming picocyanobacteria in a changing world. Toxins **10**: 48.
888 doi:10.3390/toxins10010048

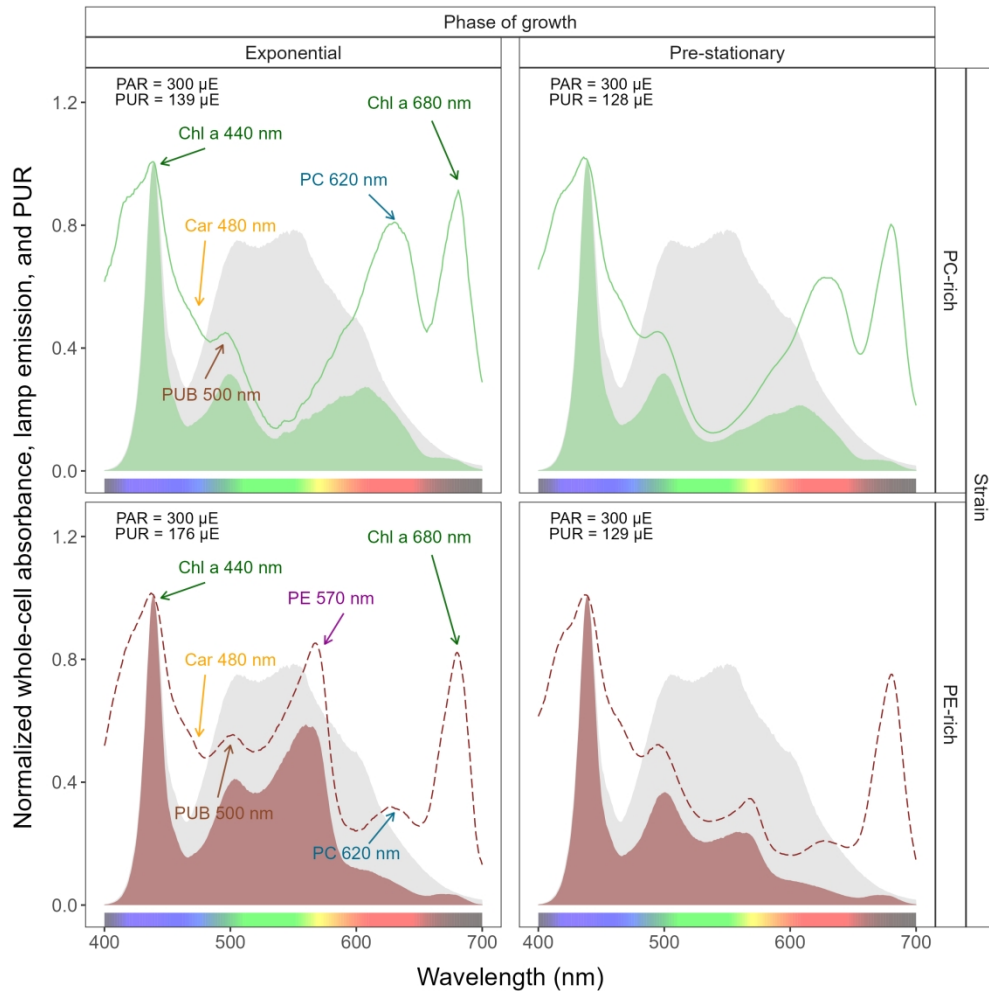
- 889 Stadnichuk, I. N., P. M. Krasilnikov, and D. V. Zlenko. 2015. Cyanobacterial phycobilisomes
890 and phycobiliproteins. *Microbiology* **84**: 101–111. doi:10.1134/S0026261715020150
- 891 Stomp, M., J. Huisman, L. Vörös, F. R. Pick, M. Laamanen, T. Haverkamp, and L. J. Stal. 2007.
892 Colourful coexistence of red and green picocyanobacteria in lakes and seas. *Ecology Letters* **10**:
893 290–298. doi:10.1111/j.1461-0248.2007.01026.x
- 894 Strickland, J. D., and T. R. Parsons. 1972. Practical Hand Book of Seawater Analysis. Fisheries
895 Research Board of Canada **167 (2nd edition)**: 1–311. doi:DOI: <http://dx.doi.org/10.25607/OBP-1791>
- 896
- 897 Theus, M. E., T. J. Layden, N. McWilliams, S. Crafton-Tempel, C. T. Kremer, and S. B. Fey.
898 2022. Photoperiod influences the shape and scaling of freshwater phytoplankton responses to
899 light and temperature. *Oikos* **2022**: e08839. doi:10.1111/oik.08839
- 900 Torremorell, A., M. E. Llames, G. L. Pérez, R. Escaray, J. Bustingorry, and H. Zagarese. 2009.
901 Annual patterns of phytoplankton density and primary production in a large, shallow lake: The
902 central role of light. *Freshwater Biology* **54**: 437–449. doi:10.1111/j.1365-2427.2008.02119.x
- 903 Tortell, P., and D. J. Suggett. 2021. A user guide for the application of Single Turnover active
904 chlorophyll fluorescence for phytoplankton productivity measurements. Version 1. Report
905 Scientific Committee on Oceanic Research (SCOR) Working Group 156.
- 906 van Alphen, P., H. Abedini Najafabadi, F. Branco dos Santos, and K. J. Hellingwerf. 2018.
907 Increasing the photoautotrophic growth rate of *Synechocystis* sp. PCC 6803 by identifying the
908 limitations of its cultivation. *Biotechnology Journal* **13**: 1700764. doi:10.1002/biot.201700764

- 909 Velichko, N., S. Smirnova, S. Averina, and A. Pinevich. 2021. A survey of Antarctic
910 cyanobacteria. *Hydrobiologia* **848**: 2627–2653.
- 911 Vincent, W. F., J. P. Bowman, L. M. Rankin, and T. A. McMeekin. 2000. Phylogenetic diversity
912 of picocyanobacteria in Arctic and Antarctic ecosystems. *Microbial biosystems: new frontiers.*
913 Proceedings of the 8th International Symposium on Microbial Ecology 317–322.
- 914 Wickham, H. 2016. Data Analysis, p. 189–201. *In* H. Wickham [ed.], *Ggplot2: Elegant Graphics*
915 for Data Analysis. Springer International Publishing.
- 916 Wood, S. N. 2017. Generalized Additive Models: An Introduction with R, Second Edition, 2nd
917 ed. Chapman and Hall/CRC.
- 918 Xi, H., S. N. Losa, A. Mangin, and others. 2020. Global retrieval of phytoplankton functional
919 types based on empirical orthogonal functions using CMEMS GlobColour merged products and
920 further extension to OLCI data. *Remote Sensing of Environment* **240**: 111704.
921 doi:10.1016/j.rse.2020.111704
- 922 Xu, K., J. L. Grant-Burt, N. Donaher, and D. A. Campbell. 2017. Connectivity among
923 Photosystem II centers in phytoplankters: Patterns and responses. *Biochimica et Biophysica Acta*
924 (BBA) - Bioenergetics **1858**: 459–474. doi:10.1016/j.bbabi.2017.03.003
- 925 Xu, K., J. Lavaud, R. Perkins, E. Austen, M. Bonnanfant, and D. A. Campbell. 2018.
926 Phytoplankton σ PSII and excitation dissipation; implications for estimates of primary
927 productivity. *Frontiers in Marine Science* **5**. doi:10.3389/fmars.2018.00281



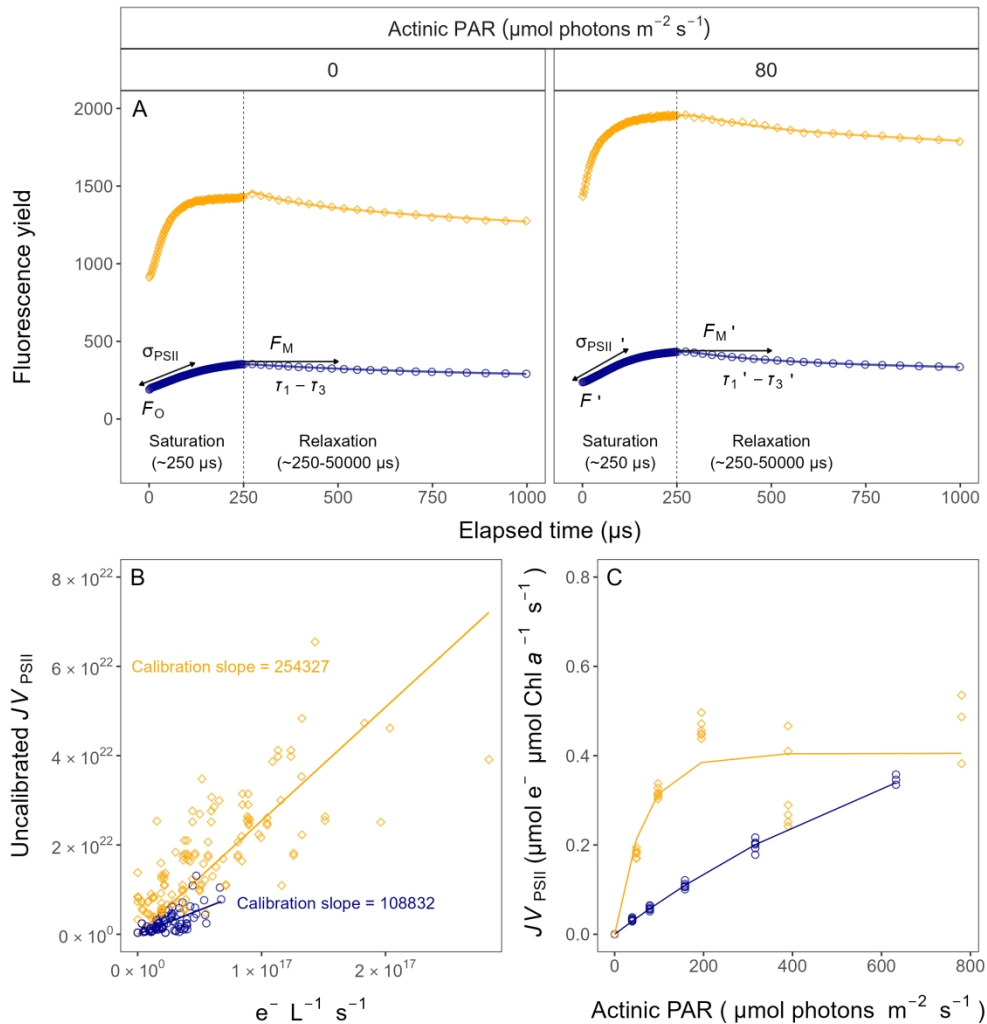
Example of a growth curve (tracked as OD₇₂₀, OD₆₈₀, or Δ OD; red solid lines, left y-axis) of PE-rich culture of *Synechococcus* sp. (048) vs. elapsed time (d, x-axis).

452x290mm (118 x 118 DPI)



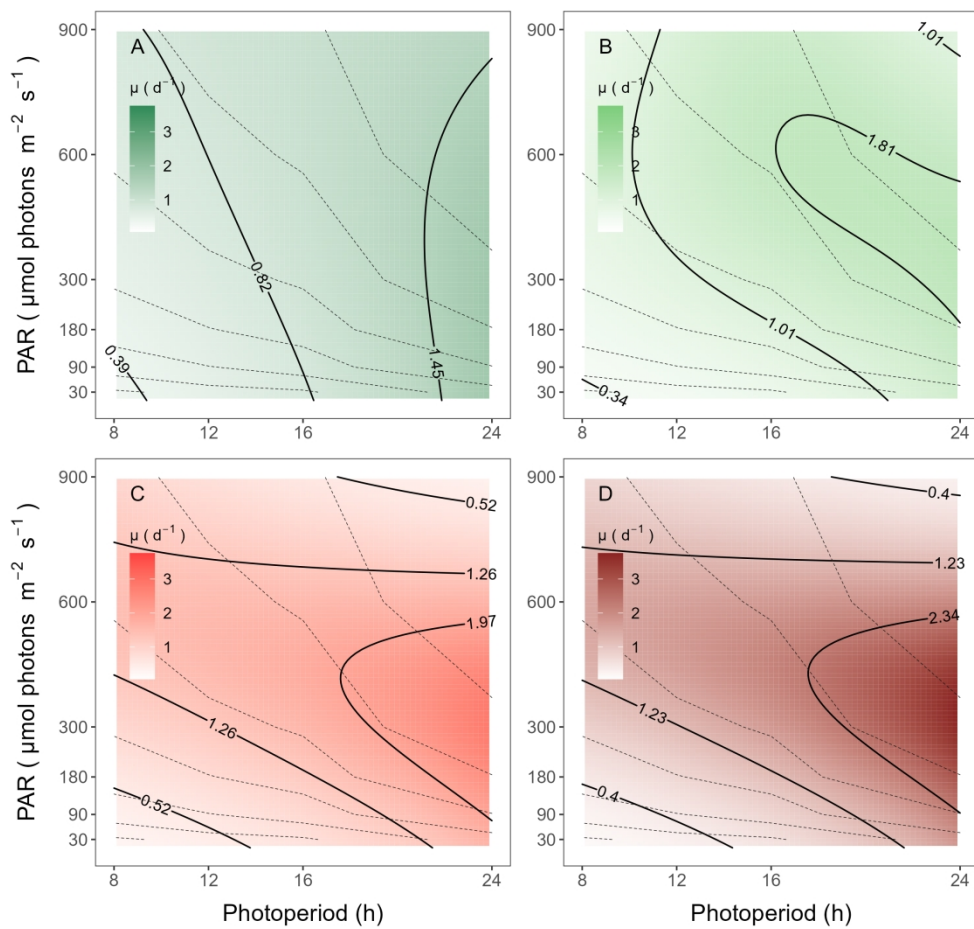
Whole-cell absorbance spectra of PC-rich (solid green lines) or PE-rich (dashed red lines) cultures of *Synechococcus* sp.

581x581mm (118 x 118 DPI)



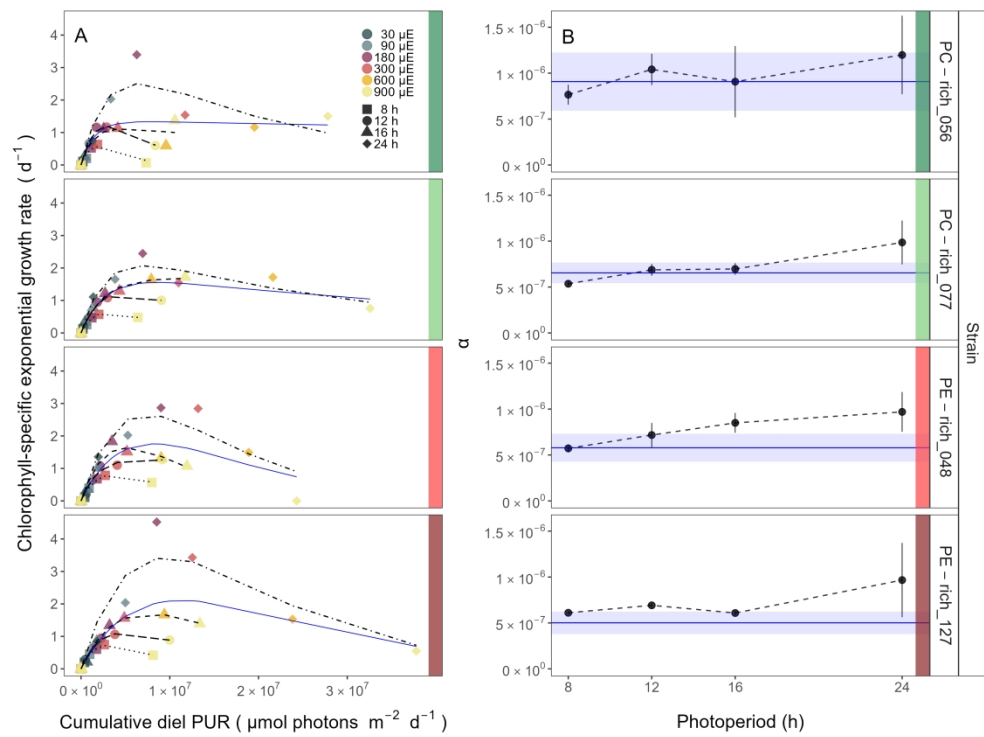
Single turnover (ST) fluorescence induction by Fast Repetition Rate fluorometry (FRRf).

613x645mm (118 x 118 DPI)



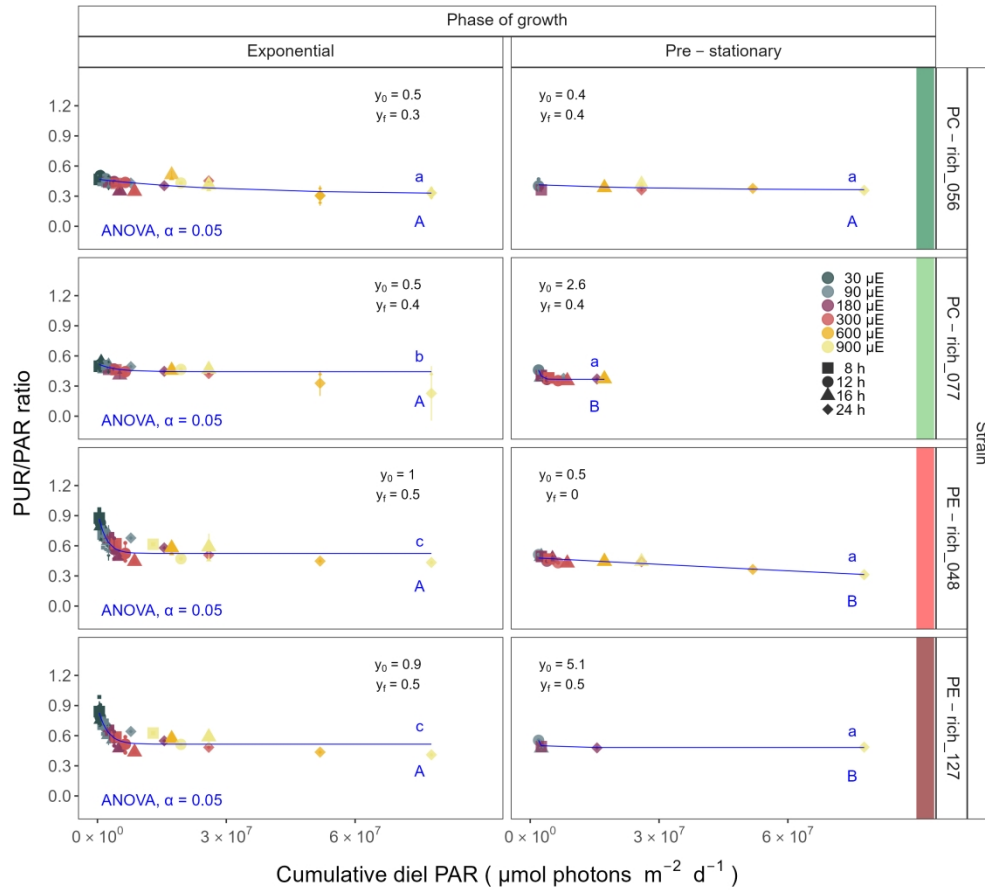
A contour plot of a Generalized Additive Model (GAM) of chlorophyll-specific growth rates (d^{-1}) for two PC-rich cultures: (A) 056, (B) 077 and two PE-rich cultures: (C) 048, (D) 127 of *Synechococcus* sp. originating from the Baltic Sea.

613x581mm (118 x 118 DPI)



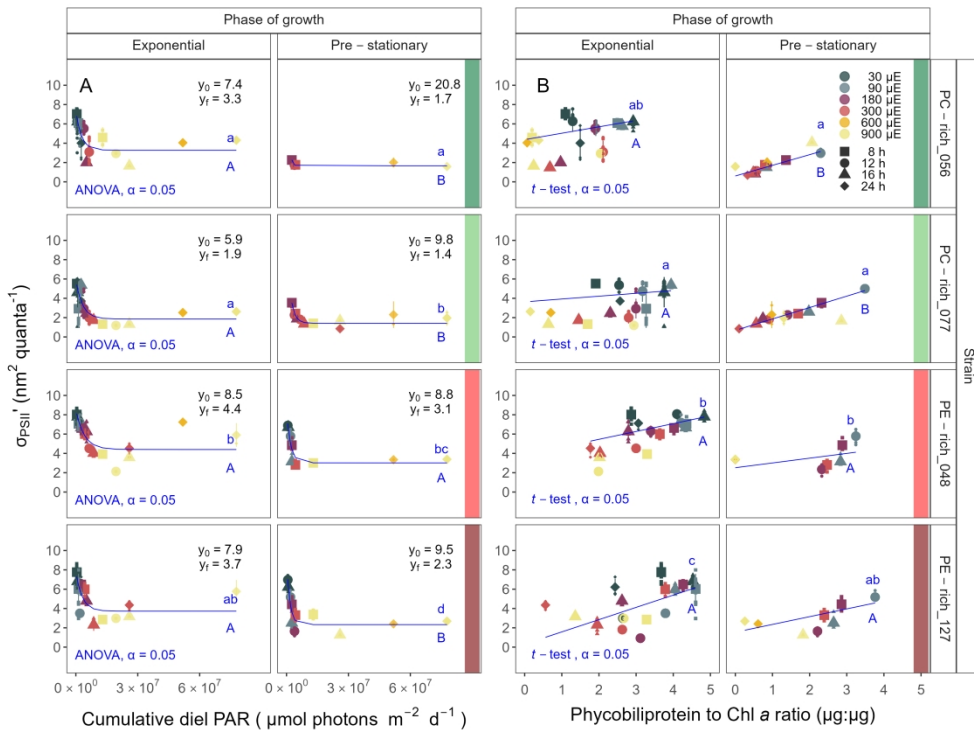
Chlorophyll-specific exponential growth rates (d^{-1}) vs. cumulative diel Photosynthetically Usable Radiation (PUR, $\mu\text{mol photons m}^{-2} d^{-1}$).

774x581mm (118 x 118 DPI)



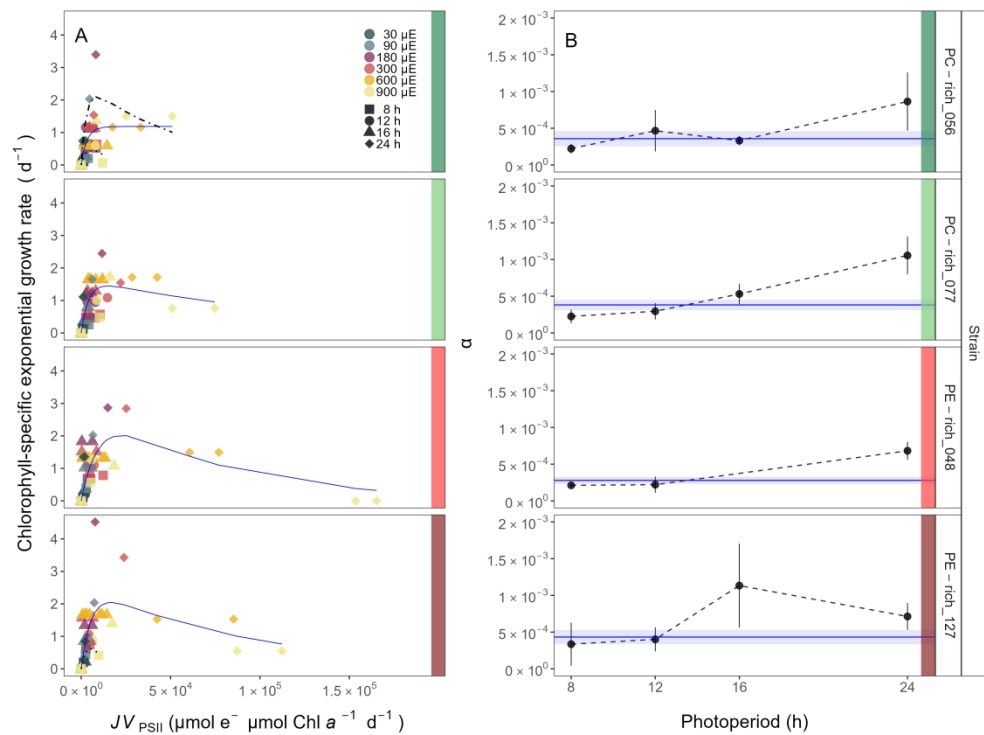
Changes in PUR/PAR ratio vs. cumulative diel PAR ($\mu\text{mol photons m}^{-2}\text{d}^{-1}$).

645x581mm (118 x 118 DPI)



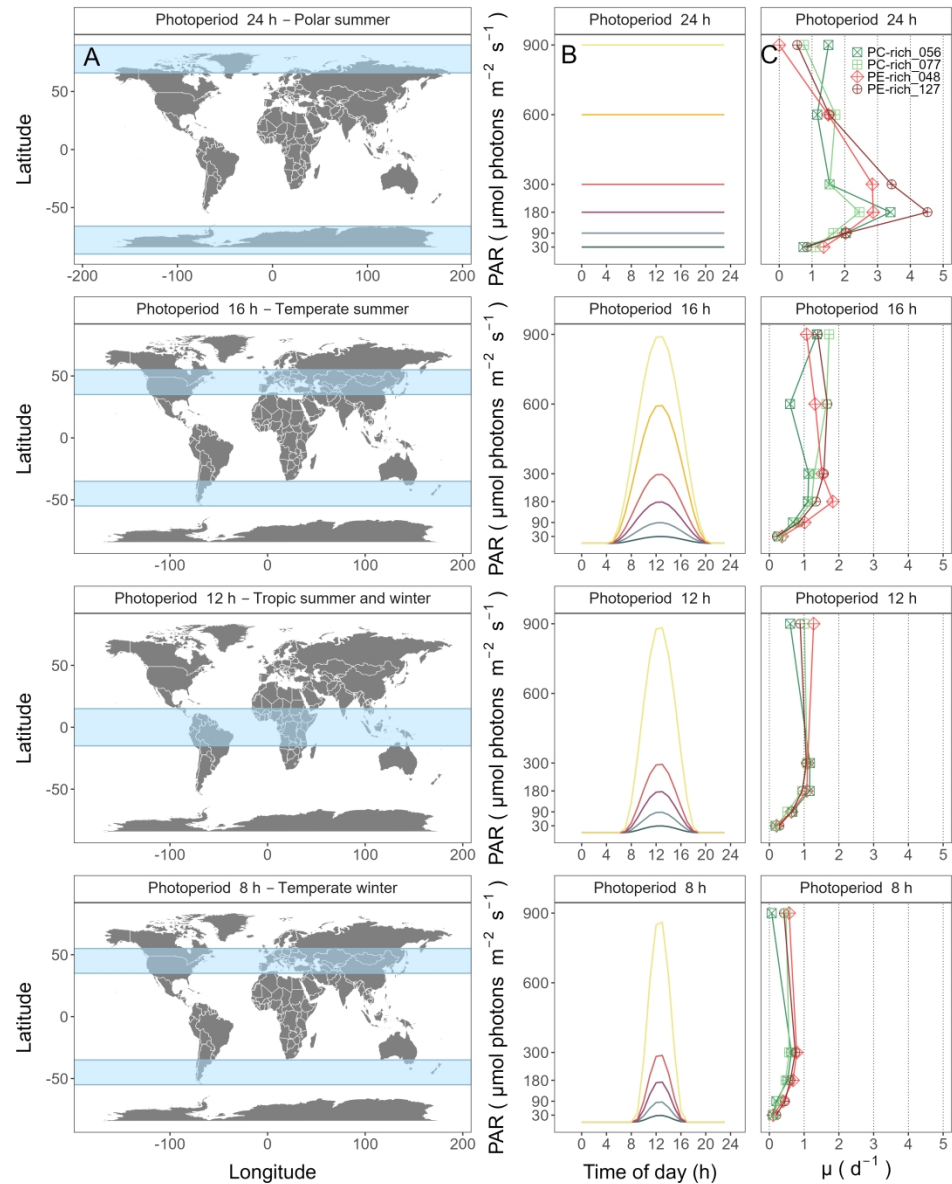
Effective absorption cross section of PSII ($\sigma_{\text{PSII}'}$; $\text{nm}^2 \text{ quanta}^{-1}$) measured under diel peak PAR growth light.

774x581mm (118 x 118 DPI)



Chlorophyll-specific exponential growth rates (d^{-1}) vs. cumulative diel PSII electron flux (JV_{PSII} ; $\mu\text{mol e}^- \mu\text{mol Chl } a^{-1} d^{-1}$) measured under diel peak PAR growth light.

774x581mm (118 x 118 DPI)



Latitudinal bands, equivalent summer or winter photoperiods, and picocyanobacterial growth responses.

774x968mm (118 x 118 DPI)

1 **Growth yields and light-capture in PhycoCyanin and**
2 **PhycoErythrin-rich picocyanobacteria, across photic**
3 **regimes and growth phases**

4

5 **Sylwia Śliwińska-Wilczewska^{1,2}, Marta Konik^{3,4}, Mireille Savoie¹, Anabella**
6 **Aguilera^{5,6§}, Naaman M. Omar¹, and Douglas A. Campbell^{1,*}**

7

8 ¹ Department of Biology, Mount Allison University, 53 York St., Sackville, NB, E4L 1C9,
9 Canada

10 ² Institute of Oceanography, University of Gdańsk, 46 Piłsudskiego St, 81-378, Gdynia, Poland

11 ³ Department of Geography, University of Victoria, Victoria, BC, V8P 5C2, Canada

12 ⁴ Institute of Oceanology, Polish Academy of Sciences, 81-712 Sopot, Poland

13 ⁵ Department of Biology and Environmental Science, Centre for Ecology and Evolution in
14 Microbial Model Systems (EEMiS), Linnaeus University, Kalmar, Sweden

15 ^{6§} Department of Aquatic Sciences and Assessment, Swedish University of Agricultural
16 Sciences, Uppsala, Sweden

17 * Correspondence: Douglas A. Campbell: dubhglascambeuil@gmail.com

18

19 **Running head:** *Picocyanobacteria across photic regimes*

20 **Keywords:** Cumulative diel photon dose; Light-capture, PAR; Photic regime; Phase of growth;
21 Photoperiod; Picocyanobacteria; PUR

22 ***Supporting Information***

23

For Review Only

25 **Tab. S1.** Linear regression, coefficient of determination (R square), Pearson correlation coefficients (R), and *p*-value
 26 used to calculate the pigment content ($\mu\text{g mL}^{-1}$) of two PhycoCyanin(PC)-rich cultures (056, 077) and two
 27 PhycoErythrin(PE)-rich cultures (048, 127) (Culture Collection of Baltic Algae) of *Synechococcus* sp. based on
 28 absorbance (A) measurements.
 29

Pigment	Abs	Linear_regression	R_square	R	<i>p</i> _value
Chl a	665	Chl a $\mu\text{g/mL} = (\text{Abs}_{665} * 13.411029) + 0.154793$	0.865	0.930	0.000
Car	480	Car $\mu\text{g/mL} = (\text{Abs}_{480} * 5.469880) + 0.089971$	0.791	0.890	0.000
PE	565	PE $\mu\text{g/mL} = (\text{Abs}_{565} * 26.760737) - 0.143872$	0.698	0.840	0.000
PC	620	PC $\mu\text{g/mL} = (\text{Abs}_{620} * 29.979866) - 0.182611$	0.807	0.900	0.000
APC	650	APC $\mu\text{g/mL} = (\text{Abs}_{650} * 3.873803) + 0.021964$	0.087	0.300	0.000

30
 31 **Tab. S2.** Three-way factorial ANOVA testing whether peak PAR, photoperiod, strain, and their interactions
 32 (Source_of_variation), significantly influence the chlorophyll specific exponential growth rate ($\mu; \text{d}^{-1}$), estimated
 33 from logistic fits of chlorophyll proxy OD₆₈₀ – OD₇₂₀ vs. cumulative diel PUR, for two PhycoCyanin(PC)-rich
 34 cultures (056, 077) and two PhycoErythrin(PE)-rich cultures (048, 127) (Culture Collection of Baltic Algae) of
 35 *Synechococcus* sp., grown at 30, 90, 180, 300, 600, or 900 peak PAR $\mu\text{mol photons m}^{-2}\text{s}^{-1}$; and photoperiods of 8,
 36 12, 16, or 24 h. Df – degrees of freedom; Sum Sq – sum of squares; Mean Sq – mean sum of squares; *F*_value –
 37 Fisher's *F*-test statistic; *p*_value - level of significance.
 38

Source_of_variation	Df	Sum Sq	Mean Sq	<i>F</i> _value	<i>p</i> _value
Par_ue	5	0.049	0.010	3.276e+30	0.000
Photoperiod	3	0.076	0.025	8.367e+30	0.000
Strain	3	0.003	0.001	3.151e+29	0.000
Par_ue:Photoperiod	13	0.040	0.003	1.025e+30	0.000
Par_ue:Strain	15	0.007	0.000	1.593e+29	0.000
Photoperiod:Strain	9	0.004	0.000	1.306e+29	0.000
Par_ue:Photoperiod:Strain	39	0.017	0.000	1.434e+29	0.000
Residuals	88	0.000	0.000	NA	N/A

39

41 **Tab. S3.** One-way ANOVA of a three parameter model (Harrison and Platt 1986) from pooled data (All) and data fit
 42 across different photoperiods (8, 12, 16, or 24) from chlorophyll specific exponential growth rate vs. cumulative diel
 43 PUR (Fit_model), for two PhycoCyanin(PC)-rich cultures (056, 077) and two PhycoErythrin(PE)-rich cultures (048,
 44 127) of *Synechococcus* sp., grown at 30, 90, 180, 300, 600, or 900 peak PAR $\mu\text{mol photons m}^{-2}\text{s}^{-1}$; and
 45 photoperiods of 8, 12, 16, or 24 h. Res.Df - residual degrees of freedom for each model; Res.Sum Sq - residual sum
 46 of squares for each model; F _value – Fisher's F -test statistic; p _value - level of significance.
 47

Strain	Fit_model	Res.Df	Res.Sum Sq	F _value	p _value
PC-rich_056	8_All	41	8.063	1.807e+03	0.000
PC-rich_056	12_All	41	8.063	2.822e+01	0.001
PC-rich_056	16_All	41	8.063	8.566e+00	0.012
PC-rich_056	24_All	41	8.063	2.333e+01	0.001
PC-rich_077	8_All	41	3.015	6.193e+01	0.000
PC-rich_077	12_All	41	3.015	2.477e+01	0.001
PC-rich_077	16_All	41	3.015	1.855e+01	0.002
PC-rich_077	24_All	41	3.015	1.073e+01	0.007
PE-rich_048	8_All	41	6.731	1.443e+01	0.004
PE-rich_048	12_All	41	6.731	8.361e+01	0.000
PE-rich_048	16_All	41	6.731	8.403e+00	0.013
PE-rich_048	24_All	41	6.731	8.234e+01	0.000
PE-rich_127	8_All	41	13.016	1.453e+02	0.000
PE-rich_127	12_All	41	13.016	2.060e+03	0.000
PE-rich_127	16_All	41	13.016	6.908e+00	0.020
PE-rich_127	24_All	41	13.016	7.812e+01	0.000



48
 49
 50
 51
 52
 53
 54
 55
 56
 57
 58

60 **Tab. S4.** One-way ANOVA of a three parameter model (Harrison and Platt 1986) from pooled data (All) and data fit
 61 across different peak PAR (30, 90, 180, 300, 600 together with 900) from chlorophyll specific exponential growth
 62 rate vs. cumulative diel PUR (Fit_model), for two PhycoCyanin(PC)-rich cultures (056, 077) and two
 63 PhycoErythrin(PE)-rich cultures (048, 127) of *Synechococcus* sp., grown at 30, 90, 180, 300, 600, or 900 peak PAR
 64 $\mu\text{mol photons m}^{-2}\text{s}^{-1}$; and photoperiods of 8, 12, 16, or 24 h. Res.Df - residual degrees of freedom for each model;
 65 Res.Sum Sq - residual sum of squares for each model; F _value – Fisher's F -test statistic; p _value - level of
 66 significance.
 67

Strain	Fit_model	Res.Df	Res.Sum Sq	F _value	p _value
PC-rich_056	30_All	41	8.063	1.807e+03	0.000
PC-rich_056	90_All	41	8.063	2.822e+01	0.001
PC-rich_056	180_All	41	8.063	8.566e+00	0.012
PC-rich_056	300_All	41	8.063	2.333e+01	0.001
PC-rich_056	900_All	41	8.063	3.360e+00	0.030
PC-rich_077	30_All	41	3.015	6.193e+01	0.000
PC-rich_077	90_All	41	3.015	2.477e+01	0.001
PC-rich_077	180_All	41	3.015	1.855e+01	0.002
PC-rich_077	300_All	41	3.015	1.073e+01	0.007
PC-rich_077	900_All	41	3.015	6.508e-01	0.822
PE-rich_048	30_All	41	6.731	1.443e+01	0.004
PE-rich_048	90_All	41	6.731	8.361e+01	0.000
PE-rich_048	180_All	41	6.731	8.403e+00	0.013
PE-rich_048	300_All	41	6.731	8.234e+01	0.000
PE-rich_048	900_All	41	6.731	1.357e+00	0.328
PE-rich_127	30_All	41	13.016	1.453e+02	0.000
PE-rich_127	90_All	41	13.016	2.060e+03	0.000
PE-rich_127	180_All	41	13.016	6.908e+00	0.020
PE-rich_127	300_All	41	13.016	7.812e+01	0.000
PE-rich_127	900_All	41	13.016	3.523e+00	0.026

68

69

71 **Tab. S5.** One-way ANOVA of a three parameter model (Harrison and Platt 1986) from pooled data (All) and data fit
 72 across different photoperiods (8, 12, 16, or 24) from chlorophyll specific exponential growth rate vs. cumulative diel
 73 PAR (Fit_model), for two PhycoCyanin(PC)-rich cultures (056, 077) and two PhycoErythrin(PE)-rich cultures (048,
 74 127) of *Synechococcus* sp., grown at 30, 90, 180, 300, 600, or 900 peak PAR $\mu\text{mol photons m}^{-2}\text{s}^{-1}$; and
 75 photoperiods of 8, 12, 16, or 24 h. Res.Df - residual degrees of freedom for each model; Res.Sum Sq - residual sum
 76 of squares for each model; F _value – Fisher's F -test statistic; p _value - level of significance.
 77

Strain	Fit_model	Res.Df	Res.Sum Sq	F _value	p _value
PC-rich_056	8_All	135	18.854	1.089e+03	0.000
PC-rich_056	12_All	135	18.854	1.412e+01	0.000
PC-rich_056	16_All	135	18.854	7.420e+00	0.000
PC-rich_056	24_All	135	18.854	1.279e+01	0.000
PC-rich_077	8_All	131	5.672	2.749e+01	0.000
PC-rich_077	12_All	131	5.672	8.972e+00	0.000
PC-rich_077	16_All	131	5.672	5.640e+00	0.000
PC-rich_077	24_All	131	5.672	4.027e+00	0.000
PE-rich_048	8_All	133	16.660	2.122e+01	0.000
PE-rich_048	12_All	133	16.660	1.997e+01	0.000
PE-rich_048	16_All	133	16.660	3.576e+00	0.000
PE-rich_048	24_All	133	16.660	8.068e+01	0.000
PE-rich_127	8_All	133	26.508	6.568e+01	0.000
PE-rich_127	12_All	133	26.508	6.758e+03	0.000
PE-rich_127	16_All	133	26.508	1.515e+01	0.000
PE-rich_127	24_All	133	26.508	5.207e+01	0.000



78
 79

81 **Tab. S6.** One-way ANOVA of a three parameter model (Harrison and Platt 1986) from pooled data (All) and data fit
 82 across different peak PAR (30, 90, 180, 300, 600 together with 900) from chlorophyll specific exponential growth
 83 rate vs. cumulative diel PAR (Fit_model), for two PhycoCyanin(PC)-rich cultures (056, 077) and two
 84 PhycoErythrin(PE)-rich cultures (048, 127) of *Synechococcus* sp., grown at 30, 90, 180, 300, 600, or 900 peak PAR
 85 $\mu\text{mol photons m}^{-2}\text{s}^{-1}$; and photoperiods of 8, 12, 16, or 24 h. Res.Df - residual degrees of freedom for each model;
 86 Res.Sum Sq - residual sum of squares for each model; F_{value} – Fisher's F -test statistic; p_{value} - level of
 87 significance.
 88

Strain	Fit_model	Res.Df	Res.Sum Sq	F_{value}	p_{value}
PC-rich_056	30_All	135	18.854	1.089e+03	0.000
PC-rich_056	90_All	135	18.854	1.412e+01	0.000
PC-rich_056	180_All	135	18.854	7.420e+00	0.000
PC-rich_056	300_All	135	18.854	1.279e+01	0.000
PC-rich_056	900_All	135	18.854	2.573e+00	0.003
PC-rich_077	30_All	131	5.672	2.749e+01	0.000
PC-rich_077	90_All	131	5.672	8.972e+00	0.000
PC-rich_077	180_All	131	5.672	5.640e+00	0.000
PC-rich_077	300_All	131	5.672	4.027e+00	0.000
PC-rich_077	900_All	131	5.672	7.428e-01	0.844
PE-rich_048	30_All	133	16.660	2.122e+01	0.000
PE-rich_048	90_All	133	16.660	1.997e+01	0.000
PE-rich_048	180_All	133	16.660	3.576e+00	0.000
PE-rich_048	300_All	133	16.660	8.068e+01	0.000
PE-rich_048	900_All	133	16.660	1.893e+00	0.034
PE-rich_127	30_All	133	26.508	6.568e+01	0.000
PE-rich_127	90_All	133	26.508	6.758e+03	0.000
PE-rich_127	180_All	133	26.508	1.515e+01	0.000
PE-rich_127	300_All	133	26.508	5.207e+01	0.000
PE-rich_127	900_All	133	26.508	2.800e+00	0.002

89

90

92 **Tab. S7.** One-way ANOVA of a three parameter model (Harrison and Platt 1986) from pooled data (All) and data fit
 93 across different photoperiods (8, 12, 16, or 24) from chlorophyll specific exponential growth rate vs. PSII electron
 94 flux (JV_{PSII} ; $\mu\text{mol e}^- \mu\text{mol Chl } a^{-1} d^{-1}$) (Fit_model), for two PhycoCyanin(PC)-rich cultures (056, 077) and two
 95 PhycoErythrin(PE)-rich cultures (048, 127) of *Synechococcus* sp., grown at 30, 90, 180, 300, 600, or 900 peak PAR
 96 $\mu\text{mol photons m}^{-2}\text{s}^{-1}$; and photoperiods of 8, 12, 16, or 24 h. Res.Df - residual degrees of freedom for each model;
 97 Res.Sum Sq - residual sum of squares for each model; F _value – Fisher's F -test statistic; p _value - level of
 98 significance.
 99

Strain	Fit_model	Res.Df	Res.Sum Sq	F _value	p _value
PC-rich_056	8_All	61	11.802	3.972e+00	0.016
PC-rich_056	12_All	61	11.802	7.712e-01	0.730
PC-rich_056	16_All	61	11.802	2.287e-01	1.000
PC-rich_056	24_All	61	11.802	3.332e+00	0.037
PC-rich_077	8_All	61	9.014	1.125e+00	0.459
PC-rich_077	12_All	61	9.014	1.377e+00	0.350
PC-rich_077	16_All	61	9.014	6.146e-01	0.861
PC-rich_077	24_All	61	9.014	1.562e+00	0.260
PE-rich_048	8_All	61	16.583	1.332e+00	0.339
PE-rich_048	12_All	61	16.583	1.977e+00	0.174
PE-rich_048	16_All	61	16.583	5.540e-01	0.903
PE-rich_048	24_All	61	16.583	6.716e-01	0.817
PE-rich_127	8_All	53	21.117	7.994e+00	0.004
PE-rich_127	12_All	53	21.117	4.159e+00	0.057
PE-rich_127	16_All	53	21.117	5.525e-01	0.882
PE-rich_127	24_All	53	21.117	1.100e+00	0.504

100

101

103 **Tab. S8.** One-way ANOVA of a three parameter model (Harrison and Platt 1986) from pooled data (All) and data fit
 104 across different peak PAR (30, 90, 180, 300, 600 together with 900) from chlorophyll specific exponential growth
 105 rate vs. PSII electron flux (JV_{PSII} ; $\mu\text{mol e}^{-} \mu\text{mol Chl } a^{-1} d^{-1}$) (Fit_model), for two PhycoCyanin(PC)-rich cultures
 106 (056, 077) and two PhycoErythrin(PE)-rich cultures (048, 127) of *Synechococcus* sp., grown at 30, 90, 180, 300,
 107 600, or 900 peak PAR $\mu\text{mol photons m}^{-2}s^{-1}$; and photoperiods of 8, 12, 16, or 24 h. Res.Df - residual degrees of
 108 freedom for each model; Res.Sum Sq - residual sum of squares for each model; F_value – Fisher's F-test statistic;
 109 p_value - level of significance.

110

Strain	Fit_model	Res.Df	Res.Sum Sq	F_value	p_value
PC-rich_056	30_All	61	11.802	3.972e+00	0.016
PC-rich_056	90_All	61	11.802	7.712e-01	0.730
PC-rich_056	180_All	61	11.802	2.287e-01	1.000
PC-rich_056	300_All	61	11.802	3.332e+00	0.037
PC-rich_056	900_All	61	11.802	2.156e+00	0.044
PC-rich_077	30_All	61	9.014	1.125e+00	0.459
PC-rich_077	90_All	61	9.014	1.377e+00	0.350
PC-rich_077	180_All	61	9.014	6.146e-01	0.861
PC-rich_077	300_All	61	9.014	1.562e+00	0.260
PC-rich_077	900_All	61	9.014	1.295e+00	0.287
PE-rich_048	30_All	61	16.583	1.332e+00	0.339
PE-rich_048	90_All	61	16.583	1.977e+00	0.174
PE-rich_048	180_All	61	16.583	5.540e-01	0.903
PE-rich_048	300_All	61	16.583	6.716e-01	0.817
PE-rich_048	900_All	61	16.583	3.125e+00	0.007
PE-rich_127	30_All	53	21.117	7.994e+00	0.004
PE-rich_127	90_All	53	21.117	4.159e+00	0.057
PE-rich_127	180_All	53	21.117	5.525e-01	0.882
PE-rich_127	300_All	53	21.117	1.100e+00	0.504
PE-rich_127	900_All	53	21.117	3.784e+00	0.002

111

112

114 **Tab. S9.** One-way ANOVA of single phase exponential decay fit model (Fit_model) of pooled data across different
 115 strains for a given phase of growth (exponential; _Exp, pre-stationary; _St) and across different phase of growth for
 116 a given strain (_Exp_St) from PUR/PAR ratio in relation to the cumulative diel PAR ($\mu\text{mol photons m}^{-2}\text{d}^{-1}$), for two
 117 PhycoCyanin(PC)-rich cultures (056, 077) and two PhycoErythrin(PE)-rich cultures (048, 127) of *Synechococcus*
 118 sp., grown at 30, 90, 180, 300, 600, or 900 peak PAR $\mu\text{mol photons m}^{-2}\text{s}^{-1}$; and photoperiods of 8, 12, 16, or 24 h.
 119 Res.Df - residual degrees of freedom for each model; Res.Sum Sq - residual sum of squares for each model; F_value
 120 – Fisher's F-test statistic; p_value - level of significance.

121

Fit_model	Res.Df	Res.Sum Sq	F_value	p_value
056_077_Exp	43	0.025	2.813e+01	0.000
048_127_Exp	51	0.217	NA	N/A
056_048_Exp	51	0.307	2.762e+01	0.000
077_048_Exp	51	0.307	5.976e+01	0.000
056_127_Exp	51	0.217	1.607e+01	0.000
077_127_Exp	51	0.217	4.064e+01	0.000
056_077_St	20	0.006	-1.491e-01	1.000
048_127_St	2	0.000	5.386e+00	0.168
056_048_St	17	0.009	9.648e-02	0.999
077_048_St	17	0.009	-2.066e+00	1.000
056_127_St	2	0.000	1.415e+01	0.067
077_127_St	2	0.000	2.812e+00	0.294
056_Exp_St	7	0.008	1.882e+00	0.195
077_Exp_St	20	0.006	3.039e+00	0.007
048_Exp_St	17	0.009	1.681e+01	0.000
127_Exp_St	2	0.000	4.128e+01	0.024

122

123

125 **Tab. S10.** One-way ANOVA of single phase exponential decay fit model (Fit_model) of pooled data across
 126 different strains for a given phase of growth (exponential; _Exp, pre-stationary; _St) and across different phase of
 127 growth for a given strain (_Exp_St) from Phycobiliprotein to Chl a ratio in relation to the cumulative diel PAR
 128 ($\mu\text{mol photons m}^{-2}\text{d}^{-1}$), for two PhycoCyanin(PC)-rich cultures (056, 077) and two PhycoErythrin(PE)-rich
 129 cultures (048, 127) of *Synechococcus* sp., grown at 30, 90, 180, 300, 600, or 900 peak PAR $\mu\text{mol photons m}^{-2}\text{s}^{-1}$;
 130 and photoperiods of 8, 12, 16, or 24 h. Res.Df - residual degrees of freedom for each model; Res.Sum Sq - residual
 131 sum of squares for each model; F _value – Fisher's F -test statistic; p _value - level of significance.
 132

Fit_model	Res.Df	Res.Sum Sq	F _value	p _value
056_077_Exp	49	38.089	1.531e+01	0.000
048_127_Exp	52	54.559	NA	N/A
056_048_Exp	52	39.302	4.333e+00	0.005
077_048_Exp	52	39.302	5.202e-01	0.670
056_127_Exp	52	54.559	1.067e+01	0.000
077_127_Exp	52	54.559	7.063e+00	0.000
056_077_St	24	3.580	-1.005e+01	1.000
048_127_St	19	3.343	NA	N/A
056_048_St	19	2.239	-2.229e-01	1.000
077_048_St	19	2.239	2.276e+00	0.088
056_127_St	19	3.343	-1.195e+00	1.000
077_127_St	19	3.343	2.686e-01	0.925
056_Exp_St	25	2.081	1.399e+01	0.000
077_Exp_St	24	3.580	9.255e+00	0.000
048_Exp_St	19	2.239	9.531e+00	0.000
127_Exp_St	19	3.343	8.820e+00	0.000

133

134

136 **Tab. S11.** One-way ANOVA of single phase exponential decay fit model (Fit_model) of pooled data across
 137 different strains for a given phase of growth (exponential; _Exp, pre-stationary; _St) and across different phase of
 138 growth for a given strain (_Exp_St) from effective absorption cross section of PSII (σ_{PSII}' ; nm² quanta⁻¹) measured
 139 under diel peak PAR growth light under Ex590nm (orange) excitation in relation to the cumulative diel PAR (μmol
 140 photons m⁻²d⁻¹), for two PhycoCyanin(PC)-rich cultures (056, 077) and two PhycoErythrin(PE)-rich cultures (048,
 141 127) of *Synechococcus* sp., grown at 30, 90, 180, 300, 600, or 900 peak PAR μmol photons m⁻²s⁻¹; and
 142 photoperiods of 8, 12, 16, or 24 h. Res.Df - residual degrees of freedom for each model; Res.Sum Sq - residual sum
 143 of squares for each model; F_value – Fisher's F-test statistic; p_value - level of significance.

144

Fit_model	Res.Df	Res.Sum Sq	F_value	p_value
056_077_Exp	97	116.359	9.926e-01	0.469
048_127_Exp	72	106.728	-1.652e+00	1.000
056_048_Exp	97	116.359	3.764e+01	0.000
077_048_Exp	112	134.219	8.037e+00	0.000
056_127_Exp	72	106.728	2.599e-01	1.000
077_127_Exp	72	106.728	4.636e-01	0.995
056_077_St	41	3.366	1.522e+01	0.000
048_127_St	45	38.775	3.762e+00	0.001
056_048_St	34	17.489	1.158e+02	0.000
077_048_St	34	17.489	-3.922e+00	1.000
056_127_St	45	38.775	1.566e+02	0.000
077_127_St	45	38.775	1.078e+02	0.000
056_Exp_St	17	0.150	1.650e+02	0.000
077_Exp_St	41	3.366	2.245e+01	0.000
048_Exp_St	34	17.489	1.146e+00	0.339
127_Exp_St	45	38.775	2.921e+00	0.001

145

146

148 **Tab. S12.** *T*-test of linear fit model (Fit_model) of pooled data across different strains for a given phase of growth
 149 (exponential; _Exp, pre-stationary; _St) and across different phase of growth for a given strain (_Exp_St) from
 150 effective absorption cross section of PSII (σ_{PSII}' ; nm² quanta⁻¹) measured under diel peak PAR growth light under
 151 Ex_{445nm} (blue) excitation in relation to the cumulative diel PAR ($\mu\text{mol photons m}^{-2}\text{d}^{-1}$, for two PhycoCyanin(PC)-
 152 rich cultures (056, 077) and two PhycoErythrin(PE)-rich cultures (048, 127) of *Synechococcus* sp., grown at 30, 90,
 153 180, 300, 600, or 900 peak PAR $\mu\text{mol photons m}^{-2}\text{s}^{-1}$; and photoperiods of 8, 12, 16, or 24 h. Estimate - estimation
 154 statistics; Std.Error - standard error of the estimate; *t*_value – *t*-test statistic; *p*_value - level of significance.
 155

Fit_model	Estimate	Std.Error	<i>t</i> _value	<i>p</i> _value
056_077_Exp	-1.451e-09	1.058e-09	-1.372	0.171
056_048_Exp	-2.188e-09	1.313e-09	-1.666	0.097
056_127_Exp	-8.236e-10	1.412e-09	-0.583	0.560
048_127_Exp	1.365e-09	1.603e-09	0.851	0.395
077_048_Exp	-7.373e-10	1.233e-09	-0.598	0.550
077_127_Exp	6.274e-10	1.336e-09	0.470	0.639
056_077_St	2.453e-09	1.349e-09	1.818	0.071
056_048_St	5.254e-09	2.098e-09	2.505	0.014
056_127_St	1.745e-09	1.862e-09	0.937	0.350
048_127_St	-3.509e-09	1.658e-09	-2.116	0.036
077_048_St	2.801e-09	1.263e-09	2.217	0.028
077_127_St	-7.077e-10	1.209e-09	-0.586	0.559
056_Exp_St	2.487e-09	1.643e-09	1.514	0.132
077_Exp_St	6.391e-09	9.166e-10	6.973	0.000
048_Exp_St	9.930e-09	1.695e-09	5.860	0.000
127_Exp_St	5.056e-09	1.621e-09	3.120	0.002

156

157

159 **Tab. S13.** *T*-test of linear fit model (Fit_model) of pooled data across different strains for a given phase of growth
 160 (exponential; _Exp, pre-stationary; _St) and across different phase of growth for a given strain (_Exp_St) from
 161 effective absorption cross section of PSII (σ_{PSII}' ; nm² quanta⁻¹) measured under diel peak PAR growth light under
 162 Ex_{445nm} (blue) excitation in relation to Phycobiliprotein to Chl *a* ratio, for two PhycoCyanin(PC)-rich cultures (056,
 163 077) and two PhycoErythrin(PE)-rich cultures (048, 127) of *Synechococcus* sp., grown at 30, 90, 180, 300, 600, or
 164 900 peak PAR $\mu\text{mol photons m}^{-2}\text{s}^{-1}$; and photoperiods of 8, 12, 16, or 24 h. Estimate - estimation statistics;
 165 Std.Error - standard error of the estimate; *t*_value - *t*-test statistic; *p*_value - level of significance.
 166

Fit_model	Estimate	Std.Error	<i>t</i> _value	<i>p</i> _value
056_077_Exp	0.003	0.008	0.424	0.672
056_048_Exp	0.078	0.009	9.082	0.000
056_127_Exp	0.039	0.009	4.382	0.000
048_127_Exp	-0.039	0.009	-4.416	0.000
077_048_Exp	0.075	0.008	8.954	0.000
077_127_Exp	0.036	0.009	4.117	0.000
056_077_St	-0.023	0.007	-3.495	0.000
056_048_St	-0.062	0.016	-3.788	0.000
056_127_St	-0.037	0.014	-2.606	0.009
048_127_St	0.026	0.023	1.143	0.253
077_048_St	-0.039	0.014	-2.823	0.005
077_127_St	-0.013	0.012	-1.117	0.264
056_Exp_St	0.083	0.013	6.327	0.000
077_Exp_St	0.057	0.009	6.590	0.000
048_Exp_St	-0.057	0.018	-3.217	0.001
127_Exp_St	0.008	0.020	0.389	0.698

167

168

170 **Tab. S14.** *T*-test of linear fit model (Fit_model) of pooled data across different strains for a given phase of growth
 171 (exponential; _Exp, pre-stationary; _St) and across different phase of growth for a given strain (_Exp_St) from
 172 effective absorption cross section of PSII (σ_{PSII}' ; nm² quanta⁻¹) measured under Ex_{590nm} (orange) excitation in
 173 relation to the Phycobiliprotein to Chl *a* ratio, for two PhycoCyanin(PC)-rich cultures (056, 077) and two
 174 PhycoErythrin(PE)-rich cultures (048, 127) of *Synechococcus* sp., grown at 30, 90, 180, 300, 600, or 900 peak PAR
 175 μmol photons m⁻²s⁻¹; and photoperiods of 8, 12, 16, or 24 h. Estimate - estimation statistics; Std.Error - standard
 176 error of the estimate; *t*_value – *t*-test statistic; *p*_value - level of significance.
 177

Fit_model	Estimate	Std.Error	<i>t</i> _value	<i>p</i> _value
056_077_Exp	-0.369	0.092	-4.000	0.000
056_048_Exp	0.149	0.082	1.812	0.070
056_127_Exp	0.606	0.099	6.122	0.000
048_127_Exp	0.457	0.090	5.084	0.000
077_048_Exp	0.518	0.083	6.267	0.000
077_127_Exp	0.976	0.097	10.089	0.000
056_077_St	0.077	0.029	2.669	0.008
056_048_St	-0.610	0.079	-7.751	0.000
056_127_St	-0.299	0.071	-4.191	0.000
048_127_St	0.311	0.177	1.759	0.080
077_048_St	-0.688	0.076	-9.099	0.000
077_127_St	-0.377	0.070	-5.371	0.000
056_Exp_St	0.440	0.117	3.761	0.000
077_Exp_St	0.887	0.091	9.780	0.000
048_Exp_St	-0.319	0.148	-2.164	0.031
127_Exp_St	-0.465	0.247	-1.882	0.060

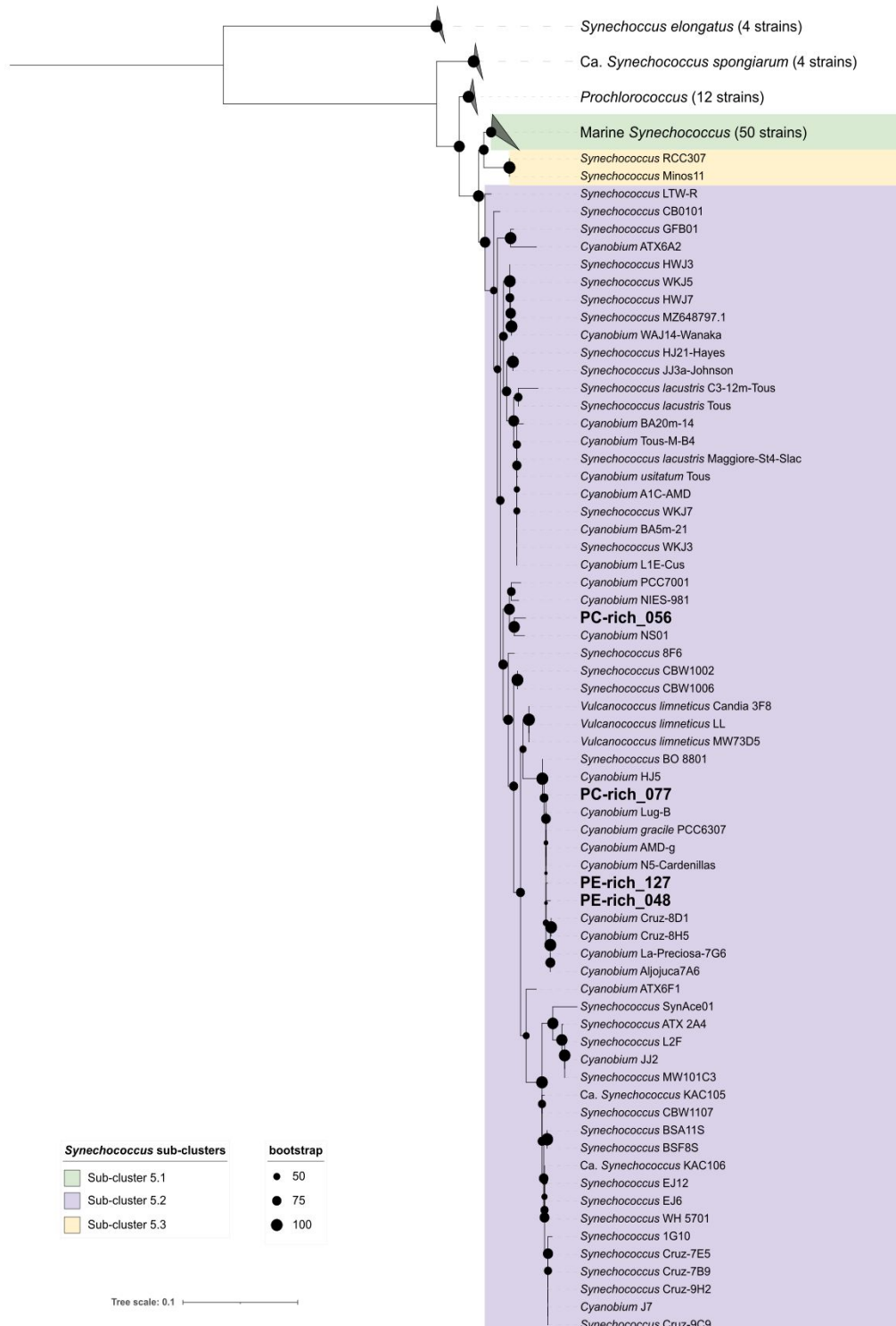
178

179

181 **Tab. S15.** *T*-test of linear fit model (Fit_model) of pooled data across different strains for a given phase of growth
182 (exponential; _Exp, pre-stationary; _St) and across different phase of growth for a given strain (_Exp_St) from
183 effective absorption cross section of PSII (σ_{PSII} ; nm² quanta⁻¹) measured under Ex590nm (orange) excitation in
184 relation to the Phycobiliprotein to Chl *a* ratio, for two PhycoCyanin(PC)-rich cultures (056, 077) and two
185 PhycoErythrin(PE)-rich cultures (048, 127) of *Synechococcus* sp., grown at 30, 90, 180, 300, 600, or 900 peak PAR
186 μmol photons m⁻²s⁻¹; and photoperiods of 8, 12, 16, or 24 h. Estimate - estimation statistics; Std.Error - standard
187 error of the estimate; *t*_value – *t*-test statistic; *p*_value - level of significance.
188

Fit_model	Estimate	Std.Error	<i>t</i> _value	<i>p</i> _value
056_077_Exp	-0.118	0.060	-1.962	0.050
056_048_Exp	0.216	0.058	3.693	0.000
056_127_Exp	0.841	0.076	11.067	0.000
048_127_Exp	0.625	0.076	8.187	0.000
077_048_Exp	0.334	0.060	5.526	0.000
077_127_Exp	0.959	0.075	12.806	0.000
056_077_St	0.397	0.027	14.566	0.000
056_048_St	-0.120	0.064	-1.873	0.062
056_127_St	0.086	0.061	1.411	0.159
048_127_St	0.206	0.114	1.801	0.073
077_048_St	-0.516	0.048	-10.776	0.000
077_127_St	-0.310	0.044	-7.121	0.000
056_Exp_St	0.317	0.075	4.234	0.000
077_Exp_St	0.831	0.061	13.656	0.000
048_Exp_St	-0.019	0.122	-0.155	0.877
127_Exp_St	-0.438	0.209	-2.099	0.036

189



190

191 **Fig. S1.** Phylogenetic tree derived from partial 16S rRNA gene sequences using topology given by Maximum
 192 Likelihood (1000 bootstraps). Support values are indicated by the size of internal nodes. Strains used in this study
 193 are shown in bold.

194

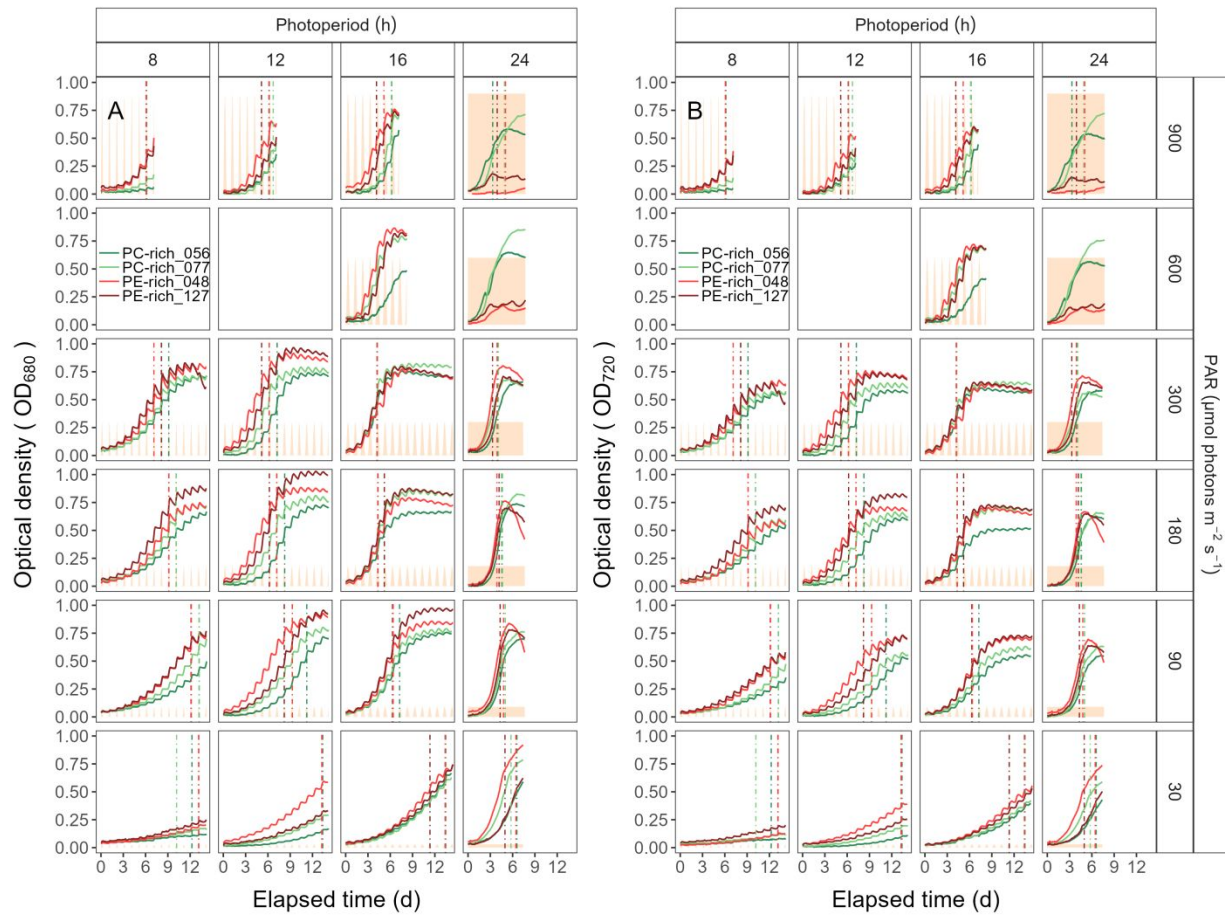


Fig. S2. Growth curves, tracked as OD_{680} (**A**) and OD_{720} (**B**) vs. elapsed time (d). Growth curves were estimated over 5-min intervals for two PC-rich cultures (056; dark green, 077; light green) and two PE-rich cultures (048; light red, 127; dark red) of *Synechococcus* sp. grown at 30, 90, 180, 300, 600, or 900 peak PAR $\mu\text{mol photons m}^{-2}\text{s}^{-1}$; and photoperiods of 8, 12, 16, or 24 h. The vertical lines represent the time when the cultures reached the maximum of the 1st derivative of OD_{680} , or maximum absolute hourly growth (tMaxAHG), taken as an index of transition from exponential to pre-stationary growth phases. The orange area represents the photoperiods, with peak PAR x 1/1000 to scale to the Y axis.

195

196

197

198

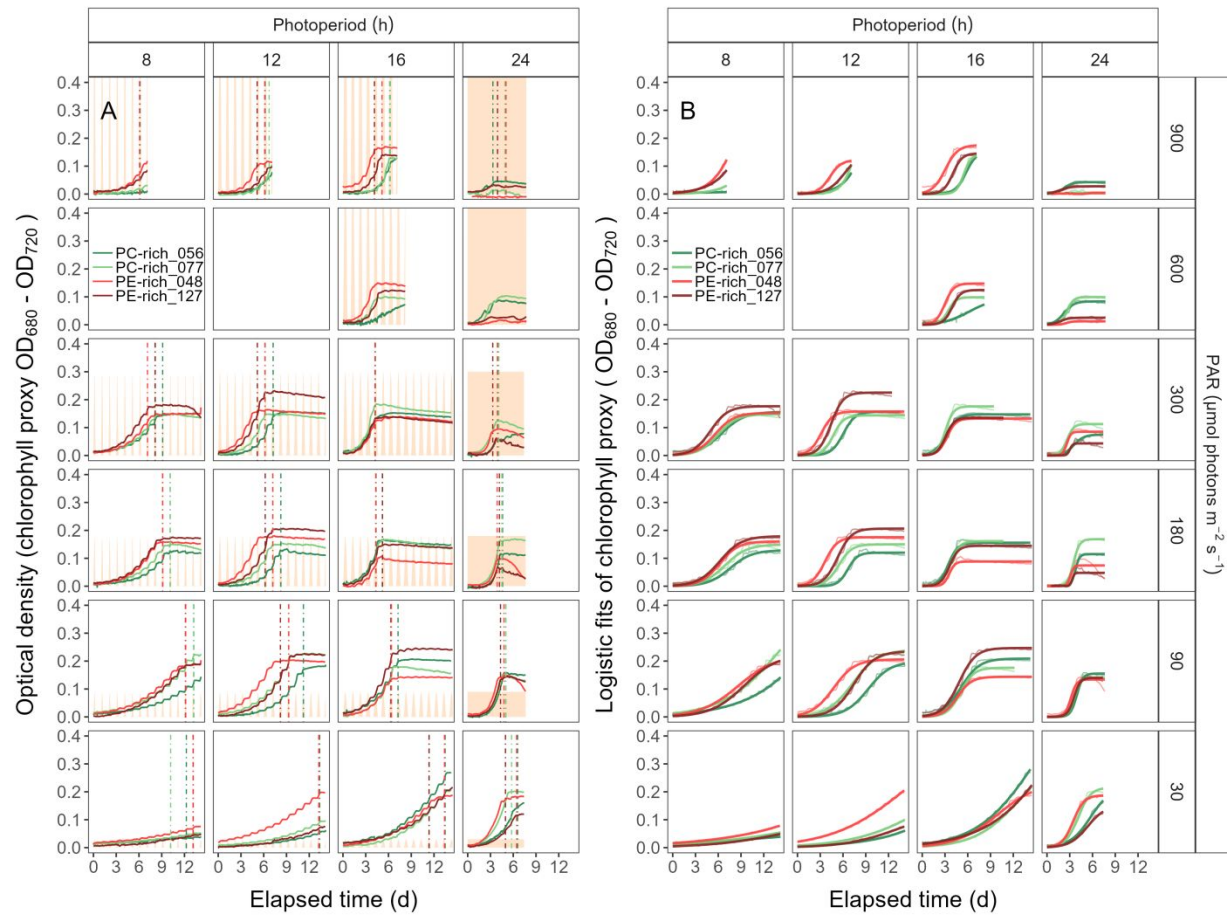
199

200

201

202

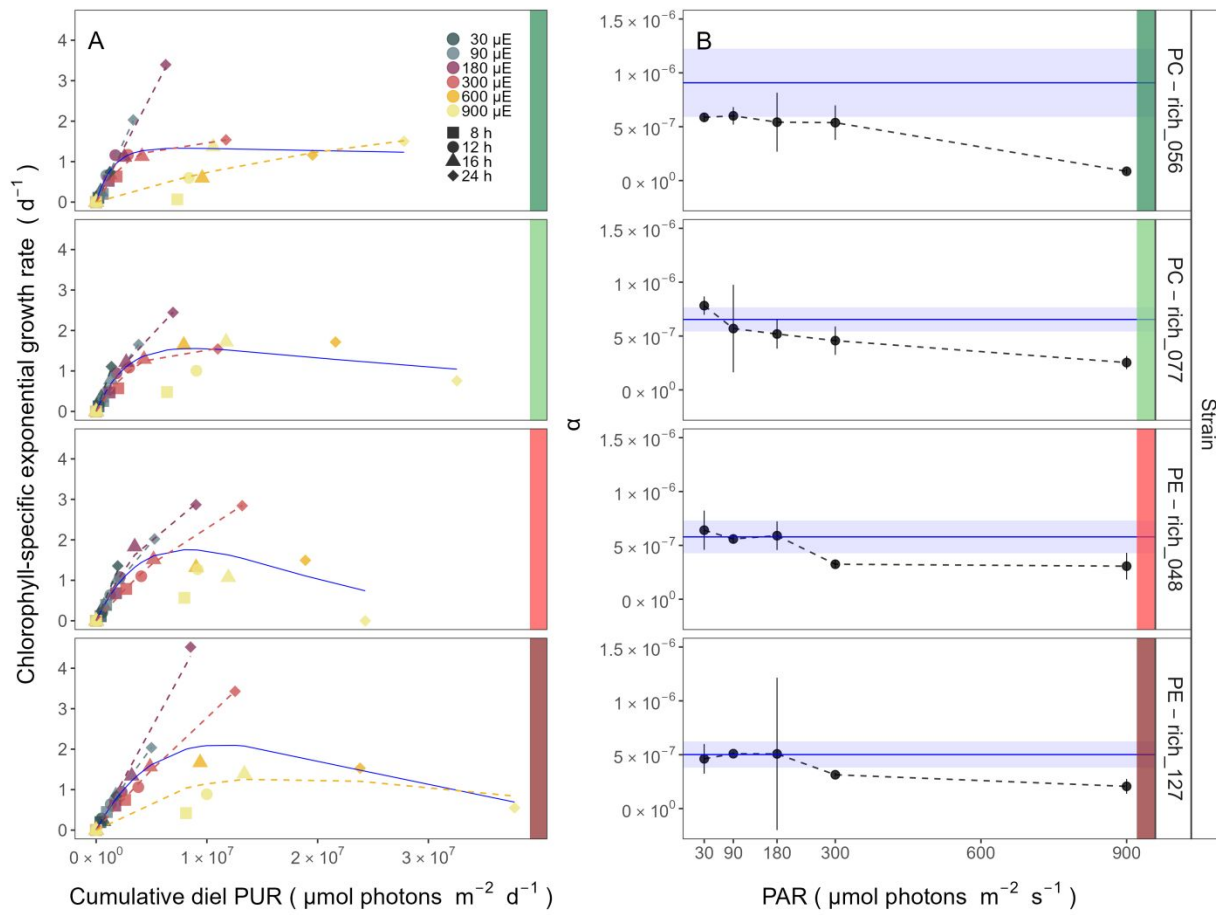
203



204

Fig. S3. (A) Growth curves (tracked as chlorophyll proxy $\text{OD}_{680}-\text{OD}_{720}; \Delta \text{OD}$) vs. elapsed time (d). Growth curves were estimated over 5-min intervals for two PC-rich cultures (056; dark green, 077; light green) and two PE-rich cultures (048; light red, 127; dark red) of *Synechococcus* sp. grown at 30, 90, 180, 300, 600, or 900 peak PAR $\mu\text{mol photons m}^{-2}\text{s}^{-1}$; and photoperiods of 8, 12, 16, or 24 h. The vertical lines represent the time when the cultures reached the maximum of the 1st derivative of OD_{680} , or maximum absolute hourly growth (tMaxAHG), taken as an index of transition from exponential to pre-stationary growth phases. The orange area represents the photoperiods, with peak PAR $\times 1/2000$ to scale to the Y axis. (B) Logistic fits (thick lines) of chlorophyll proxy $\text{OD}_{680}-\text{OD}_{720} (\Delta \text{OD})$ vs. elapsed time (d). Growth curves (thin line) measured over 5-min intervals for each strain were also presented.

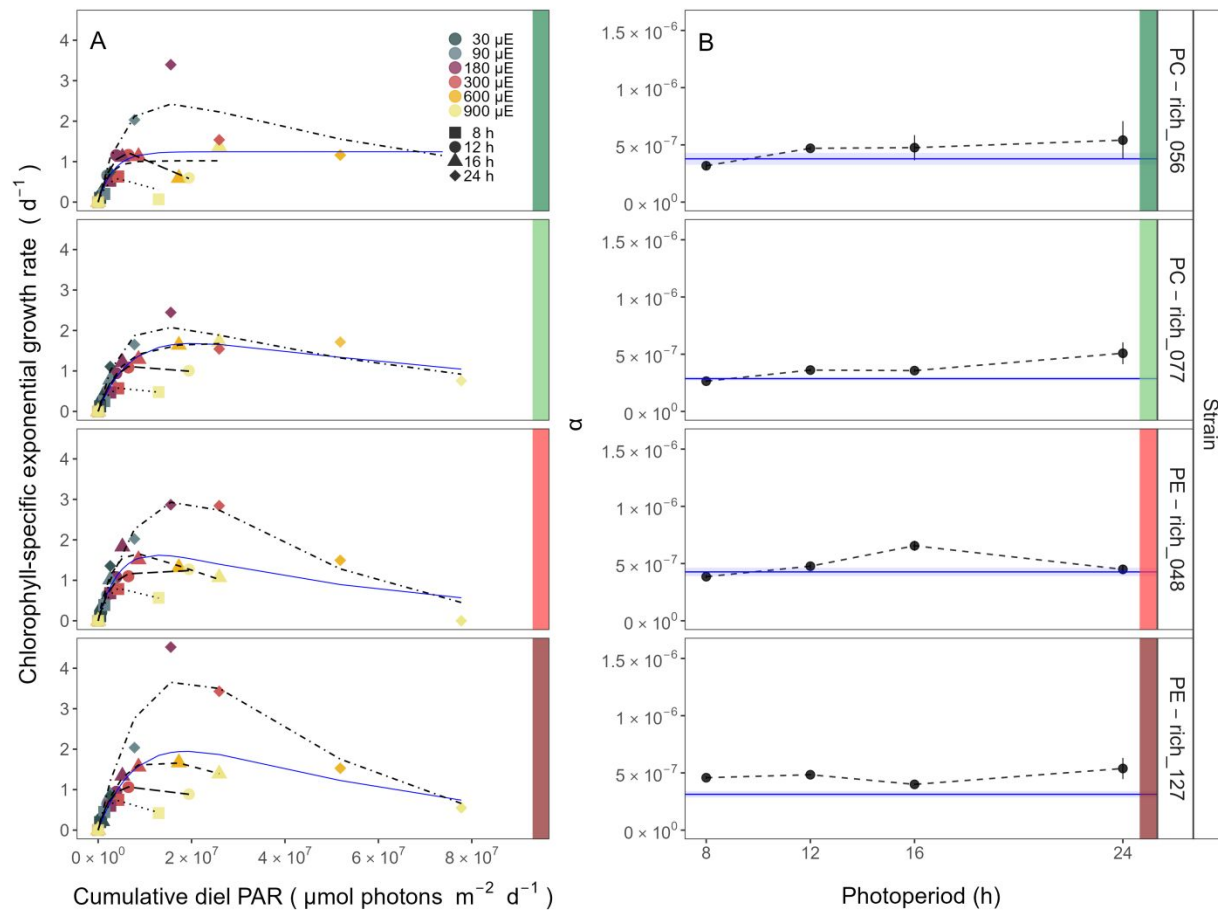
214



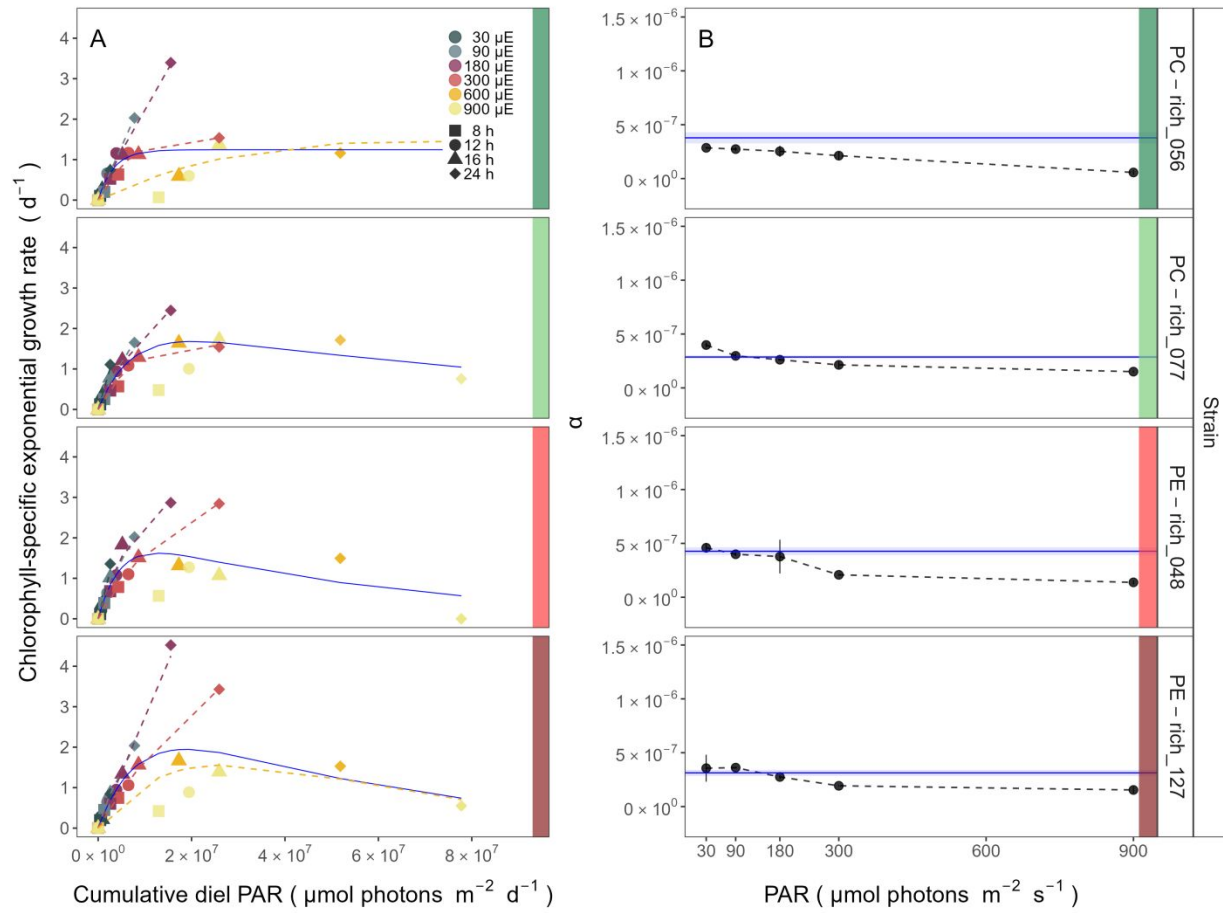
215

Fig. S4. (A) Chlorophyll-specific exponential growth rates (d^{-1}) vs. cumulative diel Photosynthetically Usable Radiation (PUR, $\mu\text{mol photons m}^{-2}\text{d}^{-1}$). Growth rates (\pm SE falling within symbols) were estimated from logistic fits of chlorophyll proxy OD₆₈₀ – OD₇₂₀ (ΔOD) vs. elapsed time (Fig. 1, Fig. S3B), for two PC-rich cultures (056; dark green, 077; light green) and two PE-rich cultures (048; light red, 127; dark red) of *Synechococcus* sp. grown at 30 (dark gray), 90 (light gray), 180 (purple), 300 (red), 600 (orange), or 900 (yellow) peak PAR $\mu\text{mol photons m}^{-2}\text{s}^{-1}$ (μE); and photoperiods of 8 (square), 12 (circle), 16 (triangle), or 24 (diamond) h. Solid blue line shows a fit of the pooled growth rates through peak PAR for each strain, with a three parameter model (Harrison and Platt, 1986). We also fit the same model separately for 30 (dark gray), 90 (light gray), 180 (purple), 300 (red), 600 together with 900 (orange) peak PAR $\mu\text{mol photons m}^{-2}\text{s}^{-1}$, only when they were each significantly different (ANOVA, $p < 0.05$) from the fit of pooled data. (B) Alpha parameters of the initial rise of growth rate (α) vs. cumulative diel Photosynthetically Usable Radiation (PUR), estimated from data pooled for each peak PAR (points (\pm SE) connected by dashed lines), and estimated for all data across all peak PAR, for each strain (solid blue horizontal line \pm SE).

229



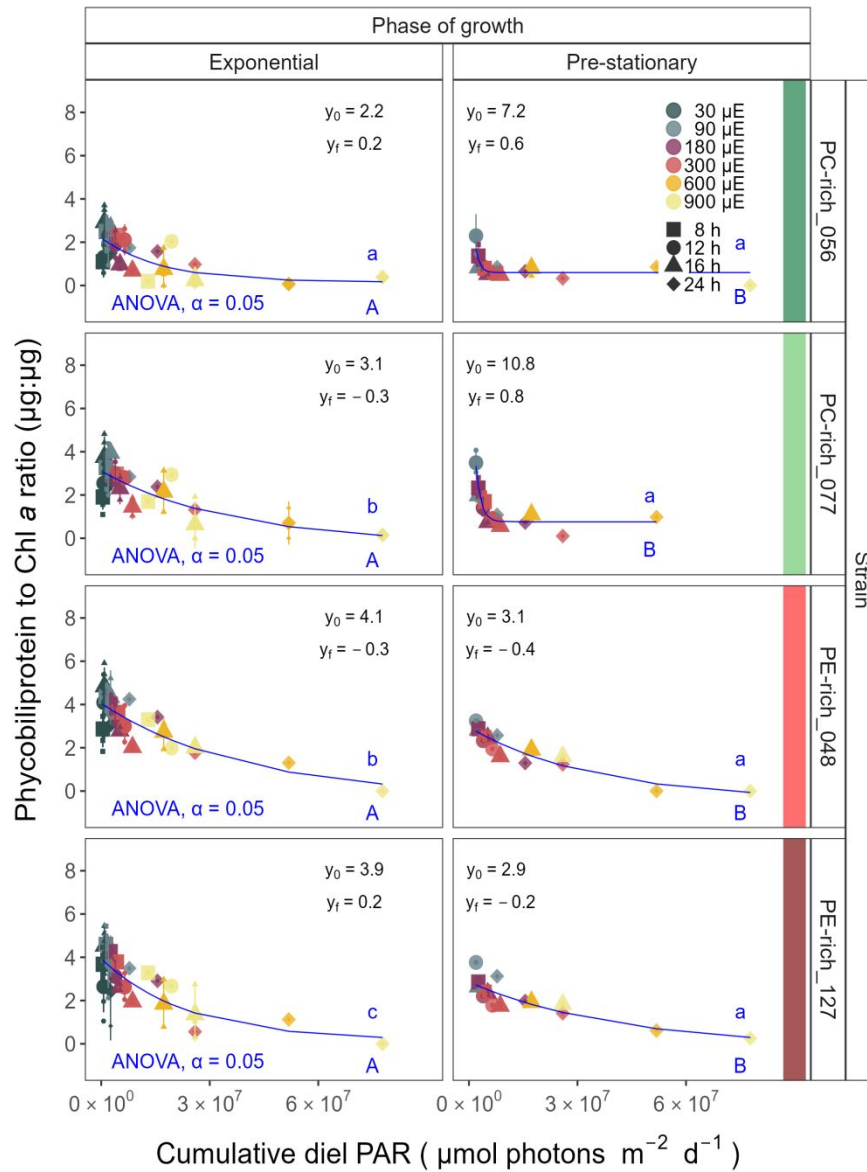
230
231 **Fig. S5.** (A) Chlorophyll-specific exponential growth rates (d^{-1}) vs. cumulative diel PAR ($\mu\text{mol photons m}^{-2} \text{d}^{-1}$).
232 Growth rates (\pm SE falling within symbols) were estimated from logistic fits of chlorophyll proxy OD₆₈₀ – OD₇₂₀
233 (ΔOD) vs. elapsed time (Fig. 1, Fig. S3B), for two PC-rich cultures (056; dark green, 077; light green) and two PE-
234 rich cultures (048; light red, 127; dark red) of *Synechococcus* sp. grown at 30 (dark gray), 90 (light gray), 180
235 (purple), 300 (red), 600 (orange), or 900 (yellow) peak PAR $\mu\text{mol photons m}^{-2}\text{s}^{-1}$ (μE); and photoperiods of 8
236 (square), 12 (circle), 16 (triangle), or 24 (diamond) h. Solid blue line shows a fit of the pooled growth rates through
237 photoperiod (h) for each strain, with a three parameter model (Harrison and Platt 1986). We also fit the same model
238 separately for 8 (dotted line), 12 (long dash line), 16 (dashed line), or 24 (two dash line) h photoperiods, since for all
239 strains they were each significantly different (ANOVA, $p < 0.05$) from the fit of pooled data. (B) Alpha parameters
240 of the initial rise of growth rate (α) vs. cumulative diel PAR, estimated from data pooled for each photoperiod
241 (points (\pm SE) connected by dashed lines), and estimated for all data across photoperiods (solid blue horizontal line
242 \pm SE), for each strain.
243



244

245 **Fig. S6.** (A) Chlorophyll-specific exponential growth rates (d^{-1}) vs. cumulative diel PAR ($\mu\text{mol photons m}^{-2} \text{d}^{-1}$).
 246 Growth rates (\pm SE falling within symbols) were estimated from logistic fits of chlorophyll proxy OD₆₈₀ – OD₇₂₀
 247 (ΔOD) vs. elapsed time (Fig. 1, Fig. S3B), for two PC-rich cultures (056; dark green, 077; light green) and two PE-
 248 rich cultures (048; light red, 127; dark red) of *Synechococcus* sp. grown at 30 (dark gray), 90 (light gray), 180
 249 (purple), 300 (red), 600 (orange), or 900 (yellow) peak PAR $\mu\text{mol photons m}^{-2}\text{s}^{-1}$ (μE); and photoperiods of 8
 250 (square), 12 (circle), 16 (triangle), or 24 (diamond) h. Solid blue line shows a fit of the pooled growth rates through
 251 peak PAR for each strain, with a three parameter model (Harrison and Platt, 1986). We also fit the same model
 252 separately for 30 (dark gray), 90 (light gray), 180 (purple), 300 (red), 600 together with 900 (orange) peak PAR
 253 $\mu\text{mol photons m}^{-2}\text{s}^{-1}$, only when they were each significantly different (ANOVA, $p < 0.05$) from the fit of pooled
 254 data. (B) Alpha parameters of the initial rise of growth rate (α) vs. cumulative diel PAR, estimated from data pooled
 255 for each peak PAR (points (\pm SE) connected by dashed lines), and estimated for all data across all peak PAR, for
 256 each strain (solid blue horizontal line \pm SE).

257



258

259

260

261

262

263

264

265

266

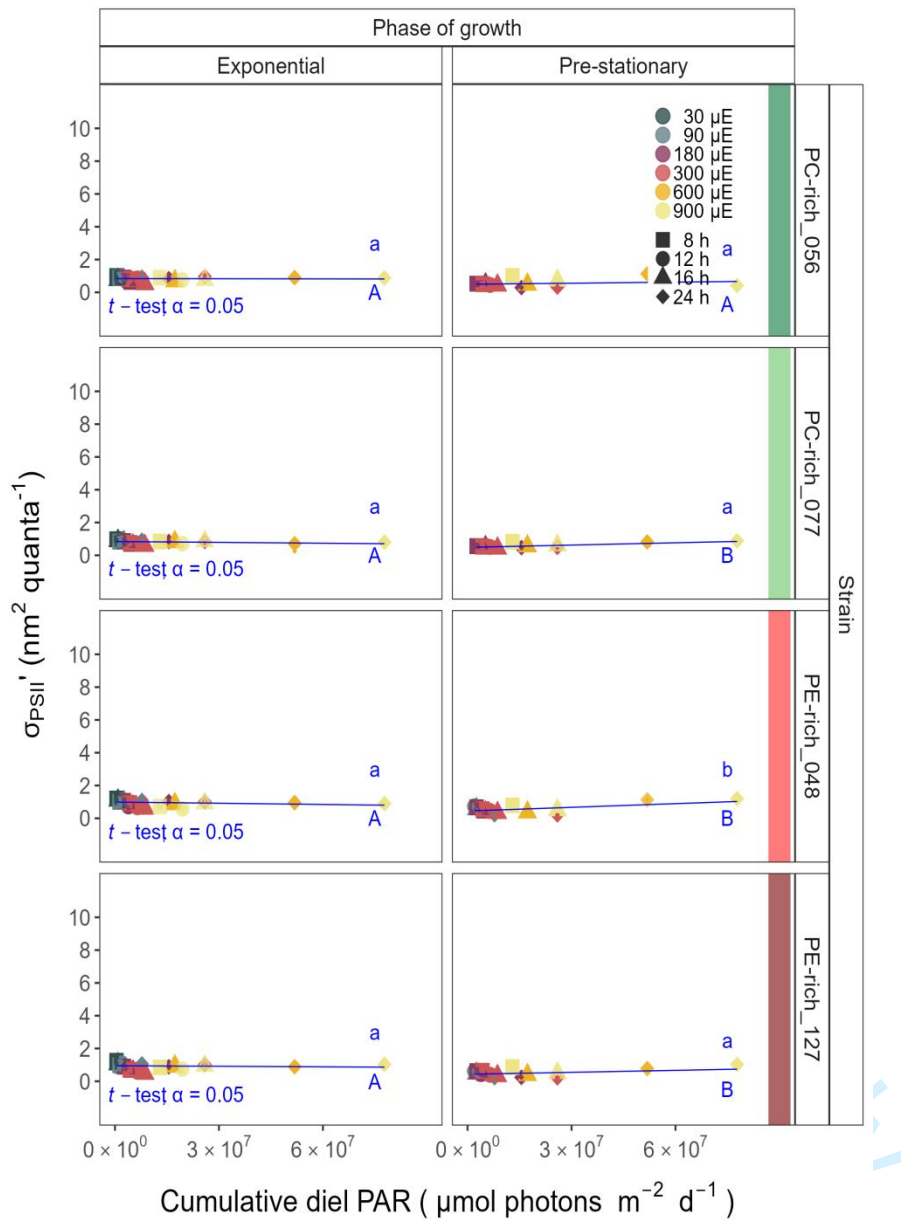
267

268

269

Fig. S7. Changes of Phycobiliprotein to Chl *a* ratio ($\mu\text{g}:\mu\text{g}$) vs. cumulative diel PAR ($\mu\text{mol photons m}^{-2}\text{d}^{-1}$).

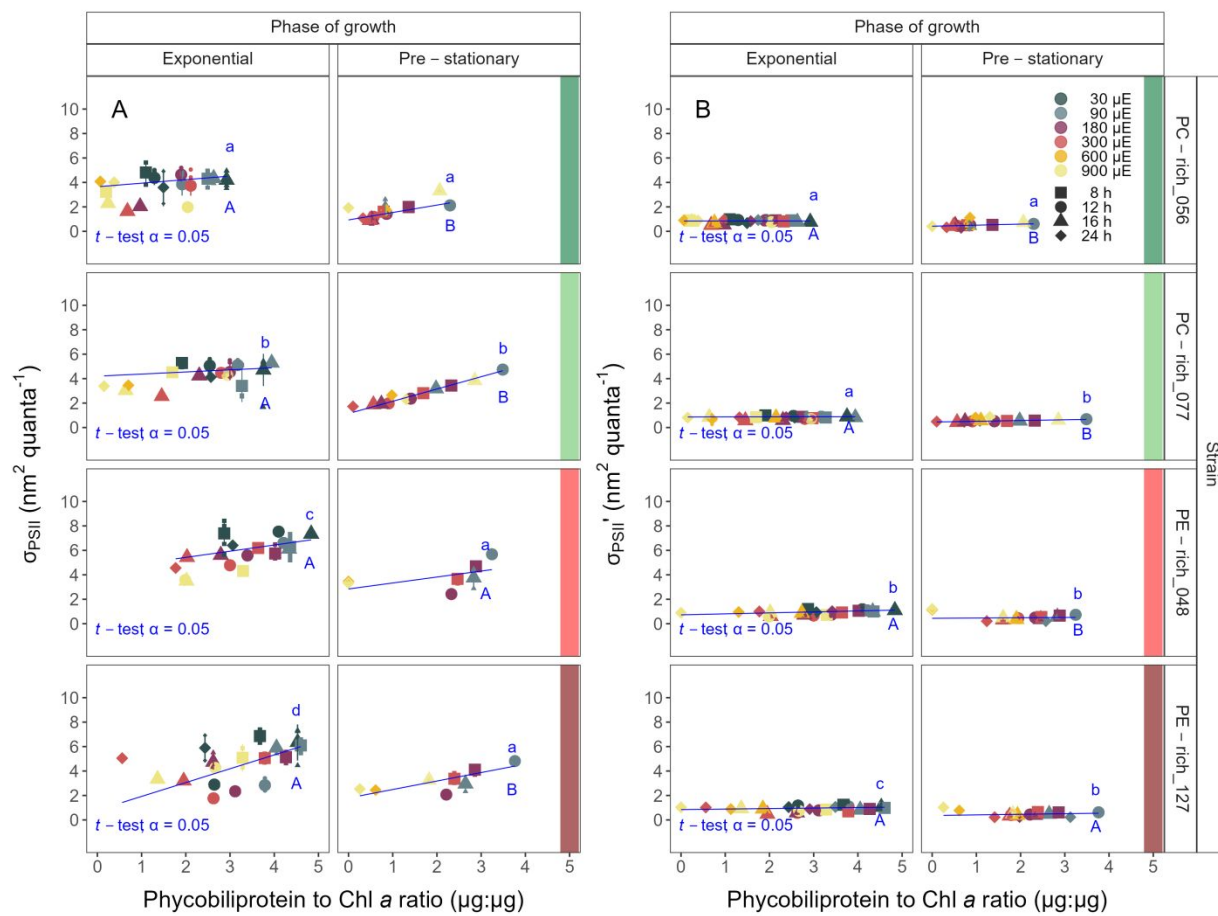
Phycobiliprotein to Chl *a* ratio was estimated for two PC-rich cultures (056; dark green, 077; light green) and two PE-rich cultures (048; light red, 127; dark red) of *Synechococcus* sp. grown at 30 (dark gray), 90 (light gray), 180 (purple), 300 (red), 600 (orange), or 900 (yellow) peak PAR $\mu\text{mol photons m}^{-2}\text{s}^{-1}$ (μE); and photoperiods of 8 (square), 12 (circle), 16 (triangle), or 24 (diamond) h. Figure presents data (smaller symbols) and means (bigger symbols) from exponential or pre-stationary phase of growth. Blue solid line shows single phase exponential decay fit for data from each strain and growth phase, fit parameters are presented. Different lowercase letters indicate statistically significant differences between the fit models for different strains within a given phase of growth. Different uppercase letters indicate statistically significant differences between the fit models for different phases of growth within a given strain (ANOVA; $p < 0.05$).



270

271 **Fig. S8.** Effective absorption cross section of PSII ($\sigma_{\text{PSII}'}$; nm² quanta⁻¹) measured under diel peak PAR growth light
 272 under blue (Ex_{445nm}) excitation vs. cumulative diel PAR (μmol photons m⁻²d⁻¹). $\sigma_{\text{PSII}'}$ was estimated for two PC-rich
 273 cultures (056; dark green, 077; light green) and two PE-rich cultures (048; light red, 127; dark red) of
 274 *Synechococcus* sp. grown at 30 (dark gray), 90 (light gray), 180 (purple), 300 (red), 600 (orange), or 900 (yellow)
 275 peak PAR μmol photons m⁻²s⁻¹ (μE); and photoperiods of 8 (square), 12 (circle), 16 (triangle), or 24 (diamond) h.
 276 Figure presents data (smaller symbols) and means (bigger symbols) from exponential or pre-stationary phase of
 277 growth. Blue solid line shows linear model fit for data from each strain and growth phase. Different lowercase
 278 letters indicate statistically significant differences between the fit models for different strains within a given phase of
 279 growth. Different uppercase letters indicate statistically significant differences between the fit models for different
 280 phases of growth within a given strain (*t*-test; $p < 0.05$).

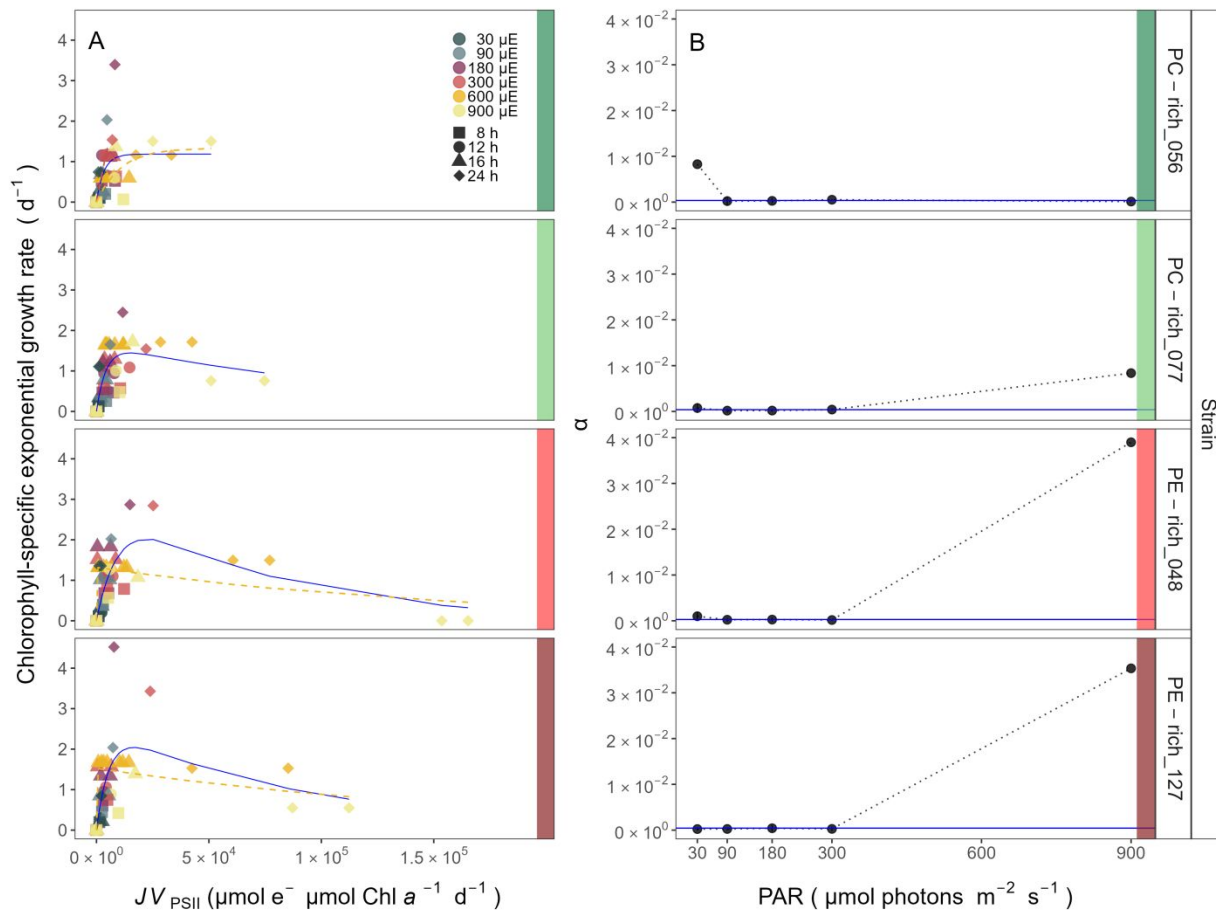
281



282

Fig. S9. (A) Changes of effective absorption cross section of PSII (σ_{PSII} ; $\text{nm}^2 \text{ quanta}^{-1}$) measured at the dark period under orange ($Ex_{590\text{nm}}$) excitation vs. the ratio of sum of μg phycobilins (PE, PC, APC protein, Phycobiliprotein) to μg Chl a. **(B)** Changes of effective absorption cross section of PSII (σ_{PSII}' ; $\text{nm}^2 \text{ quanta}^{-1}$) measured under diel peak PAR growth light under blue ($Ex_{445\text{nm}}$) excitation vs. the ratio of sum of μg phycobilins (PE, PC, APC protein, Phycobiliprotein) to μg Chl a. σ_{PSII}' was estimated for two PC-rich cultures (056; dark green, 077; light green) and two PE-rich cultures (048; light red, 127; dark red) of *Synechococcus* sp. grown at 30 (dark gray), 90 (light gray), 180 (purple), 300 (red), 600 (orange), or 900 (yellow) peak PAR $\mu\text{mol photons m}^{-2}\text{s}^{-1}$ (μE); and photoperiods of 8 (square), 12 (circle), 16 (triangle), or 24 (diamond) h. Figure presents data (smaller symbols) and means (bigger symbols) from exponential or pre-stationary phase of growth. Blue solid line shows linear model fit for data from each strain and growth phase. Different lowercase letters indicate statistically significant differences between the fit models for different strains within a given phase of growth. Different uppercase letters indicate statistically significant differences between the fit models for different phases of growth within a given strain (t -test; $p < 0.05$).

295



296

Fig. S10. (A) Chlorophyll specific exponential growth rates (d^{-1}) vs. cumulative diel PSII electron flux (JV_{PSII} ; $\mu\text{mol e}^- \mu\text{mol Chl } a^{-1} d^{-1}$) measured under diel peak PAR growth light. Growth rates (\pm SE falling within symbols) were estimated from logistic fits of chlorophyll proxy $OD_{680} - OD_{720}$ (ΔOD) vs. elapsed time (Fig. S3). PSII flux was estimated using FRRf induction curves with excitation of chlorophyll ($Ex_{445\text{nm}}$, blue), for two PC-rich cultures (056; dark green, 077; light green) and two PE-rich cultures (048; light red, 127; dark red) of *Synechococcus* sp. grown at 30 (dark gray), 90 (light gray), 180 (purple), 300 (red), 600 (orange), or 900 (yellow) peak PAR $\mu\text{mol photons m}^{-2} s^{-1}$; and photoperiods of 8 (square), 12 (circle), 16 (triangle), or 24 (diamond) h. Solid blue line shows a fit of the pooled growth rates for each strain, with a three parameter model (Harrison and Platt 1986). We also fit the same model separately for 600 together with 900 (orange) peak PAR $\mu\text{mol photons m}^{-2} s^{-1}$, when they were significantly different (ANOVA, $p < 0.05$) from the fit of pooled data. (B) Alpha parameters of the initial rise of growth rate (α) vs. cumulative diel JV_{PSII} , estimated from data pooled for each peak PAR (points (\pm SE) connected by dashed lines), and estimated for all data across all peak PAR, for each strain (solid blue horizontal line \pm SE).

309

310 **References**

- 311 Harrison, W. G., and T. Platt. 1986. Photosynthesis-irradiance relationships in polar and
312 temperate phytoplankton populations. *Polar biology* **5**: 153–164.